

INFLUENCE OF THE NEOSTRIATAL PATCH SYSTEM ON THE  
PREDICTION-BASED CODING OF MIDBRAIN DOPAMINERGIC  
NEURONS

BY

THOMAS WILLAM FAUST

A DISSERTATION SUBMITTED TO THE GRADUATE SCHOOL – NEWARK  
RUTGERS, THE STATE UNIVERSITY OF NEW JERSEY

IN PARTIAL FULFILLMENT OF THE REQUIREMENTS FOR THE DEGREE OF  
DOCTOR OF PHILOSOPHY

GRADUATE PROGRAM IN BEHAVIORAL AND NEURAL SCIENCES

WRITTEN UNDER THE DIRECTION OF

TIBOR KOÓS

AND APPROVED BY

---

---

---

---

---

---

---

NEWARK, NEW JERSEY

OCTOBER 2017

©2017

Thomas W Faust

ALL RIGHTS RESERVED

# ABSTRACT OF THE DISSERTATION

Influence of the Neostriatal Patch System on the Prediction-Based Coding of  
Midbrain Dopaminergic Neurons

By THOMAS WILLIAM FAUST

Dissertation Director:

Tibor Koós

Dopaminergic neurons of the ventral midbrain signal deviations from expected values, and have profound effects on motivated behavior. It has been hypothesized that these neurons produce these signals by integrating prediction and outcome information from distinct afferent structures, and update representations of prediction by dopamine-dependent synaptic plasticity. I therefore attempted to characterize the coding properties of one of their primary source of synaptic inhibition, the patches of the dorsal striatum, in an attempt to determine whether it could serve to provide prediction information to the dopaminergic neurons. The coding differences between the patch and matrix subpopulations of the dorsal striatum have thus far remained unknown, but due to the recent availability of new transgenic mouse lines targeting these neuronal populations, they can now be investigated. Based on their unique monosynaptic innervation of dopaminergic neurons of the substantia

nigra, receipt of dopaminergic innervation from the substantia nigra, and dopamine-dependent synaptic plasticity, I therefore hypothesized that the neurons of the dorsal striatal patches provide the prediction signal by which dopaminergic neurons report deviations in expected value. I used in vitro whole cell recording and optogenetics to determine the synaptic physiology of projections from the patches to dopaminergic neurons, and used in vivo multielectrode recording and optogenetics to characterize the coding properties of striatal patch and matrix neurons. The patches of the dorsal striatum were observed to provide biophysically distinct fast and slow inhibition to the dopaminergic neurons of the substantia nigra, and dorsal striatal patch neurons were observed to encode signals which conform to the notion of a prediction signal. Therefore these results support the hypothesis that dopaminergic neurons encode deviations from predicted outcomes, and that the dorsal striatal patches provide a prediction signal necessary for this type of coding.

## ACKNOWLEDGMENTS

First of all, I'd like to thank my committee members, who took time, energy and thoughtful analysis out of their busy lives to provide useful feedback and advice which has helped guide this thesis project to completion and improve it along the way. I'd like to thank NINDS, Rutgers University and specifically the BNS graduate program, and the Rutgers Graduate School – Newark for their support during my time here as a graduate student. I'd like to thank multiple of my peers, graduate students past and present, and postdocs, for their technical, intellectual, and emotional contributions to my training. I'd additionally like to thank two of my family members, my brother Rudolf P. Faust and my wife Adria L. Faust. I fondly remember having many intellectually-stimulating conversations with my brother about my thesis project, the basal ganglia, and neuroscience in general. Lastly I'd like to acknowledge that without the support of my wife during this difficult time, while we were taking care of our young baby Theodore, this thesis would not have been finalized in the form that it was, in a timely manner. You are a wonderful partner and I'm grateful for your support.

# TABLE OF CONTENTS

## **Chapter 1:**

<b>Introduction</b>	<b>1</b>
The neurotransmitter dopamine	2
The role of dopaminergic neurons in reward-based learning	4
On the circuit mechanisms of RPE coding in dopaminergic neurons	18
The patch compartment of the dorsal striatum	23
GABAergic transmission by midbrain dopaminergic neurons	26
Striatal GABAergic interneuron identity and circuitry	27

## **Chapter 2:**

### **Novel Fast Adapting Interneurons Mediate Cholinergic-Induced Fast GABA**

<b>Inhibitory Postsynaptic Currents in Striatal Spiny Neurons</b>	<b>29</b>
Abstract	30
Introduction	31
Materials and Methods	32
Animals	32
Intracerebral viral injection	33
Immunocytochemistry	34
Slice preparation and visualized in vitro whole cell recording	35
Data analysis	36
Results	38
Discussion	45

FAIs represent a novel type of GABAergic interneuron in the neostriatum	45
FAIs are not a major source of the fIPSC elicited in SPNs by synchronous activation of cholinergic interneurons	47
Implications for organization of the circuitry of the neostriatum	48
Possible significance for behavioral functions of acetylcholine	50
Acknowledgements	51
References	51

### **Chapter 3:**

#### **Neostriatal GABAergic Interneurons Mediate Cholinergic Inhibition of Spiny**

<b>Projection Neurons</b>	<b>66</b>
Abstract	67
Significance Statement	68
Introduction	68
Materials and Methods	70
Subjects	70
Intracerebral viral injection	71
Slice preparation and visualized in vitro whole-cell recording	71
In vitro optical stimulation	72
Results	73
Discussion	77
References	80

## **Chapter 4:**

### **Neostriatal patch and matrix neurons differentially encode reward**

<b>prediction</b>	<b>90</b>
Abstract	91
Significance Statement	92
Introduction	92
Materials and Methods	94
Animals	94
Intracerebral viral injection	95
Slice preparation and in vitro whole-cell recording	96
Immunohistochemistry	96
Behavior	97
Multi-tetrode and fiberoptic drive fabrication and implantation	98
In vivo recording	99
Analysis and statistics	100
Results	101
Discussion	106
References	111

## **Chapter 5:**

<b>General Discussion</b>	<b>122</b>
---------------------------	------------

**Chapter 6:**

**References**

**127**

## LIST OF TABLES

Table 1	Electrophysiological properties of Htr3a-Cre interneurons	60
---------	---	----

## LIST OF FIGURES

### Chapter 2:

Figure 1	Immunocytochemical characterization of HTR3a-Cre interneurons	56
Figure 2	Electrophysiological identification of FAIs	58
Figure 3	Characterization of synaptic transmission between FAIs and SPNs	61
Figure 4	Characterization of optogenetic responses in slices prepared from double transgenic ChAT-ChR2-EYFP; HTR3a-Cre mice	62
Figure 5	Nicotinic cholinergic synaptic responses of FAIs	64

### Chapter 3:

Figure 1	Schematic for examining interneuronal contributions to cholinergic-induced inhibition	84
Figure 2	Cholinergic-induced inhibition in SPNs before and after inhibition of Htr3a-Cre interneurons	85
Figure 3	Inhibition of Htr3a-Cre interneurons delays cholinergic-induced IPSC	86
Figure 4	Statistical analysis of HR3.0 effect on IPSC kinetics	87
Figure 5	Relationship between IPSC reduction and amplitude	89

### Chapter 4:

Figure 1	Targeting of striatal neurons in the SepW1_NP67 transgenic mouse	115
----------	--	-----

Figure 2	Inhibition of substantia nigra dopaminergic and GABAergic neurons by the patch	116
Figure 3	Schematic for instrumental task	117
Figure 4	SNC dopaminergic neurons encode RPE in the instrumental task	118
Figure 5	Matrix and patch SPN responses during the instrumental task	119
Figure 6	Contralateral responses in matrix and patch SPNs are increased between the CS and UCS	120
Figure 7	Differential coding of patch and matrix neurons to reward expectation	120

# CHAPTER 1:

## Introduction

## **The neurotransmitter dopamine**

In order to survive and reproduce, most animals must obtain scarce resources in a frequently changing environment. In vertebrates, a diverse set of neural circuits throughout the brain have proven critical to evaluating and solving this evolutionary problem. These circuits, or at least components of them, must produce resource-seeking behaviors, generate flexible representations of resource availability, solve optimization problems related to resource acquisition strategy and provide feedback to update history-dependent representations. The history-dependence of flexible representations and the feedback required to update them suggests that these functions should be produced by heavily interconnected circuits. The neurotransmitter dopamine and the dopaminergic neurons that release it appear to occupy a central position in these circuits. In the following section I will describe what we know about how dopamine and the coding of dopaminergic neurons produces behaviors of reward seeking and facilitates reward learning. As most of these observations take place within a laboratory setting, I will be using the term reward but expect that these processes generalize for appetitive stimuli in more ethological settings.

First confirmed as a neurotransmitter by Arvid Carlsson in 1957, dopamine was quickly observed to exert a strong influence over movement control. Carlsson and colleagues demonstrated that reserpine depleted brain dopamine levels while its precursor 3,4-Dihydroxyphenylalanine, also known as L-DOPA, increased brain dopamine levels (Carlsson et al., 1957). When L-DOPA was administered to animals following treatment with reserpine it reduced the reserpine-mediated immobility of these animals (Carlsson et al., 1958). This finding soon led to the discovery that dopamine loss was responsible for

the symptoms of Parkinson's disease (Ehringer and Hornykiewicz, 1960) and eventually lead to the adoption of L-DOPA as the primary treatment for the disease.

The neostriatum contains the highest brain concentrations of dopamine (Bertler and Rosengren, 1959), and the dopaminergic neurons of the ventral midbrain were found to project there (Andén et al., 1964). The behavioral effects of dopamine depletion by reserpine or Parkinson's disease suggested that the recipient structures, including the neostriatum, were responsible for the phenotype. The majority of ascending dopaminergic neurons were found to reside in three ventral midbrain nuclei, the ventral tegmental area (VTA), the substantia nigra pars compacta (SNc), and the retrorubral field, containing dopaminergic neurons from the cell groups A10, A9, and A8, respectively. The dopaminergic neurons of the VTA primarily innervate the ventral striatum, olfactory tubercle, and limbic cortical areas while those of the SNc and retrorubral field primarily innervate the dorsal striatum (Dahlström & Fuxe, 1964).

The early observance of dopamine's effects on motor control led to a profusion of ideas about its function and many lines of investigation of its behavioral effects. The first animal model of Parkinsonian syndrome to be developed was the 6-hydroxydopamine (6-OHDA) mediated lesioning of midbrain dopamine neurons (Ungerstedt, 1971). Similar to Parkinson's disease, 6-OHDA lesioning produced a loss of motor control in animals, and also what could be characterized as a lack of motivation. Based on evidence from Parkinson's patients, Parkinsonian animal models, dopamine antagonism, and drugs of abuse, multiple theories have arisen for how dopamine influences motor control, motivation and reward learning. For reviews on these topics, see (Wise, 2004; Salamone and Correa, 2012; Berridge, 2007; Palmiter, 2008; Bromberg-Martin et al., 2010).

### **The role of dopaminergic neurons in reward-based learning**

Midbrain dopaminergic neurons exhibit three firing patterns in vivo, a tonic, pace-making firing pattern, a random firing pattern, and a phasic burst firing pattern (Grace and Bunney, 1983; Grace and Bunney, 1984; Grace and Bunney, 1984). The pace-making firing pattern is generated by a combination of voltage depending sodium and calcium conductances, and establishes a normal working range of tonic extracellular dopamine in recipient brain structures (Puopolo et al., 2007), without which Parkinsonian symptoms would occur. The burst firing pattern of these neurons is strongly influenced by intracellular calcium and potassium (Grace and Bunney, 1984). Midbrain dopamine neurons exhibit a low terminal release probability (Cragg, 2003), and extracellular dopamine in the dorsal and ventral striatum is limited by uptake (Stamford et al., 1988; Giros et al., 1996; Floresco et al., 2003) so the consequence of burst firing is to greatly increase extracellular dopamine in a phasic manner (Gonon, 1988).

The burst firing pattern of dopamine neurons appears to be under both excitatory and inhibitory control, such that disinhibition of these neurons is required for the production of bursts, rather than just direct excitatory input (Paladini et al., 1999; Lobb et al., 2010; Lobb et al., 2011). In vivo, the occurrence and probability of burst firing in dopamine neurons is perhaps unsurprisingly also under control of multiple inhibitory structures projecting to these neurons within the basal ganglia. For SNc dopamine neurons, this includes most of the major GABAergic structures in the basal ganglia: the striatum, globus pallidus (GP), and substantia nigra pars reticulata (SNr). In anesthetized animals, stimulation of these nuclei produces inhibition of SNc dopamine neuron firing that is

mediated by GABA<sub>A</sub> and GABA<sub>B</sub> receptors (Tepper et al., 1995; Paladini et al., 1999; Brazhnik et al., 2008). Antagonism of GABA<sub>A</sub> receptors in the substantia nigra promotes the burst firing of dopamine neurons, while antagonism of GABA<sub>B</sub> receptors promotes a pace-making firing pattern (Tepper et al., 1995; Paladini and Tepper, 1999). The cause of the latter observation, however, remains ambiguous as GABA<sub>B</sub> receptor antagonism will reduce inhibitory currents in both SNc neurons and presynaptic inhibitory terminals due to their autoreceptors (Boyes and Bolam, 2003).

Despite observations of how pallidal stimulation inhibits dopamine neurons, the net effect of pallidal activation with respect to dopamine neuron firing is likely disinhibitory, presumably due to the stronger effect of inhibiting their primary target, the SNr neurons (Celada et al., 1999). Inhibition of the GP serves to increase pacemaking activity despite its direct inhibition of SNc dopamine neurons, and disinhibition of the GP serves to increase burst firing. Indeed, the modulation of pallidal control over SNc dopamine neurons has meagre control over baseline firing rate but large control over dopamine levels in recipient structures (Lee et al., 2004), again this is assumed to be due to release kinetics.

From the earliest observations of how dopamine controls movement, motivation and learning, investigation of the coding properties of these neurons has revealed that they phasically respond to many sensory stimuli. In multiple species, a subset of dopamine neurons display phasic excitatory or inhibitory responses to multiple types of somatosensory stimuli such as limb and tail pinches, heat exposure, vaginal stimulation, air puff, or peripheral nerve stimulation (Chiodo et al., 1980; Tsai et al., 1980; Maeda and Mogenson, 1982; Schultz and Romo, 1987). Unconditioned visual, auditory, and olfactory stimuli can also generate similar responses (Chiodo et al., 1980; Steinfels et al., 1983).

In addition to sensory stimuli, both trained and untrained arm movements are capable of eliciting phasic responses in many dopamine neurons (Schultz et al., 1983). The motor coding of dopamine neurons has recently been re-examined in spontaneous, untrained movements of head-fixed mice, and in these scenarios dopamine neurons of the SNc phasically encode motor activity in addition to, or in some cases preferentially to, reward (Howe et al., 2016; Parker et al., 2016; Dodson et al., 2016).

These observed nonselective responses to unconditioned stimuli or sensorimotor activity don't provide a great explanation of how dopamine coding exerts its influence over motor control, motivation and reward learning, and don't describe whether dopamine neurons simply generate mixed sensorimotor transients in their recipient structures. In several studies, more complex events produced phasic responses, such as prolonged decreases in firing after orienting to the experimenter (Steinfels et al., 1983), and increases or decreases in firing rate to conditioned and unconditioned appetitive stimuli in Pavlovian and instrumental tasks (Miller et al., 1981). Whether these complex events were produced by purely sensory or motor stimuli, or were representative of higher order associations was unknown at the time.

In a series of subsequent experiments, phasic responses to stimuli appeared to follow a predictable pattern that diverged from purely sensory or motor coding. In well-trained monkeys, the presentation of a conditioned stimulus in an appetitive Pavlovian task increases the firing of dopamine neurons specifically to that conditioned stimulus more than the subsequent motor activation or motor response (Schultz et al., 1986). During retrieval of food reward, dopamine neurons' burst response to self-initiated grasping movements was contingent on the presence of food (Schultz and Romo, 1990). The absence

of food failed to produce the same response. In this example, the same sensorimotor program or stimulus of reaching to collect food had far less control over the firing of dopamine neurons than the presence of a food reward.

Further examination of these apparent departures from purely sensorimotor responses revealed several more reward-related features of dopamine neuron coding. Reward-predicting stimuli that generated orienting behavior prior to reward delivery would selectively induce burst firing of dopamine neurons compared with neutral stimuli, as would either unpredicted or randomly delivered rewards. During training however, as animals learned to anticipate rewards, habituation to reward delivery decreased reward responses in dopamine neurons (Ljungberg et al., 1992; Mirenowicz and Schultz, 1994). This process of burst suppression was observed to extend to predicted conditioned stimuli in second order conditioning, where the response to a predicted appetitive trigger stimulus decreased after it was preceded by another conditioned stimulus (Schultz et al., 1993). Omission of conditioned stimuli in second order conditioning recovered reward-related bursting in dopamine neurons that had previously been reduced (Pan et al., 2005), as this stimulus pattern no longer conformed to previous trial history.

Following the learning of a task, when reward responses in dopamine neurons were reduced, omission of expected rewards produced a decrease or pause in the tonic firing of dopamine neurons (Schultz et al., 1993; Schultz et al., 1997; Hollerman and Schultz, 1998). Expectation-based encoding of conditioned stimuli or rewards was sensitive to temporal deviations of stimulus delivery (Schultz et al., 1993; Hollerman and Schultz, 1998), with early or late stimuli eliciting a burst, while the expected delay produced no bursting. Despite working memory and attentional processes being required for these behaviors and

coding properties, dopamine neurons do not usually display increased activity between conditioned stimuli and rewards, indicating that their coding doesn't reflect these properties in real time. In tasks where increased delay period activity occurs, it appears to be due to uncertainty (Fiorillo et al., 2005).

Dopamine neurons are also observed to encode reward magnitude and reward prediction magnitude, such that larger rewards produced larger burst responses, and that stimuli predicting larger rewards produced larger burst responses (Tobler et al., 2005; Eshel et al., 2016). Smaller than expected reward delivery generate decreases in firing similar to reward omission (Tobler et al., 2005). These quantitative reward-related responses appear to reflect a weighted average of reward history (Bayer and Glimcher, 2005). This might reflect both quantitative coding or a motivational signal, however, as dopamine neurons' phasic responses to reward-predicting phasic stimuli correlate both with reward expectation and with reaction times (Sato et al., 2003).

In similar operant tasks, when observing dopamine release in terminal regions at high frequency by cyclic voltammetry, the response of extracellular dopamine levels to predicted and unpredicted reward-related stimuli retains similar prediction-based reward responses that occur in the somatic spiking of ventral midbrain dopamine neurons (Day et al., 2007; Hart et al., 2014; Saddoris et al., 2015; Hamid et al., 2016). As an extension, the effects of this coding for animals' learning and behavior likely occurs through dopamine neurons' targets in the dorsal and ventral striatum. The reward-predictive coding of phasically released dopamine was also observed to follow principles of delay discounting, in which value is reduced with increasing temporal delays (Ainslie, 1974). With increasing delays, phasic dopamine responses in the nucleus accumbens are reduced, to the point

where differences in phasic dopamine response to small and large rewards were eventually indistinguishable with long enough delay between a predictive conditioned stimulus and the reward itself (Day et al., 2010; Saddoris et al., 2015). Dopamine neurons did not display quantitative encoding of a cost-benefit relationship (Gan et al., 2010).

Thus, apart from the diverse types of observed sensorimotor responses, dopamine neurons quantitatively encode reward-associated stimuli that deviate from expected values, also known as reward prediction errors (RPE). However, dopamine neurons do not exclusively encode these types of conditioned events. Other conditioned and unconditioned stimuli, both appetitive and aversive, generate phasic responses in dopamine neurons that differ from the RPE valence and response type, across multiple timescales.

The relationship between dopaminergic coding and aversive stimuli remains less clear and responses to these events are more heterogeneous amongst dopamine neurons compared to that of appetitive stimuli. In some of the earliest observations, dopamine neurons appeared to segregate into those that were excited or inhibited by multiple types of noxious unconditioned stimuli (Chiodo et al., 1980). This segregation of dopamine neurons by response type has also been observed with conditioned aversive stimuli, with most dopamine neurons predictively encoding aversive stimuli by increases in firing similar that produced by appetitive conditioned stimuli, while a minority decrease their tonic firing rates (Matsumoto and Hikosaka, 2009). Dopamine neurons response types to aversive conditioned stimuli in this study reflected an anatomical organization, where the neurons increasing their firing to aversive events are more likely to be found in dorsal regions of the SNc, while those decreasing their firing to aversive events are more likely to be found in the ventral regions of the SNc (Matsumoto and Hikosaka, 2009). Despite

this observation, dopamine neurons seem to encode appetitive stimuli with greater phasic responses than aversive stimuli (Mirenowicz and Schultz, 1996), and other studies have failed to find a discrete segregation of dopamine neurons into two categories based on their responses to aversive events (Fiorillo et al., 2013), or a prediction error basis for the encoding of aversive events by the population of dopamine neurons (Fiorillo, 2013). Some of this diversity might be explained by the diversity of anatomical and intrinsic properties, and long term response to behavioral events of these neurons, particularly in the VTA (Lammel et al., 2008; Lammel et al., 2011). So while dopaminergic neurons phasically encode aversive events in a prediction-based manner, there are differences in the coding throughout the dopaminergic population, and the anatomical or other bases of these phenomena remain unknown. As a population dopamine neurons don't appear to have a dominant coding pattern for these type of events.

The phasic responses to behavioral stimuli observed by recording extracellular action potentials or extracellularly released dopamine last for hundreds of milliseconds, yet longer timescale responses of lower magnitude are also observable during behavior. Within its normal homeostatic range, tonic dopamine levels appear to display characteristic responses to behavioral events. Unpredictability of rewards generates a slow and moderate increase of dopamine neuron firing between conditioned stimuli and reward (Fiorillo et al., 2005). In the terminal structures of the dorsal and ventral striatum, extracellular dopamine increases during reward approach with respect to reward value and proximity (Howe et al., 2013), similar to the delay discounting observed for phasic coding, yet unrelated to predictability. And while still containing a prediction error signal, extracellular dopamine levels in the nucleus accumbens encode a temporally discounted prediction of future

reward over many rewarded and unrewarded trials (Hamid et al., 2016). Some of these changes in tonic coding may be region specific. In nucleus accumbens core, dopamine release has been observed to be mostly phasic and associated with reward prediction, while in the nucleus accumbens shell it displays longer lasting tonic responses during behavioral sequences that have been associated with incentive motivation (Saddoris et al., 2015).

Dopaminergic neurons generate several overlapping codes, including phasic responses to sensorimotor stimuli, as well as to conditioned and unconditioned appetitive and aversive stimuli, and slow tonic responses during behavioral sequences preceding expected rewards. However only the reward-related and predictive stimuli seem to follow a consistent pattern with respect to animals' learning and behavior, at least as far as they have been studied. The RPE coding of dopamine neurons strongly resembles the behavior of several learning algorithms generated to describe how behavioral conditioning occurs in animals.

A classic and influential learning theory introduced by Robert Rescorla and Allan Wagner, termed the Rescorla-Wagner model, described how conditioned stimuli become associated with unconditioned stimuli over many trials and produce conditioned responses (Rescorla and Wagner, 1972). In this model, association between a conditioned stimulus and an unconditioned stimulus is generated over multiple trials based on learning rates and expectation, to the point where the expectation of the unconditioned stimulus by the conditioned stimulus should be the same as the outcome. Importantly, in this model learning occurs when outcomes don't meet expectation. This theory accurately described behavioral conditioning in many paradigms, including blocking, but did not successfully describe all reinforcement learning phenomena, such as reinstatement. A subsequent

adaptation of this theory was introduced by Richard Sutton and Andrew Barto in the form of the temporal difference learning algorithm (TD) (Sutton and Barto, 1981). This model provided several benefits over the Rescorla-Wagner model for describing animal learning behavior, including an eligibility trace component  $\bar{x}$  which described temporal relationships between stimuli and a different treatment of conditioned and unconditioned stimuli that allowed for the model to describe second order conditioning (Sutton and Barto, 1990). In this model, prediction of events in a trial is accomplished by an adaptive element  $y - \bar{y}$ , which integrates and reports differences between predictions  $\bar{y}$ , and outcomes  $y$ , of events. Deviations from predicted outcomes then update predictive information about events or stimuli, such that over time a steady state of no prediction error occurs following many similar trials.

The prediction error coding of dopamine neurons was unsurprisingly observed to be similar to the  $y - \bar{y}$  component of the TD model (Schultz et al., 1997). If dopamine neurons' coding of RPE occurs in a similar manner to the TD model, dopamine neurons would be expected to resemble the characteristics of this component, namely that they not only encode prediction errors but also receive prediction information and update synaptic weights of inputs representing this predictive information. There is strong evidence that dopamine neurons satisfy the latter of these two criteria.

Dopamine receptors are metabotropic rather than ionotropic, in that release of dopamine in itself does not result in direct excitation or inhibition of recipient neurons. In the striatum, which receives the vast majority of ascending dopamine inputs, the recipient striatal spiny projection neurons (SPN) are composed of two primary types: direct pathway neurons targeting the SNr, which express the D1 dopamine receptor, and indirect pathway

neurons targeting the GP, which express the D2 dopamine receptor (Gerfen et al., 1990; Gong et al., 2003). The other isoforms D3, D4, and D5 are expressed at much lower levels. Activations of D1 receptors in direct pathway SPNs increase excitatory conductances of L-type voltage-gated calcium channels while reducing inhibitory conductances of potassium channels (Kitai and Surmeier, 1993; Surmeier et al., 1995; Galarraga et al., 1997). Activation of the D2 receptor in contrast has nearly the opposite effect in indirect pathway SPNs, decreasing excitatory conductances of L-type voltage-gated calcium channels and increasing inhibitory conductances of potassium channels (Kitai and Surmeier, 1993; Greif et al., 1995; Hernández-López et al., 2000; Olson et al., 2005). In addition to these effects on intrinsic excitability, D1 and D2 receptors again have opposing effects on postsynaptic excitability, with D1 activation in direct pathway neurons increasing NMDA receptor currents and postsynaptic trafficking (Cepeda et al., 1993; Levine et al., 1996; Hallett et al., 2006), while D2 activation in indirect pathway neurons decreases AMPA receptor currents (Cepeda et al., 1993; Hernández-Echeagaray et al., 2004).

Thus when dopamine levels increase either phasically or tonically, direct pathway neurons are expected to become more excitable and indirect pathway neurons are expected to become less excitable. Decreases in dopamine levels would be expected to produce the opposite effect. While the contributions of these various effects on intrinsic and postsynaptic excitability may explain the role of dopamine in normal behavior, Parkinson's disease, or the effects of pharmacological manipulations, this does not distinguish between the effect of dopamine receptor activation on the various contributions of dopamine to motor control, motivation, and reward learning.

Some of this ambiguity can be addressed using simplified preparations. In vitro and in vivo, the neural bases of learning and memory can be studied using the paradigms of long term potentiation (LTP), long term depression (LTD), and other various types (Bliss and Collinridge, 1993). In the acute slice preparation, plasticity-inducing stimulation of corticostriatal fibers in most cases produces LTD of postsynaptic responses. In an early observation of the contributions of dopamine to the synaptic basis of learning and memory, addition of dopamine to the extracellular solution was sufficient to reverse corticostriatal LTD to LTP (Wickens et al., 1996). Depletion of dopamine or D1 receptor antagonism was capable of preventing corticostriatal LTP (Kerr and Wickens, 2001). Spike-timing-dependent potentiation (STDP) of corticostriatal inputs was again observed to be D1 receptor sensitive, where D1 receptor antagonism generated spike-timing-dependent depression (STDD) of corticostriatal inputs (Pawlak and Kerr, 2008). And in vivo stimulation of ascending dopaminergic fibers in a pattern which produced intracranial self-stimulation (ICSS) was sufficient to potentiate corticostriatal postsynaptic responses in SPNs (Reynolds et al., 2001).

However, these earlier observations of dopamine's effects on synaptic potentiation and depression appear to hold true only for direct pathway neurons. For indirect pathway neurons, D2 receptor activation is observed to reverse STDP, resulting in postsynaptic depression, while D2 receptor inactivation reverses STDD. Plasticity of indirect pathway neurons was also modulated by A2a adenosine receptors. For direct pathway neurons, STDP was reversed by D1 receptor antagonism. Stimulation of D1 receptors or D2 receptors in slices from dopamine-depleted animals was sufficient to recover the normal

direction of either potentiation or depression for direct and indirect pathway neurons (Shen et al., 2008).

The effects of dopamine or dopamine receptor stimulation of postsynaptic plasticity are not only observed with bath application of agonists or antagonists. Pairing of optogenetically released dopamine combined with glutamate uncaging on SPN dendritic spines results in spike-timing dependent increases in spine head volume, in a manner which requires temporally close pairing of dopamine release with dendritic spine stimulation (Yagishita et al., 2014). Additionally, pairing optogenetically released dopamine with an odor-like burst from olfactory inputs to olfactory tubercle SPNs results in a D1 receptor-dependent potentiation (Wieland et al., 2015).

As simplified postsynaptic plasticity induction paradigms are by necessity artificial, additional evidence for the roles of dopamine in modulating postsynaptic plasticity comes from *ex vivo* examination of postsynaptic responses following learning. Following the acquisition of goal-directed actions, corticostriatal postsynaptic responses in D1-containing direct pathway neurons were increased and in D2-containing indirect pathway neurons were decreased (Shan et al., 2014). In this case the direction of postsynaptic plasticity is the same as that observed *in vitro* in these two pathways following dopamine receptor activation, which is assumed to occur during the learning of this task in the form of RPE coding and which may be responsible for it.

Although the earliest observations of Parkinson's patients, dopamine depletion or pharmacological antagonism generated support for theories about the role of dopamine in reward learning, motivation, or incentive salience, the role of different types of dopamine signaling for these processes could not be disambiguated, whether tonic, phasic, or for

specific types of behavioral events. One of the first tools that allowed for the selective investigation of the different effects of dopaminergic coding was the dopamine-deficient mouse. This mouse line was generated to have the rate-limiting dopamine synthetic enzyme tyrosine hydroxylase knocked out specifically in dopamine neurons, but not in norepinephrine neurons (Zhou and Palmiter, 1995). These mice displayed great deficits in movement and feeding several weeks after birth, which were reversible by L-DOPA but lethal in its absence. Consistent L-DOPA treatment allowed these mice to feed, drink and survive similar to littermates. Viral rescue of dopamine synthesis in the striatum was sufficient to restore feeding behavior in these mice (Szczycka et al., 2001).

Under regular administration of L-DOPA, dopamine-deficient mice displayed preference for sucrose over water similar to normal mice, but following long term removal of L-DOPA these mice were less likely to generate sucrose-seeking behavior, despite displaying the preference (Cannon and Palmiter, 2003). These mice were also capable of learning reward-based associations in conditioning tasks, but were only capable of correctly executing them in the presence of dopamine (Robinson et al., 2005). Taken together, these observations support the notion of dopamine being essential for motivation but not necessary for reward learning.

Yet in the context of this transgenic model, it is unknown whether tonic or phasic dopamine generates these motivational behaviors, or whether these two distinct types of signaling display different behavioral properties at all. Tonic elevation of dopamine levels in a transgenic model in which expression of the dopamine transporter was knocked down had the effect of increasing motivation for food, while reward learning was unaffected (Cagniard et al., 2006). This observation taken together with the results from the dopamine

deficient mice support the theory that tonic dopamine influences motivation while phasic dopamine influences reinforcement learning.

One subsequent model which clarified this issue is the cell type specific knockout of the essential NMDA receptor subunit NR1 in dopamine neurons. In these mice, lack of functional NMDA receptors in dopamine neurons generated a deficit of burst firing of dopamine neurons while tonic firing was unaffected. These mice displayed selective deficits in cued reward learning, but not motivation to work for rewards (Zweifel et al., 2009), in contrast to the observed effects of manipulating tonic dopamine levels.

Multiple studies using optogenetic stimulation of dopamine neurons demonstrate that phasic release of dopamine has profound consequences for reward learning. Phasic stimulation of VTA dopamine neurons on its own was able to generate conditioned place preference, while tonic stimulation was not (Tsai et al., 2009). Furthermore phasic stimulation of dopaminergic neurons even when not paired with any reward was sufficient to generate operant behavior (Kim et al., 2012). In these examples even in the absence of a primary reinforcer, dopamine was capable of inducing behavioral conditioning.

Optogenetic dopamine transients paired with behavioral stimuli after task learning has the effect of changing the expected patterns of reinforcement learning in the tasks used. Phasic dopamine release is capable of recovering the conditioning to a normally blocked stimulus and impairing the typical behavioral responses to reward value decrement and extinction (Steinberg et al., 2013), as well as increasing behaviorally-measured associations between cues (Sharpe et al., 2017). In both of these examples, in behavioral states in which reward-related dopamine transients were likely either reduced or absent, introduction of them had profound consequences for reinforcement learning which

deviated from both theoretical expectations and observed outcomes. Phasic reduction of dopamine is similarly capable of influencing reinforcement learning patterns as phasic dopamine release. Brief optogenetic inhibition of dopamine neurons during the time of reward delivery decreased animals' future responses to cues predicting that reward (Chang et al., 2016).

Synthesizing this series of studies we can confidently say that increases or decreases of tonic dopamine levels have consequences for motivation, while disruption of normal phasic dopamine coding selectively affects appetitive reinforcement learning. Thus, dopamine neurons are well-situated to phasically encode RPE to behavioral stimuli, and these phasic signals modulate synaptic plasticity and affect reward learning. If these functions are similarly accomplished as in the TD model, we expect that examination of afferent inputs to dopamine neurons would reveal circuits responsible for generating these signals.

### **On the circuit mechanisms of RPE coding in dopaminergic neurons**

If the reward prediction coding of dopamine neurons is responsible for influencing synaptic plasticity and learning, and the mechanism of RPE coding resembles the TD model, then the identity of some of the inputs responsible for certain phasic responses can be inferred. Specific excitatory and/or disinhibitory inputs representing outcome should arrive at the time of reward to produce a burst in dopamine neurons, performing the function of the  $y$  component of the TD model. Specific inhibitory inputs performing the function of the  $\bar{y}$  component of the TD model should encode the prediction of reward events that either

balances, shunts, or presynaptically inhibits the input representing outcome, or  $y$ . Such a system would allow for the RPE and reward magnitude coding of dopaminergic neurons.

The identity of these relevant inputs remains mostly unknown. For the  $y$  component, inputs representing outcome may arrive from circuits encoding innate information about specific reward modalities such as thirst, hunger and reproduction. Higher order outcome information may originate elsewhere, in the case of social rewards or sensory cues based on higher order conditioning. For the  $\bar{y}$  component, inputs representing prediction are expected to provide inhibitory input, but also must receive dopaminergic input either monosynaptically or multisynaptically to redistribute synaptic weight and update prediction representations.

From the basis of this information several criteria can be expected from the source of this prediction signal, whether or not comprised of a single cellular identity. First, to reduce the burst-firing of dopamine neurons to predicted stimuli, the prediction source must be inhibitory. Secondly, to redistribute synaptic weights representing predictive information it must receive dopamine input and undergo synaptic plasticity in a dopamine-dependent manner. Lastly, the prediction source must represent reward prediction within the same time interval in which outcome information arrives.

Before identifying candidate sources of this prediction signal, the heterogeneity amongst dopamine neurons must be acknowledged. Although the majority of recorded dopamine neurons display RPE coding (Eshel et al., 2016; Schultz et al., 1993; Matsumoto and Hikosaka, 2009), significant heterogeneity exists for their intrinsic properties, efferent targets and coding properties, particularly for the VTA (Lammel et al., 2008; Lammel et al., 2011). In addition, the VTA and SNc have notable differences amongst their afferent

inputs, (Yetnikoff et al., 2014; Watabe-Uchida et al., 2012), and may have different cellular sources for the prediction input. Because of these differences, the remainder of this exploratory exercise concerns the SNc exclusively. For the SNc, putative inhibitory structures which may provide the prediction signal include the dorsal striatum, GP, SNr, the central amygdala, and the rostromedial tegmental nucleus (RMTg). The first three basal ganglia structures have ventral analogues which likely perform similar roles for the VTA, and the last structure projects to both the VTA and SNc (Jhou et al., 2009).

Amongst these, little evidence has been provided for their influence on dopaminergic encoding of RPE except for the RMTg. First identified as a GABAergic structure immediately posterior to the VTA, it receives input from the lateral habenula (LHb) through the fasciculus retroflexus and provides strong inhibitory input to midbrain dopamine neurons (Jhou et al., 2009; Kaufling et al., 2009; Matsui and Williams, 2011). Although the lateral habenula projects to some dopaminergic neurons in the VTA (Omelchenko et al., 2009), its control over the dopaminergic midbrain is thought to occur primarily through its projection to the RMTg. The lateral habenula appears to encode a similar RPE signal to that of dopamine neurons, but with an inverse valence (Bromberg-Martin and Hikosaka 2011). Since the lateral habenula neurons are glutamatergic, the inhibitory effect of the LHb over dopaminergic neurons has been demonstrated to be mediated disynaptically through the GABAergic RMTg, which displays similar RPE coding to the LHb (Jhou et al., 2009; Hong et al., 2011; Balcita-Pedicino et al., 2011; Brown et al., 2017). Lesioning of the lateral habenula reduced the magnitude of dopaminergic coding of RPE to reward-predictive cues, rewards, and reward omissions,

but did not affect the prediction-based coding of dopamine neurons to aversive stimuli (Tian and Uchida, 2015).

If the lateral habenula-RMTg circuit displays RPE coding, by the description of the TD model it is expected to be part of the  $y - \bar{y}$  component of the model, contributing to the RPE coding of these neurons by indirectly inhibiting and disinhibiting dopamine neurons. By inference the lateral habenula must also receive prediction and outcome information from other sources. Sources of prediction or outcome input to the lateral habenula could arrive from cortical regions through the stria medullaris, or could arrive from the basal forebrain, the lateral hypothalamus, or the entopeduncular nucleus (EP)/GP internal segment (GPi) (Herkenham and Nauta, 1977). The EP at least appears to encode either outcome or prediction errors similarly to the lateral habenula (Stephenson-Jones et al., 2016), so would not be the source for either of these types of input.

The contribution of the central amygdala (CeA) to the coding of dopaminergic neurons is unknown. The CeA provides inhibitory input to all regions of the dopaminergic midbrain (Price and Amaral, 1981; Gonzalez and Chesselet, 1990; Fudge and Haber, 2000; Watabe-Uchida et al., 2012), and also receives dopaminergic inputs (Freedman and Cassell, 1994). Although in the latter case, CeA only receives moderate innervation from most of the dopaminergic midbrain, with the majority of CeA-projecting dopamine neurons residing in certain VTA subregions and the periaqueductal gray (Hasue and Shammah-Lagnado, 2002; Lammel et al., 2008). This anatomical specificity would imply that the phasic coding of the majority of dopamine neurons would not be responsible for updating their own suppression as expected from the TD model, if the source of it were the CeA. This information, combined with the known coding properties of the CeA (Calu et al., 2010;

Ciocchi et al., 2010; Duvarci et al., 2011), casts the CeA as a dubious fit for the prediction signal.

The GP and SNr are possible candidates, fitting most of the criteria listed above, yet as spiny neurons little is known about their synaptic plasticity and its dopamine-dependence. Importantly, these regions receive the majority of their input from the last candidate region, the dorsal striatum, which also fits the criteria listed above, and is better suited to redistribute synaptic weight in a dopamine-dependent manner. Thus, any prediction coding of the GP and SNr would be expected to be under strong control from the dorsal striatum. Out of the structures explored, this last one provides the best candidate for providing dopaminergic neurons with a prediction signal which can be updated by dopamine-dependent synaptic plasticity.

The dorsal striatum exhibits the greatest levels of dopamine in the brain and the synaptic plasticity of its projection neurons are heavily modulated by it. Out of all the explored structures, the dorsal striatum alone exhibits a strong dopamine-dependent synaptic plasticity, and thus is the only one to fit that requirement of the  $\bar{y}$  component to update representations of prediction in a dopamine-dependent manner. This anatomical and physiological difference equips it with a distinct advantage over the other candidate structures. For the SNc, the vast majority of anatomical inputs originate from the dorsal striatum (Yetnikoff et al., 2014; Watabe-Uchida et al., 2012). As for the last criteria, many striatal SPNs are observed to be phasically active around the time of reward (Jog et al., 1999; Schmitzer-Torbert and Redish, 2004; Gage et al., 2010). These reward-related responses are acquired during task learning (Jog et al., 1999), during which dopamine neurons are reducing their reward-related responses (Hollerman et al., 1998). In this

hypothetical scenario reward-related dopamine transients would induce synaptic plasticity in striatal SPNs, some of which acquire or increase reward-related responses, and if they project to dopamine neurons gradually reduce reward-related dopamine transients until a steady state is reached in the coding of both cell populations.

### **The patch compartment of the dorsal striatum**

Amongst dorsal striatal SPNs, there are at least two overlapping dichotomies of cell type. First, as described earlier, SPNs are segregated by dopamine receptor type and efferent target, where direct pathway SPNs targeting the SNr express the D1 dopamine receptor and the neuropeptide substance P, and indirect pathway SPNs targeting the GP express the D2 dopamine receptor and the neuropeptide enkephalin (Gerfen et al., 1990; Gong et al., 2003). Additionally, there is another dichotomy of cell type with both gross anatomical differences as well as afferent and efferent target differences.

This dichotomy was first observed as clusters of dense opiate receptor staining in the caudate putamen termed patches (Pert et al., 1976), which also received no input from parafascicular thalamus and exhibited lower acetylcholinesterase (AChE) staining (Graybiel and Ragsdale, 1978; Herkenham and Pert, 1981). These patches were observed to receive different inputs from the surrounding matrix and project to different regions of the substantia nigra, with the matrix projecting to the substantia nigra pars reticulata and the patch projecting to the substantia nigra pars compacta (Gerfen, 1984; Gerfen, 1985). Although the ventral striatum displays different expression patterns for the markers of dorsal patch and matrix, distinct subregions or cell groups within the ventral striatum appear to target VTA dopaminergic neurons selectively, perhaps constituting a ventral

analog of the dorsal striatal patches (Watabe-Uchida et al., 2012).

In one of these first studies, prelimbic cortex was observed to project selectively to the patches, while motor and sensory cortices were observed to project selectively to the matrix (Gerfen, 1984). This pattern has been observed to be segregated more by cortical layers than cortical areas, with cortical layers 2, 3, and the superficial layer of 5 (5a) projecting to the matrix and the deep cortical layer of 5 (5b), and layer 6 projecting to the patches (Gerfen, 1989; Kincaid and Wilson, 1996). The exception to this rule appears to be the somatosensory cortex, which doesn't project to the patches (Kincaid and Wilson, 1996; Flaherty and Graybiel, 1994). In higher mammals some cortical areas appear to preferentially target patches (Ragsdale and Graybiel, 1990; Eblen and Graybiel, 1995). Neostriatal patch and matrix compartments also receive different dopaminergic inputs from the SNc, with the matrix receiving primarily dorsal tier input and the patch ventral tier input (Gerfen et al., 1987; Gerfen et al., 1987; Prensa and Parent, 2001).

Both patch and matrix compartments contain both striatonigral and striatopallidal neurons (Gerfen and Young, 1988), however their innervation of efferent targets differs between patch and matrix neurons. Patch striatonigral neurons innervate all downstream basal ganglia nuclei innervated by the matrix, but display less innervation of the GP and SNr while greater innervation of the EP and exclusive innervation of the SNc (Fujiyama et al., 2011). Patch axons heavily target the ventral dendrites and ventral tier of SNc dopaminergic neurons, while matrix axons avoid them and target the SNr (Crittenden et al., 2016). Both patch and matrix striatopallidal neurons exclusively innervate the GP. Patch and matrix innervation of the EP is segregated along a rostrocaudal axis, where the patch preferentially innervates the rostral pole and the matrix the caudal pole of the EP

(Rajakumar et al., 1993). The rostral pole of the EP receiving patch input projects to the LHb (Stephenson-Jones et al., 2016).

Within the EP, there are two different classes of projection neurons targeting the LHb, one exclusively providing mixed glutamatergic and GABAergic input to the LHb and another targeting both the LHb and the thalamus that provides glutamatergic input to the LHb (Wallace et al., 2017). Both of these populations appear to be mostly targeted by patch neurons rather than matrix neurons, whereas other populations of EP neurons that do not target the LHb appear to receive predominantly matrix input. This disynaptic targeting of the LHb by patch neurons may have consequences for the control of dopaminergic neuronal coding by the LHb.

In addition to differences in opioid receptor and AChE expression, the matrix displays increased expression of the calcium binding protein calbindin compared to the patches (Gerfen et al., 1985). The patch and matrix calbindin expression patterns and the patch innervation of midbrain dopaminergic neurons and LHb-projecting GP appear to be conserved in evolutionary biology back to the lamprey (Stephenson-Jones et al., 2013). This conservation likely indicates an essential role of this circuit in vertebrates. Given the specific anatomical niche that patch SPNs operate within, and the smaller number of synapses between Patch SPNs and SNc dopaminergic neurons than matrix SPNs and SNc dopaminergic neurons, they appear to be the candidate most likely to provide a prediction signal to dopaminergic neurons necessary for successful RPE coding.

### **GABAergic transmission by midbrain dopaminergic neurons**

The role of dopaminergic neurons in transmitting dopamine to the forebrain and their influence over their downstream targets in the dorsal and ventral striatum described in these earlier sections relies on the assumption that dopaminergic neurons are indeed primarily accomplishing this by transmitting dopamine. This normally straightforward assumption based on decades of work has recently been challenged, following in vitro evidence that dopaminergic terminals co-release both glutamate and/or GABA (Tecuapetla et al., 2010; Tritsch et al., 2012). Compared to the weak effects of dopamine on the intrinsic membrane properties of SPNs, strong GABAergic inhibition would be much more likely to transmit any phasic signals of dopaminergic signaling, if this was their predominant method of neurotransmission. If we assume that this GABAergic co-transmission occurs similarly in vivo as it is observed in vitro, and that it displays fast synaptic recovery, then this would completely disrupt the model of dopaminergic neurons functioning in a TD model-like circuit and recruiting their own prediction-based inhibition by dopamine-dependent synaptic plasticity. This would render the foundational hypotheses of this thesis void, and require a complete reassessment of how the dorsal striatal patches might be organized into the information processing circuits of the basal ganglia.

GABAergic transmission from SNc terminals has also been credited to the phasic behavioral responses of striatal cholinergic interneurons (Nelson et al., 2014). Cholinergic interneurons (CINs) are the only known intrinsic source of excitation within the striatum, providing nicotinic input to a subset of striatal interneurons and nigrostriatal terminals (Sullivan et al., 2008; English et al., 2012; Threlfell et al., 2012; Cachepe et al., 2012). They have also been observed to provide a disynaptic GABAergic inhibition of striatal

SPNs which has been attributed to both striatal interneurons and nigrostriatal terminals (English et al., 2012; Nelson et al., 2014). As the optogenetic stimulation of CINs is sufficient to elicit phasic dopamine release in vitro (Threlfell et al., 2012; Cachope et al., 2012), the identification of the intervening source of cholinergic-induced inhibition of SPNs would do much to satisfy questions about whether SNc dopaminergic neurons primarily influence their downstream targets by releasing dopamine or GABA.

### **Striatal GABAergic interneuron identity and circuitry**

Apart from the CINs, all other known striatal interneurons are GABAergic. These GABAergic interneurons were first identified as aspiny neurons exhibiting greater uptake of tritiated GABA (Bolam et al., 1983), and greater expression of glutamate decarboxylase (GAD) than SPNs (Bolam et al., 1985). Striatal GABAergic interneurons were also observed to selectively express a number of different proteins including somatostatin, parvalbumin (PV), and calretinin (Vincent and Johansson, 1983; Chesselet and Graybiel, 1986; Cowan et al., 1990; Kita et al., 1990; Bennett and Bolam, 1993). A combination of differences in expression patterns, morphology, and intrinsic properties typified the three classical types of striatal interneurons, these being the PV-expressing fast-spiking interneuron (FSI), the CIN, and the plateau-potential exhibiting low-threshold spike (PLTS) interneurons, which express somatostatin, nitric oxide synthase, and neuropeptide-Y (NPY) (Kawaguchi, 1993). More recently, a number of other striatal interneurons have been identified which do not conform to the characteristics of these initial three types, including tyrosine hydroxylase-expressing interneurons (THINs), NPY-expressing neurogliaform interneurons (NPY-NGFs), and neurons targeted in the 5HT3a-EGFP mouse line (Ibáñez-

Sandoval et al., 2010; Ibáñez-Sandoval et al., 2011; Muñoz-Manchado et al., 2014). Interestingly, most of these more recently-discovered interneurons do not express any known markers of striatal or cortical interneurons.

FSIs and PLTS interneurons display a common circuitry with respect to their afferent and efferent targets. FSIs receive excitatory input from cortex and intralaminar thalamus (Ramanathan et al., 2002; Sidibé and Smith, 1999; Rudkin and Sadikot, 1999), and provide strong inhibition to SPNs (Koós and Tepper, 1999). PLTS interneurons also receive excitatory cortical input (Vuillet et al., 1989), and also provide inhibitory input to SPNs (Gittis et al., 2010; Straub et al., 2016), but their excitation by cortical stimulation is weaker than that of FSIs (Gittis et al., 2010), and their innervation of SPNs is dendritic rather than perisomatic (Straub et al., 2016). Nonetheless, this type of circuit organization, at least with respect to the FSI, constitutes feed-forward inhibition, as FSIs and their synaptic target, the SPNs, are both excited by the same cortical input.

However, amongst the other classes of striatal interneurons, another type of circuitry has been revealed. THINs and NPY-NGFs receive nicotinic excitation (English et al., 2012; Luo et al., 2013; Ibáñez-Sandoval et al., 2015), and for the NPY-NGF, the source of this input has been confirmed to be CINs (English et al., 2012). Thus it is possible that THINs, and perhaps as of yet unidentified striatal interneurons (Sullivan et al., 2008), might also be driven by this source. This semiautonomous circuitry of intrastriatal excitation of GABAergic interneurons, rather than cortical excitation, may underlie the influence of CINs in the striatum rather than through cholinergic-mediated nigrostriatal GABA release.

## CHAPTER 2:

# Novel Fast Adapting Interneurons Mediate Cholinergic-Induced Fast GABA<sub>A</sub> Inhibitory Postsynaptic Currents in Striatal Spiny Neurons

Thomas W. Faust, Maxime Assous, Fulva Shah, James M. Tepper and Tibor Koós  
Center for Molecular and Behavioral Neuroscience, Rutgers, the State University of New  
Jersey, 197 University Avenue, Newark, NJ 07102, USA

Published in:

Faust TW, Assous M, Shah F, Tepper JM, Koós T (2015) Novel fast adapting  
interneurons mediate cholinergic-induced fast GABA<sub>A</sub> inhibitory postsynaptic currents  
in striatal spiny neurons. *Eur J Neurosci* 42:1764–1774.

## Abstract

Previous work suggests that neostriatal cholinergic interneurons control the activity of several classes of GABAergic interneurons through fast nicotinic receptor-mediated synaptic inputs. Although indirect evidence has suggested the existence of several classes of interneurons controlled by this mechanism, only one such cell type, the neuropeptide-Y-expressing neurogliaform neuron, has been identified to date. Here we tested the hypothesis that in addition to the neurogliaform neurons that elicit slow GABAergic inhibitory responses, another interneuron type exists in the striatum that receives strong nicotinic cholinergic input and elicits conventional fast GABAergic synaptic responses in projection neurons. We obtained in vitro slice recordings from double transgenic mice in which Channelrhodopsin-2 was natively expressed in cholinergic neurons and a population of serotonin receptor-3a-Cre-expressing GABAergic interneurons were visualized with tdTomato. We show that among the targeted GABAergic interneurons a novel type of interneuron, termed the fast-adapting interneuron, can be identified that is distinct from previously known interneurons based on immunocytochemical and electrophysiological criteria. We show using optogenetic activation of cholinergic inputs that fast-adapting interneurons receive a powerful supra-threshold nicotinic cholinergic input in vitro. Moreover, fast adapting neurons are densely connected to projection neurons and elicit fast, GABA<sub>A</sub> receptor-mediated inhibitory postsynaptic current responses. The nicotinic receptor-mediated activation of fast-adapting interneurons may constitute an important mechanism through which cholinergic interneurons control the activity of projection neurons and perhaps the plasticity of their synaptic inputs when animals encounter reinforcing or otherwise salient stimuli.

## Introduction

The recent introduction of transgenic reporter methods into the study of striatal circuits has not only led to the discovery of several new classes of striatal GABAergic interneurons but also revealed important and unexpected features of their circuit organization. Of particular interest, direct and indirect evidence now indicates that a subset of GABAergic interneurons receives a powerful nicotinic excitatory synaptic input. This phenomenon, first inferred from evidence showing recurrent inhibition in cholinergic interneurons (Sullivan et al., 2008) and later confirmed and extended using paired recordings and optogenetics (English et al., 2012), suggests that contrary to the prevailing view some striatal GABAergic interneurons may not be driven exclusively by the cortical and thalamic inputs that they share with the main projection neuron population, but to a significant degree by intrastriatal and perhaps extrastriatal cholinergic inputs. This observation, together with the existence of feedback inhibition of cholinergic [choline-acetyltransferase-expressing (ChAT)] interneurons and the selective electrotonic and synaptic connectivity of different GABAergic interneurons, suggests that the function of interneurons may not be limited to the currently envisaged feed-forward gating of cortical and thalamic excitation of projection neurons. Instead, the interconnected ChAT and GABAergic interneurons may transmit afferent signals that are not directly received by projection neurons and integrate them with other striatal inputs through the emergent dynamics of their circuitry. The picture of a complex and perhaps semi-autonomous network of ChAT and GABAergic interneurons provides impetus for more detailed characterization of this circuitry, with particular emphasis on the number, intrinsic properties and connectivity of neurons that receive significant nicotinic synaptic inputs. To

date, only one such GABAergic interneuron, the neuropeptide-Y-expressing neurogliaform (NPY-NGF) neuron has been identified (Ibáñez-Sandoval et al., 2011; English et al., 2012). Indirect evidence however suggests that other interneurons may also be activated by nicotinic synaptic inputs. The existence of one of these putative interneurons was inferred from experiments where multiphasic disynaptic GABAergic inhibitory postsynaptic currents (IPSCs) were elicited in sympathetic preganglionic neurons (SPNs) with synchronous optogenetic activation of ChAT interneurons (English et al., 2012). This study suggested that a conventional fast GABAergic IPSC component of the compound response in SPNs may originate from a type of neuron that is distinct from the NPY-NGF interneuron. Alternatively, however, part or perhaps all of this inhibitory response may arise from axon terminals of extrastriatal afferent neurons that express presynaptic nicotinic receptors, as shown for dopaminergic inputs by Nelson et al. (2014). Here we tested the hypothesis that there exists a population of striatal GABAergic interneurons that mediate fast synaptic inhibition of SPNs in response to cholinergic excitatory signals.

## Materials and Methods

### **Animals**

All procedures used in this study were performed in agreement with the National Institutes of Health Guide to the Care and Use of Laboratory Animals and with the approval of the Rutgers University Institutional Animal Care and Use Committee. HTR3a-Cre mice (Tg(HTR3a-Cre)NO152Gsat/Mmucd, University of Davis) (Gerfen et al. 2013), ChAT-ChR2 mice (Tg(Chat-COP4\*H134R/EYFP,Slc18a3) 6Gfng/J; Jackson Labs, Bar Harbor, MA,

USA) and double transgenic mice (ChAT-ChR2-EYFP;HT3Ra-Cre) were generated and maintained as hemizygotic. Mice were housed in groups of up to four per cage and maintained on a 12-h light cycle (07:00–19:00 h) with ad libitum access to food and water. In total, 45 mice were used, including both males and females.

### **Intracerebral viral injection**

Mice were injected with recombinant, replication incompetent serotype-5 Adenovirus-associated virus vector (rAAV2/5) carrying an expression cassette consisting of double-floxed, inverted open reading frame coding sequences (CDS) for ChR2-(H134R)-eYFP or tdTomato under the respective control of EF1a or CAG promoters and, downstream of the CDS, a woodchuck hepatitis post-transcriptional regulatory element (WPRE) and a human growth hormone poly-adenylation (hGA) sequence. Virus stock was obtained from the University of North Carolina Vector Core Services (Chapel Hill, NC, USA). The surgery and viral injection took place inside a Biosafety Level-2 isolation hood. Mice were anesthetized with isofluorane (1.5–3%, delivered with O<sub>2</sub>, 1 L/min) and placed within a stereotaxic frame. A single dose of enrofloxacin (Baytril), 10 mg/kg, s.c., was given to prevent infections. Bupivacaine was used as a local anesthetic at the site of surgery. A single craniotomy was made at coordinates +0.74 mm anterior and 1.6–1.8 mm lateral to Bregma. Then, 0.6 µL of virus suspension ( $> 10^{13}$  viral genomes/mL titer) was delivered by glass pipette to three sites 1.75, 2.25 and 3.6 mm ventral to the brain surface, for a total volume of 1.8 µL. Virus was injected at 0.92 nL/s, after which the pipette was left in place for 10 min before being slowly retracted. During postsurgical recovery mice were kept under Biosafety level-2 confinement for 5 days and analgesia was provided for the first 3 days with 0.1 mg/kg buprenorphine, s.c. (at every 12 h) and ketoprofen s.c. (5 mg/kg daily).

Expression of viral transgene was allowed for at least 2 weeks before animals were used for experiments.

### **Immunocytochemistry**

Mice were deeply anesthetized with 150/25 mg/kg ketamine/xylazine, i.p. Brain tissue was fixed by transcardial perfusion of 10 mL of ice-cold artificial cerebrospinal fluid (adjusted to pH 7.2–7.4), followed by perfusion of 90–100 mL of 4% (w/v) paraformaldehyde, 15% (v/v) picric acid in phosphate buffer. Brains were post-fixed overnight in the same fixative solution. Sections 50–60  $\mu$ m thick were cut on a Vibratome 3000. Sections were cleaned with 10% (v/v) methanol, 3% (v/v) hydrogen peroxide in phosphate-buffered saline (PBS), followed by 1% (w/v) sodium borohydride in PBS. Sections were blocked in 10% (v/v) normal donkey serum, 3% (w/v) bovine serum albumin and 0.5% (v/v) Triton X-100 in PBS overnight at 4 °C. Alternating serial sections were incubated for 24 h at room temperature in the following primary antibodies and at the following concentrations: rabbit anti-parvalbumin (PV) (catalog #24428; Immunostar, Hudson, WI, USA) 1 : 1500, rabbit anti-calretinin (CR) (catalog #24445; Immunostar) 1 : 1500, goat anti-nitric oxide synthase (NOS) (catalog #Ab1376; Abcam, Cambridge, MA, USA) 1 : 1000, rabbit anti-neuropeptide-Y (NPY) (catalog #Ab30914; Abcam). Sections were incubated in the following secondary antibodies, raised in donkey, overnight at 4 °C: 1 : 400 (NOS) anti-goat Alexa Fluor® 594 (catalog #A-11058; Life Technologies, Carlsbad, CA, USA), 1 : 400 (PV, CR) anti-rabbit Alexa Fluor® 594 (catalog #A-11032; Life Technologies) and 1 : 500 (NPY) anti-rabbit Alexa Fluor® 594. In one case where tdTomato virus was injected, the tissue was processed in 1 : 1500 rabbit anti-tyrosine hydroxylase (TH) (catalog #ab152; Millipore, Billerica, MA, USA) primary antibody and its respective 1 : 300 donkey anti-

rabbit Alexa Fluor® 488 (catalog #A-21206; Life Technologies) secondary antibody. Immunocytochemical detection of TH in striatal interneurons requires prior 6-OHDA-mediated lesioning of the nigrostriatal dopaminergic projection, which was conducted as described by Ünal et al. (2013). Sections were mounted in Vectashield (Vector Labs, Burlingame, CA, USA).

### **Slice preparation and visualized in vitro whole cell recording**

Mice aged 3–7 months were deeply anesthetized with 150/25 mg/kg ketamine/xylazine, i.p., prior to surgery. Acute brain slices were prepared as previously described (Tecuapetla et al., 2009), with the following exceptions. Mice were transcardially perfused with ice cold or partially frozen N-methyl-D-glucamine (NMDG)-based solution consisting of following (in mM): 103.0 NMDG, 2.5 KCl, 1.2 NaH<sub>2</sub>PO<sub>4</sub>, 30.0 NaHCO<sub>3</sub>, 20.0 HEPES, 25.0 glucose, 101.0 HCl, 10.0 MgSO<sub>4</sub>, 2.0 thiourea, 3.0 sodium pyruvate, 12.0 N-acetyl cysteine, 0.5 CaCl<sub>2</sub> (saturated with 95% O<sub>2</sub>/5% CO<sub>2</sub>, measured to be 300–310 mOsm and 7.2–7.4 pH). Following slice preparation, slices were allowed to recover in well-oxygenated NMDG-based solution at 35 °C for an additional 5 min, after which they were transferred to well-oxygenated normal Ringer solution at 25 °C until placed in the recording chamber constantly perfused with oxygenated Ringer solution at 32–34 °C. We recorded SPNs in voltage clamp using a CsCl-based internal solution (Tecuapetla et al., 2009). This solution also contained 0.2% (w/v) Alexa Fluor® 594, used to fill and visually verify the identity of SPNs. All other neurons were recorded with normal internal solution.

Instrumentation, voltage-clamp parameters and other aspects of fluorescence-guided visualized whole-cell recording were the same as described by Tecuapetla et al.

(2009).

Optogenetic stimulation in vitro consisted of 1- to 2-ms blue light pulses (1.25 mW/mm<sup>2</sup>) delivered from an LED coupled to a 200- $\mu$ m multimode optical fiber placed at  $\sim 45^\circ$  above the slice aiming at the recorded neurons, or by wide field illumination using a high-power (750-mW) LED ( $> 5$  mW/mm<sup>2</sup> illumination intensity). Optogenetic pulses were delivered at 30- or 60-s intervals.

For the testing of synaptic transmission, 50-Hz trains (10 spikes) were elicited in the presynaptic cell with short current pulses. Trains were delivered at 30-s intervals.

### **Data analysis**

As fast-adapting interneurons (FAIs) were recognized based on subjective classification of cells, we first used unsupervised clustering to examine if these neurons could be identified in an unbiased manner among the cells exhibiting novel characteristics. As FSIs and NPY-NGFs have been previously characterized and encountered in other transgenic lines, they were excluded from clustering analysis. These cells were positively identified based on several defining intrinsic properties such as a fast spike waveform with a single fast afterhyperpolarization (AHP) for the fast-spiking interneuron (FSI), whereas NPY-NGFs exhibited a single slow AHP. FAIs and all other unclassified cells submitted for clustering exhibited both fast and slow AHPs at or close to rheobase (see Figs 2C and D, 3B, and 5C), demonstrating their difference from the other two cell types in this example. The most salient difference between FAIs and other novel cells was that all the other novel cells rapidly entered depolarization block. To use this property for classification we chose two quantitative metrics that capture interrelated but distinct aspects of how the firing of action

potentials depends on somatically injected current amplitude (Fig. 2F). The first, more straightforward one is the steepness of the current–firing frequency relationship. The second is the degree to which the cells are liable to depolarization block at higher current amplitudes. Depolarization block directly affects the total number of spikes fired during current injection in a manner that often reduces rather than increases the number of spikes with increasing current amplitudes above the level where depolarization block first develops. As a result the relationship between the injected current and the total number of spikes per episode is not monotonic but U-shaped and the increasing tendency for depolarization block results in an increasing deviation from a linear relationship between injected current and the number of elicited spikes. To capture quantitatively the degree of deviation from linearity we used linear regression to compute the coefficient of determination ( $r^2$ ) for each cell's current spike–frequency relationship. (Note that application of the linear regression to U-shaped current–frequency relationships explains the negative slope values found for several neurons, Fig. 2F.) Next, the current–frequency relationships were transformed for each cell into a 2D vector, with one dimension representing the slope of the linear fit to the spike–frequency relationship and the second dimension corresponding to the coefficient of determination for the computed fit. These vectors are plotted in the plane of the corresponding dimensions in Fig. 2F. Next we used a K-means clustering algorithm implemented in Matlab (Mathworks, Natick, MA, USA) with the number of groups chosen to be four based on an estimation of the optimal group number by the evalclusters algorithm of Matlab. One group, comprising 25 neurons that followed a near linear current–frequency function (high  $r^2$ ) and high, positive slope values could be isolated as a distinct cluster in this distribution. The Mahalanobis distances from

each of the vectors in this group to the center of the distribution were  $> 17$ . This group corresponded to the cells subjectively classified as FAI based on their rapidly developing spike frequency adaptation.

Despite the fact that the remaining 43 neurons were clustered into three separate groups by the K-means algorithm, the majority of these cells' current–frequency functions were not linear, and therefore we considered their treatment as separate groups on this basis to be ill-conceived. More specifically, because completely different non-linear functions can yield the same  $r^2$  value if a linear fit is forced to the data, a small difference in this metric is not a reliable indicator of electrophysiological similarity. We emphasize, however, that this is not a concern for reliable discrimination of approximately linear relationships from non-linear ones as high  $r^2$  requires linearity. For these reasons we identified only two distinct cell groups based on the cluster analysis, the FAI and the non-FAI groups, and post hoc statistical comparisons was performed between these two groups as described in the text. Regression analysis and statistics were performed with Origin (Originlab, Northampton, MA, USA). Population data are expressed as mean  $\pm$  SD unless otherwise indicated.

## Results

To identify GABAergic interneurons that receive nicotinic synaptic inputs our strategy was to generate double transgenic mice in which ChAT neurons natively express Chr2-eYFP and different types of candidate GABAergic interneurons express Cre-recombinase, in turn to be used for selective fluorescent visualization to guide systematic screening for

postsynaptic cholinergic responses. As previous experiments exclude (with the possible exception of subtypes of TH-expressing interneurons, THINs) the role of currently known GABAergic interneurons in mediating fast acetylcholine-induced GABAergic inhibition in SPNs (English et al., 2012) we sought to find and test new types of striatal interneurons. To this end we created a double transgenic strain using mice in which Cre-recombinase is expressed under the control of the regulatory sequence of the 5-hydroxytryptamine receptor-3-subunit-a (HTR3a) gene. Our original choice of targeting based on HTR3a gene expression was motivated by the observation that GABAergic interneurons often colocalize HT3a receptors with nicotinic receptors in other brain areas (Sudweeks et al., 2002; Lee et al., 2010). Subsequently, this correlation has also been confirmed in the neostriatum (Muñoz-Manchado et al., 2014).

We used immunocytochemistry and in vitro whole-cell recording to obtain a preliminary characterization and classification of the targeted interneurons. Currently, eight different classes of interneurons have been described in the striatum (for a review, see Tepper et al., 2010). These include PV expressing fast-spiking neurons, NPY and NOS co-expressing plateau-depolarization low-threshold spiking (PLTS) interneurons (Kawaguchi, 1993), NPY-expressing (but NOS-negative) NPY-NGF neurons which give rise to slow GABAergic inhibition in projection neurons (Ibáñez-Sandoval et al., 2011), four electrophysiologically distinct types of neurons termed THINs which can be identified in transgenic mice on the basis of GFP or Cre expression controlled by the regulatory sequence of the TH gene (Ibáñez-Sandoval et al., 2010) and, finally, interneurons with unknown electrophysiological properties that express CR (Kawaguchi et al., 1995). The existence of a class of interneurons that forms reciprocal feedback inhibitory connection

with ChAT interneurons have been inferred from indirect evidence (Sullivan et al., 2008) and, with the possible exception of CR<sup>+</sup> cells, these neurons are probably distinct from all other interneurons (English et al., 2012).

To characterize the HTR3a-Cre neuron population we first tested the expression of PV, NPY, NOS, CR and TH using immunocytochemistry (Fig. 1). Among the transfected Cre-expressing interneurons, a large fraction was positive for PV (190 PV-immunopositive neurons, 48 HTR3a-Cre neurons, 36 neurons colocalizing, 75% of HTR3a-Cre neurons PV positive). In contrast, small populations expressed NPY (165 NPY-immunopositive cells, 156 HTR3a-Cre cells, five colocalized, 3.2% of Htr3a-Cre neurons NPY positive) or CR (23 CR-immunopositive cells, 86 HTR3a-Cre cells, two colocalized, 2.3% of HTR3a-Cre neurons CR positive) while none contained NOS (130 NOS-immunopositive cells, 94 HTR3a-Cre cells, 0 colocalized) or exhibited TH expression after lesioning the nigrostriatal dopaminergic input (162 TH-immunopositive cells, 152 HTR3a-Cre cells, 0 colocalized; see Materials and methods). About 20% of HTR3a-Cre-eYFP-expressing neurons did not express any of these markers (Fig. 1). In addition, we also examined the possible expression of Cre in ChAT interneurons in double transgenic ChAT-ChR2-eYFP;HT3Ra-Cre mice virally transfected to express dTomato from a Cre-dependent (DIO) transgene (Fig. 4A). None of the HTR3a-Cre cells expressed ChR2-eYFP, demonstrating that ChAT interneurons were not part of the HTR3a-Cre neuron population (177 ChAT-ChR2-eYFP cells, 109 HTR3a-Cre cells, 0 colocalized, Fig. 4A). Finally, the possible involvement of SPN neurons could be excluded on morphological (as well as electrophysiological, see below) grounds as none of the HTR3a-Cre neurons exhibited the high dendritic spine density or other morphological characteristics of SPNs (Fig. 1; cf. Grofova, 1974; Wilson

& Groves, 1980; Somogyi et al., 1981; Gertler et al., 2008).

Next we obtained in vitro whole-cell recordings from Cre-expressing interneurons (n = 134). Consistent with the immunocytochemical detection of PV+ and NPY+ neurons, a large fraction of the recorded neurons were FSIs (n = 57, Fig. 2A) while a small population of cells exhibited the properties of NPY-NGF interneurons (n = 5) including a large-amplitude, long-lasting spike AHP, with long latency to the most negative point of the AHP (Fig. 2B) and as demonstrated in a subset of cells, slow GABAergic signaling to simultaneously recorded SPNs (Fig. 4E), which is the primary defining feature of NPY-NGF interneurons in the striatum (Ibáñez-Sandoval et al., 2010). Consistent with our morphological observations, none of these cells exhibited the electrophysiological properties of SPNs (Fig. 2; cf. Nisenbaum et al., 1994; Gertler et al., 2008).

In addition to these known cell types we also found interneurons that exhibited electrophysiological properties not previously described in the neostriatum (Kawaguchi, 1993; Kawaguchi et al., 1995; Gittis et al., 2010; Ibáñez-Sandoval et al., 2010, 2011; Tepper et al., 2010; Sciamanna & Wilson, 2011). Although these neurons were electrophysiologically heterogeneous, one class of cells could be readily recognized based on the presence of pronounced spike-frequency adaptation during repetitive firing induced by injection of depolarizing current pulses (Fig. 2D). These neurons were termed FAIs. Further characteristics of FAIs include a resting membrane potential of  $66.2 \pm 1.2$  mV, no spontaneous activity, a nearly linear sub-threshold current–voltage relationship only slightly distorted by weak time-dependent inward rectification and a moderate maximal sustained firing rate reaching  $< 100$  Hz (Fig. 2D). To test whether FAIs represented a type of neuron distinct from the remaining novel interneurons we first used unsupervised

clustering based on current–spike frequency relationships (see Materials and methods). As shown in Fig. 2E and F, this method identified distinct clusters within the recorded cell population, one of which corresponded directly to the neurons pre-classified as FAIs. To confirm statistically the validity of discriminating between FAIs and all other novel interneurons we compared several basic electrophysiological properties of FAIs and the remaining novel neurons. This revealed statistically significant differences in several parameters including the membrane time constant (FAI:  $n = 25$ ,  $22.43 \pm 1.97$  ms, mean  $\pm$  SD, other:  $n = 43$ ,  $34.61 \pm 2.42$  ms,  $t = 3.90$ , two-sample t-test,  $P < 0.001$ ), input resistance at rest (FAI:  $n = 25$ ,  $362.0 \pm 104.8$  M $\Omega$ , other:  $n = 22$ ,  $601.1 \pm 226.5$  M $\Omega$ ,  $t = 4.54$ , two-sample t-test,  $P < 0.001$ ) and the latency of the most negative point of the spike AHP following an action potential (FAI:  $n = 25$ ,  $0.85 \pm 0.23$  ms median  $\pm$  interquartile range (IQR), other:  $n = 43$ ,  $0.95 \pm 0.36$  ms median  $\pm$  IQR,  $U = 302$   $Z = 2.99$ , Mann–Whitney test,  $P < 0.003$ ). We did not attempt to further characterize or classify the novel neurons that were distinct from FAIs (these will be described in a manuscript now in preparation), but we note that they appeared to comprise more than one cell type, with many of them exhibiting features shared with subpopulations of THINs (see comments in Materials and methods). An example of the most frequently observed electrophysiological profile among these neurons is shown in Fig.2C. The basic properties of fast-spiking, NPY-NGF, FAI and the unclassified group of novel interneurons are summarized in Table 1.

As preliminary recordings demonstrated that FAIs received nicotinic synaptic inputs and therefore were a candidate for participating in a disynaptic circuit to SPNs, we concentrated on characterizing the synaptic connectivity of this cell type. First, we obtained paired recordings from FAIs and SPNs to examine the postsynaptic responses elicited by

these interneurons (Fig. 3). These tests were done using recordings from 14 FAIs and 22 SPNs, with six FAIs being tested with more than one (two or four) SPN each, and no SPN tested with more than one FAI. Postsynaptic responses could be observed in SPNs in 11 of the 22 tested connections, representing a one-way connectivity of 50%. The response was a fast GABA<sub>A</sub>-receptor-mediated IPSC as it could be blocked by bicuculline ( $n = 1$ ; Fig. 3C) and exhibited an average rise-time and decay-time constant of  $1.46 \pm 0.41$  and  $6.79 \pm 0.83$  ms, respectively. Remarkably, unlike all other inhibitory neostriatal connections in the neostriatum (Koós et al., 2004; Taverna et al., 2008; Tecuapetla et al., 2009; Gittis et al., 2010) synaptic transmission from FAIs exhibited pronounced short-term facilitation (Fig. 3A, D and F). Strikingly, in some pairs the resting release probability (the probability of observing a synaptic response to the first stimulus in 50-Hz spike trains delivered at 30-s intervals) was close to zero (Fig. 3A, inset). On average the IPSC amplitude increased by a factor of 2.17 through the first three spikes (Fig. 3D and F). In some pairs use-dependent short-term depression was also observable late in the spike train (Fig. 3D). The population mean of the maximal IPSC amplitude was  $16.9 \pm 4.8$  pA, which is significantly smaller than the unitary IPSC amplitudes recorded from FSIs (Fig. 1D, cf. Fig. 3E). Neither the short-term facilitation nor the small IPSC amplitude was an artifact of the preparation or recording methods as synaptic transmission from an FSI to an SPN exhibited typical properties including high-amplitude IPSCs and use-dependent depression (Fig. 3E and F). Normal synaptic transmission was also confirmed between four pairs of NPY-NGF interneurons and SPNs (Fig. 4E).

Next we characterized the postsynaptic responses of FAIs elicited by optogenetic activation of cholinergic inputs using double transgenic ChAT-ChR2-eYFP;HT3aR-Cre

mice virally transfected to express tdTomato from a Cre-dependent (DIO) transgene (Fig. 4A). As ChR2 was here targeted to cholinergic neurons using a transgenic and not the virus-mediated process used previously and because ChR2 expression in this preparation is not limited to ChAT interneurons but includes all cholinergic neurons such as those recently reported to project to the striatum from the brainstem (Dautan et al., 2014), we first tested if the synaptic responses of downstream circuits to optogenetic cholinergic stimulation were similar to the originally described responses (English et al., 2012). Whole-cell recording from ChAT interneurons demonstrated that these cells exhibited normal electrophysiological characteristics, including low-frequency spontaneous activity (Fig. 4B) and responded with firing action potentials to pulses of blue light (1–2 ms, Fig. 4C). Consistent with previous results, optogenetic activation of ChAT interneurons elicited multiphasic IPSCs in all recorded SPNs (Fig. 4D). The IPSC comprised an early fast component and a distinct slow component, the kinetics of which was sensitive to the blockade of GABA reuptake with NO711 (10  $\mu$ M, Fig. 4D). In addition, we also recorded NPY-NGF interneurons and showed that these neurons received nicotinic excitatory postsynaptic potential (EPSPs) and elicited slow IPSCs in SPNs ( $n = 3$ ; Fig. 4E). These results confirm that similar GABAergic circuits are activated in this preparation as in previous studies (English et al., 2012; Nelson et al., 2014).

Next we examined the postsynaptic responses of FAIs to optogenetic activation of cholinergic inputs (Fig. 5). In 13 of the 15 recorded FAIs (86.7%), brief light pulses (1–2 ms) elicited EPSPs exhibiting an average amplitude of  $10.4 \pm 6.12$  mV (Fig. 5A–C). In ten of 13 cells (76.9%) the EPSP also triggered action potentials (1–3 spikes per EPSP, Fig. 5A–C). The EPSP was mediated by nicotinic acetylcholine receptors because it could be

blocked by mecamylamine (MEC, 5  $\mu$ M, n = 7, Fig. 5A) or the  $\beta$ 2-subunit selective antagonist dihydro- $\beta$ -erythroidine (DH $\beta$ E, 1  $\mu$ M, n = 8, Fig. 5B). Interestingly, even at the relatively high concentration of 1  $\mu$ M, DH $\beta$ E was effective only in two FAIs (Fig. 5A and B), while in the remaining neurons the response was blocked by MEC (Fig. 5A), possibly revealing heterogeneity in nicotinic receptor subunit composition among FAIs. Successful receptor block by DH $\beta$ E application in these experiments was demonstrated by the complete blockade of the disynaptic IPSC elicited in simultaneously recorded SPNs (Fig. 5A).

Finally, we obtained simultaneous recordings from six pairs of connected FAIs and SPNs in the double transgenic mice and directly confirmed that the same FAIs that could be activated by optogenetic stimulation of cholinergic inputs (Fig. 5C) also provided GABAergic innervation to SPNs (Fig. 5D).

## Discussion

This study demonstrates the existence of a novel type of GABAergic interneuron in the neostriatum, the FAI, which receives strong nicotinic excitatory inputs and provides conventional fast GABAergic inhibitory inputs to SPNs.

### **FAIs represent a novel type of GABAergic interneuron in the neostriatum**

There are several lines of evidence to support the contention that FAIs represent a novel class of interneurons in the neostriatum. First, these neurons could be clearly distinguished from FSIs, NPY-PLTS and NPY-NGF interneurons based on characteristics of their firing

responses to somatically injected current pulses, the unique short-term facilitation of synaptic transmission from FAIs to SPNs, the kinetics of the IPSC and (in the case of NPY-PLTS) the absence of NOS expression in the Cre-expressing interneuron population (Figs 1 and 2). It is possible that FAIs represent one of the subtypes of the less extensively studied THINS, but the distinction of FAIs is supported by (i) specific firing and membrane potential responses to injected current pulses in THINS that are absent in FAIs, including depolarizing plateau potentials in Type I, II and III THINS and a rebound LTS at resting membrane potential in Type IV neurons; (ii) the absence of TH induction in the Cre-expressing cells, which is observed in a subset of THINS following 6-OHDA lesions of the nigrostriatal projection; and finally (iii) the absence of nicotinic EPSP/C in the subtypes of THINS (Types I and II) tested to date (Ibáñez-Sandoval et al., 2010; Ünal et al., 2013). FAIs could also be distinguished from other electrophysiologically novel interneurons based on the current–frequency relationships and other properties of these neurons, as discussed above. Although the differential expression of nicotinic receptor subunits suggests that FAIs might be further classified into subtypes, such a subdivision could not be confirmed by considering additional characteristics. Therefore, FAIs probably represent a distinct and novel cell type of the neostriatum.

In a recent study, Muñoz-Manchado et al. (2014) described several types of GABAergic interneurons targeted in HTR3a-EGFP transgenic mice. Surprisingly, despite nominally targeting the same neuron populations defined by the expression of the same gene, none of the cell types described in the HTR3a-EGFP line appears to match the properties of FAIs. In particular, among the neurons most similar to FAIs (the Type-III neurons of Muñoz-Manchado et al., 2014) many were reported to exhibit a slow

regenerative depolarizing potential that we never observed in FAIs or any other striatal interneurons targeted in the HTR3a-Cre line. Although the electrophysiological difference between FAIs and the heterogeneous Type-III neuron population may simply reflect different conditions of the recordings or preparations, or a difficulty of discerning FAIs in a different context of neuronal phenotypes, the fact that the two transgenic lines also diverge in their targeting of TH<sup>+</sup> interneurons confirms the existence of a genuine mismatch between the cell types accessible in the two transgenic lines and suggests that few or perhaps none of the FAIs are visualized in the HTR3a-EGFP mice.

### **FAIs are not a major source of the fIPSC elicited in SPNs by synchronous activation of cholinergic interneurons**

Previous experiments have shown that synchronous cholinergic activation elicits disynaptic multiphasic GABAergic inhibition in SPNs (English et al., 2012; Nelson et al., 2014). This phenomenon is of interest because activation of these GABAergic synaptic responses may be instrumental in transmitting the short-duration multi-phasic responses that ChAT interneurons exhibit during presentation of behaviorally salient stimuli. The cellular mechanism that mediates these GABAergic responses is not completely understood. As shown by English et al. (2012), at least two distinct sources are involved, one that gives rise to a conventional fast GABAergic IPSC (fIPSC) and another responsible for a slow, reuptake sensitive response (sIPSC, see Fig. 4D). In contrast to the sIPSC – a significant source of which has been identified as the NPY-NGF interneuron (English et al., 2012) – the origin of the fast inhibitory component remains unclear. We have suggested that this component may be mediated by synaptic activation of one or more additional types of interneurons (English et al., 2012). Recently, this explanation was called into question

by results showing that both fast and slow inhibition of SPNs can be triggered by acetylcholine-induced GABA release from nigrostriatal terminals (Nelson et al., 2014). Our present results directly demonstrate that there are interneurons in the striatum that elicit fast GABAergic IPSCs in SPNs and are activated by cholinergic inputs. Surprisingly, however, FAIs are unlikely to represent a major source of the cholinergically induced fIPSC observed in SPNs. This is because DH $\beta$ E can fully block the disynaptic inhibition seen in SPNs but fails to block EPSPs or prevent firing of action potentials in most FAIs. We suggest that postsynaptic responses originating from FAIs that continue firing action potentials in the presence of DH $\beta$ E are not normally observed in most experiments due to the low amplitude and very low resting release probability of the response. Additionally, the low initial release probability and strong facilitation of the FAI to SPN synapse suggest that little inhibition is provided by FAIs during the first spike in a train, which would occur when the fIPSC is observed in SPNs.

The cellular origin of the fIPSC remains unclear. It is possible that most or perhaps all of this response originates from terminals of nigrostriatal axons as suggested by Nelson et al. (2014) although in their study despite using interventions that would be expected to eliminate neurotransmitter release from dopaminergic terminals, the block of the fIPSC was incomplete, suggesting that a significant fraction of this response component may originate from other, possibly intrinsic, interneuronal sources.

### **Implications for organization of the circuitry of the neostriatum**

Our results reveal further complexity in the organization of the interneuron circuit of the neostriatum. Importantly, our results confirm that at least two types of GABAergic

interneurons, NPY-NGF and FAI, that innervate SPNs are activated by excitatory cholinergic inputs in the neostriatum. We have previously shown that the GABAergic interneurons responsible for recurrent inhibition in ChAT interneurons are distinct from those that give rise to the fIPSC or sIPSC in SPNs. As recurrent inhibition is fully blocked by low concentrations of DH $\beta$ E (Sullivan et al., 2008; English et al., 2012), the majority of FAIs are not involved in this circuit. This suggests that at least three types of GABAergic interneurons receive nicotinic excitatory inputs in the neostriatum.

An interesting possibility is that some or all of the cholinergic input to FAIs originates from cholinergic neurons in the pedunculopontine nucleus (PPN) that are known to innervate the neostriatum (Dautan et al., 2014) and the axons of which are probably activated during optogenetic experiments in slices prepared from ChAT-ChR2 mice. Although on quantitative grounds ChAT interneurons represent a more likely source of the cholinergic input than the significantly less dense input from the PPN (Dautan et al., 2014), FAIs and perhaps other interneurons may be selectively targeted by the PPN projection, a notion supported by precedents for selective innervation of striatal interneurons by extrastriatal afferents (Bevan et al., 1998; Brown et al., 2012). It is further possible that the DH $\beta$ E-sensitive and DH $\beta$ E-insensitive cholinergic receptors are localized in an input-dependent manner as is the case for specific GABA $\text{A}$  receptor subunits (Nyiri et al., 2001; Gross et al., 2011).

It is of significant interest that the cholinergic innervation of interneurons is cell type specific in the neostriatum. Rather than presenting a continuum of input strengths, the cholinergic innervation exhibits a high degree of selectivity contrasting with the complete or almost complete absence of nicotinic synaptic responses in FSIs and NPY-PLTS

neurons (Ibáñez-Sandoval et al., 2011; English et al., 2012; Nelson et al., 2014) with the extremely powerful innervation of NPY-NGF neurons (English et al., 2012), FAIs and (based on indirect evidence) that of the still unidentified recurrent inhibitory interneurons (Sullivan et al., 2008; English et al., 2012). This suggests that the GABAergic interneurons that receive nicotinic inputs serve a fundamentally different role from other striatal GABAergic interneurons – one that is intimately linked to the cholinergic control of the striatum. Furthermore, these GABAergic interneurons appear to form a complex circuitry, as suggested by feed-forward slow inhibition elicited in NPY-NGFs by cholinergic stimulation, the electrotonic coupling of these neurons to each other (English et al., 2012) and (based on their homology with cortical neurons) perhaps to other cell types (Simon et al., 2005). Consequently, the neostriatum incorporates a more intricate and functionally diverse interneuronal circuitry than that which is usually assumed based on the canonical feed-forward organization of FSIs.

### **Possible significance for behavioral functions of acetylcholine**

Cholinergic modulation is essential for the normal functioning of the neostriatum (Zackheim & Abercrombie, 2005; Pisani et al., 2007; Bonsi et al., 2011; Goldberg et al., 2012). Recent experiments have revealed a powerful although not easily conceptualized role in learning for neostriatal ChAT interneurons (Sano et al., 2003; Witten et al., 2010; Brown et al., 2012; Bradfield et al., 2013; Okada et al., 2014). Perhaps the most promising candidate to link cholinergic modulation to the regulation of learning is the brief multiphasic population response that ChAT interneurons exhibit in response to behaviorally salient stimuli. These responses consist of quickly alternating epochs of increased and reduced cholinergic activity, the precise pattern and magnitude of which

reflect several learned characteristics of sensory stimuli (Aosaki et al., 1994; Morris et al., 2004; Atallah et al., 2014). Recently, several cellular responses (including those described here) have been identified that are sufficiently rapid to transmit these fast cholinergic signals and may have significant effects on excitatory synaptic plasticity (Pakhotin & Bracci, 2007; Ding et al., 2010; Witten et al., 2010; Cachope et al., 2012; English et al., 2012; Threlfell et al., 2012). Among these, the control of GABAergic circuits by ChAT interneurons is a particularly attractive candidate because the rich integrative possibilities of networks of interneurons may provide a plausible interface for movement, attention and reinforcement-related mechanisms.

## Acknowledgements

We thank Arpan Garg for excellent technical assistance, Dr Drew Headley for advice on data analysis, Dr Jaime Kaminer for valuable suggestions on the manuscript and Dr Karl Deisseroth for optogenetic tools and advice. This research was supported by 1R01NS072950 (T.K. and J.M.T.), 5R01NS034865 (J.M.T.) and Rutgers University.

## References

- Aosaki, T., Tsubokawa, H., Ishida, A., Watanabe, K., Graybiel, A.M. & Kimura, M. (1994) Responses of tonically active neurons in the primate's striatum undergo systematic changes during behavioral sensorimotor conditioning. *J. Neurosci.*, 14, 3969–3984.
- Atallah, H.E., McCool, A.D., Howe, M.W. & Graybiel, A.M. (2014) Neurons in the ventral striatum exhibit cell-type-specific representations of outcome during learning. *Neuron*, 82, 1145–1156.

Bevan, M.D., Booth, P.A., Eaton, S.A. & Bolam, J.P. (1998) Selective innervation of neostriatal interneurons by a subclass of neuron in the globus pallidus of the rat. *J. Neurosci.*, 18, 9438–9452.

Bonsi, P., Cuomo, D., Martella, G., Madeo, G., Schirinzi, T., Puglisi, F., Ponterio, G. & Pisani, A. (2011) Centrality of striatal cholinergic transmission in basal ganglia function. *Front. Neuroanat.*, 5, 6.

Bradfield, L.A., Bertran-Gonzalez, J., Chieng, B. & Balleine, B.W. (2013) The thalamostriatal pathway and cholinergic control of goal-directed action: interlacing new with existing learning in the striatum. *Neuron*, 79, 153–166.

Brown, M.T., Tan, K.R., O'Connor, E.C., Nikonenko, I., Muller, D. & Luscher, C. (2012) Ventral tegmental area GABA projections pause accumbal cholinergic interneurons to enhance associative learning. *Nature*, 492, 452–456.

Cachope, R., Mateo, Y., Mathur, B.N., Irving, J., Wang, H.L., Morales, M., Lovinger, D.M. & Cheer, J.F. (2012) Selective activation of cholinergic interneurons enhances accumbal phasic dopamine release: setting the tone for reward processing. *Cell Rep.*, 2, 33–41.

Dautan, D., Huerta-Ocampo, I., Witten, I.B., Deisseroth, K., Bolam, J.P., Gerdjikov, T. & Mena-Segovia, J. (2014) A major external source of cholinergic innervation of the striatum and nucleus accumbens originates in the brainstem. *J. Neurosci.*, 34, 4509–4518.

Ding, J.B., Guzman, J.N., Peterson, J.D., Goldberg, J.A. & Surmeier, D.J. (2010) Thalamic gating of corticostriatal signaling by cholinergic interneurons. *Neuron*, 67, 294–307.

English, D.F., Ibáñez-Sandoval, O., Stark, E., Tecuapetla, F., Buzsaki, G., Deisseroth, K., Tepper, J.M. & Koós, T. (2012) GABAergic circuits mediate the reinforcement-related signals of striatal cholinergic interneurons. *Nat. Neurosci.*, 15, 123–130.

Gerfen, R.G., Paletzki, R. & Heintz, N. (2013) GENSAT BAC Cre-recombinase driver lines to study the functional organization of cerebral cortical and basal ganglia circuits. *Neuron*, 80, 1368–1383.

Gertler, T.S., Chan, S. & Surmeier, D.J. (2008) Dichotomous anatomical properties of adult striatal medium spiny neurons. *J. Neurosci.*, 28, 10814–10824.

Gittis, A.H., Nelson, A.B., Thwin, M.T., Palop, J.J. & Kreitzer, A.C. (2010) Distinct roles of GABAergic interneurons in the regulation of striatal output pathways. *J. Neurosci.*, 30, 2223–2234.

Goldberg, J.A., Ding, J.B. & Surmeier, D.J. (2012) Muscarinic modulation of striatal function and circuitry. *Handb. Exp. Pharmacol.*, 208, 223–241.

Grofova, I. (1974) The identification of striatal and pallidal neurons projecting to substantia nigra: an experimental study by means of retrograde axonal transport of horseradish peroxidase. *Brain Res.*, 91, 286–291.

- Gross, A., Sims, R.E., Swinny, J.D., Sieghart, W., Bolam, J.P. & Stanford, I.M. (2011) Differential localization of GABA<sub>A</sub> receptor subunits in relation to rat striatopallidal and pallidopallidal synapses. *Eur. J. Neurosci.*, 33, 868–878.
- Ibáñez-Sandoval, O., Tecuapetla, F., Unal, B., Shah, F., Koós, T. & Tepper, J.M. (2010) Electrophysiological and morphological characteristics and synaptic connectivity of tyrosine hydroxylase-expressing neurons in adult mouse striatum. *J. Neurosci.*, 30, 6999–7016.
- Ibáñez-Sandoval, O., Tecuapetla, F., Unal, B., Shah, F., Koós, T. & Tepper, J.M. (2011) A novel functionally distinct subtype of striatal neuropeptide Y interneuron. *J. Neurosci.*, 31, 16757–16769.
- Kawaguchi, Y. (1993) Physiological, morphological, and histochemical characterization of three classes of interneurons in rat neostriatum. *J. Neurosci.*, 13, 4908–4923.
- Kawaguchi, Y., Wilson, C.J., Augood, S.J. & Emson, P.C. (1995) Striatal interneurons: chemical, physiological and morphological characterization. *Trends Neurosci.*, 18, 527–535.
- Koós, T., Tepper, J.M. & Wilson, C.J. (2004) Comparison of IPSCs evoked by spiny and fast-spiking neurons in the neostriatum. *J. Neurosci.*, 24, 7916–7922.
- Lee, S., Hjerling-Leffler, J., Zagha, E., Fishell, G. & Rudy, B. (2010) The largest group of superficial neocortical GABAergic interneurons expresses ionotropic serotonin receptors. *J. Neurosci.*, 30, 16796–16808.
- Morris, G., Arkadir, D., Nevet, A., Vaadia, E. & Bergman, H. (2004) Coincident but distinct messages of midbrain dopamine and striatal tonically active neurons. *Neuron*, 43, 133–143.
- Muñoz-Manchado, A.B., Foldi, C., Szydłowski, S., Sjulson, L., Farries, M., Wilson, C., Silberberg, G. & Hjerling-Leffler, J. (2014) Novel striatal GABAergic interneuron populations labeled in the 5HT3aEGFP mouse. *Cereb. Cortex*, doi:10.1093/cercor/bhu179. [Epub ahead of print].
- Nelson, A.B., Hammack, N., Yang, C.F., Shah, N.M., Seal, R.P. & Kreitzer, A.C. (2014) Striatal cholinergic interneurons drive GABA release from dopamine terminals. *Neuron*, 82, 63–70.
- Nisenbaum, E.S., Xu, Z.C. & Wilson, C.J. (1994) Contribution of a slowly inactivating potassium current to the transition to firing of neostriatal spiny projection neurons. *J. Neurophysiol.*, 71, 1174–1189.
- Nyiri, G., Freund, T.F. & Somogyi, P. (2001) Input-dependent synaptic targeting of alpha2-subunit-containing GABA<sub>A</sub> receptors in synapses of hippocampal pyramidal cells of the rat. *Eur. J. Neurosci.*, 13, 428–442.

- Okada, K., Nishizawa, K., Fukabori, R., Kai, N., Shiota, A., Ueda, M., Tsutsui, Y., Sakata, S., Matsushita, N. & Kobayashi, K. (2014) Enhanced flexibility of place discrimination learning by targeting striatal cholinergic interneurons. *Nat. Commun.*, 5, 3778.
- Pakhotin, P. & Bracci, E. (2007) Cholinergic interneurons control the excitatory input to the striatum. *J. Neurosci.*, 27, 391–400.
- Pisani, A., Bernardi, G., Ding, J. & Surmeier, D.J. (2007) Re-emergence of striatal cholinergic interneurons in movement disorders. *Trends Neurosci.*, 30, 545–553.
- Sano, H., Yasoshima, Y., Matsushita, N., Kaneko, T., Kohno, K., Pastan, I. & Kobayashi, K. (2003) Conditional ablation of striatal neuronal types containing dopamine D2 receptor disturbs coordination of basal ganglia function. *J. Neurosci.*, 23, 9078–9088.
- Sciamanna, G. & Wilson, C.J. (2011) The ionic mechanism of gamma resonance in rat striatal fast-spiking neurons. *J. Neurophysiol.*, 106, 2936–2949.
- Simon, A., Olah, S., Molnar, G., Szabadics, J. & Tamas, G. (2005) Gap-junctional coupling between neurogliaform cells and various interneuron types in the neocortex. *J. Neurosci.*, 25, 6278–6285.
- Somogyi, P., Bolam, J.P. & Smith, A.D. (1981) Monosynaptic cortical input and local axon collaterals of identified striatonigral neurons. A light and electron microscopic study using the Golgi-peroxidase transport-degeneration procedure. *J. Comp. Neurol.*, 195, 567–584.
- Sudweeks, S.N., Hooft, J.A. & Yakel, J.L. (2002) Serotonin 5-HT(3) receptors in rat CA1 hippocampal interneurons: functional and molecular characterization. *J. Physiol.*, 544, 715–726.
- Sullivan, M.A., Chen, H. & Morikawa, H. (2008) Recurrent inhibitory network among striatal cholinergic interneurons. *J. Neurosci.*, 28, 8682–8690.
- Taverna, S., Ilijic, E. & Surmeier, D.J. (2008) Recurrent collateral connections of striatal medium spiny neurons are disrupted in models of Parkinson's disease. *J. Neurosci.*, 28, 5504–5512.
- Tecuapetla, F., Koós, T., Tepper, J.M., Kabbani, N. & Yeckel, M.F. (2009) Differential dopaminergic modulation of neostriatal synaptic connections of striatopallidal axon collaterals. *J. Neurosci.*, 29, 8977–8990.
- Tepper, J.M., Tecuapetla, F., Koós, T. & Ibáñez-Sandoval, O. (2010) Heterogeneity and diversity of striatal GABAergic interneurons. *Front. Neuroanat.*, 4, 150.
- Threlfell, S., Lalic, T., Platt, N.J., Jennings, K.A., Deisseroth, K. & Cragg, S.J. (2012) Striatal dopamine release is triggered by synchronized activity in cholinergic interneurons. *Neuron*, 75, 58–64.
- Ünal, B., Shah, F., Kothari, J. & Tepper, J.M. (2013) Anatomical and electrophysiological

changes in striatal TH interneurons after loss of the nigrostriatal dopaminergic pathway. *Brain Struct. Funct.*, 20, 331–349.

Wilson, C.J. & Groves, P.M. (1980) Fine structure and synaptic connections of the common spiny neuron of the rat neostriatum: a study employing intracellular inject of horseradish peroxidase. *J. Comp. Neurol.*, 194, 599– 615.

Witten, I.B., Lin, S.C., Brodsky, M., Prakash, R., Diester, I., Anikeeva, P., Gradinaru, V., Ramakrishnan, C. & Deisseroth, K. (2010) Cholinergic interneurons control local circuit activity and cocaine conditioning. *Science*, 330, 1677–1681.

Zackheim, J. & Abercrombie, E.D. (2005) Thalamic regulation of striatal acetylcholine efflux is both direct and indirect and qualitatively altered in the dopamine-depleted striatum. *Neuroscience*, 131, 423–436.

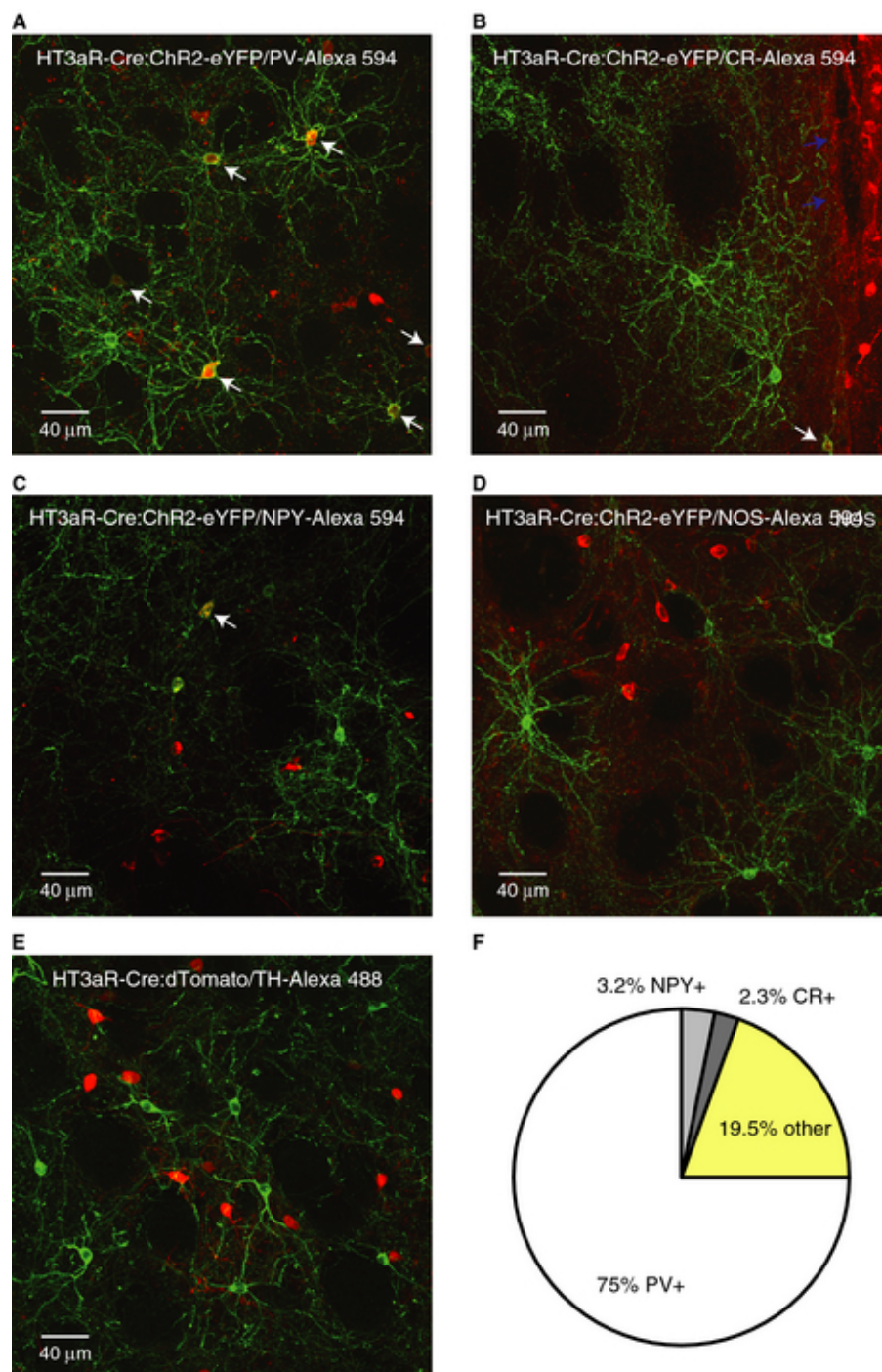


Figure 1. Immunocytochemical characterization of HTR3a-Cre interneurons. (A–D) Confocal micrographs showing interneurons transfected with ChR2-eYFP (pseudo-colored in green) and immunolabeling visualized with Alexa-594-conjugated secondary antibodies (red) to detect the different antigens indicated in the panels. (E) Confocal micrograph showing HTR3a-Cre interneurons transfected with dTomato (red) and immunolabeling visualized with Alexa-488-conjugated secondary antibody (green) to detect TH. (A–E) White arrows point to double labeled cells wherever applicable. In B blue arrows point to the border of the lateral ventricle. (F) Quantitative summary of immunocytochemical results. Neurons labeled as other refer to HTR3a-Cre interneurons that were immunonegative for PV, NPY or CR, calculated on the basis that these markers are not co-expressed in the striatum.

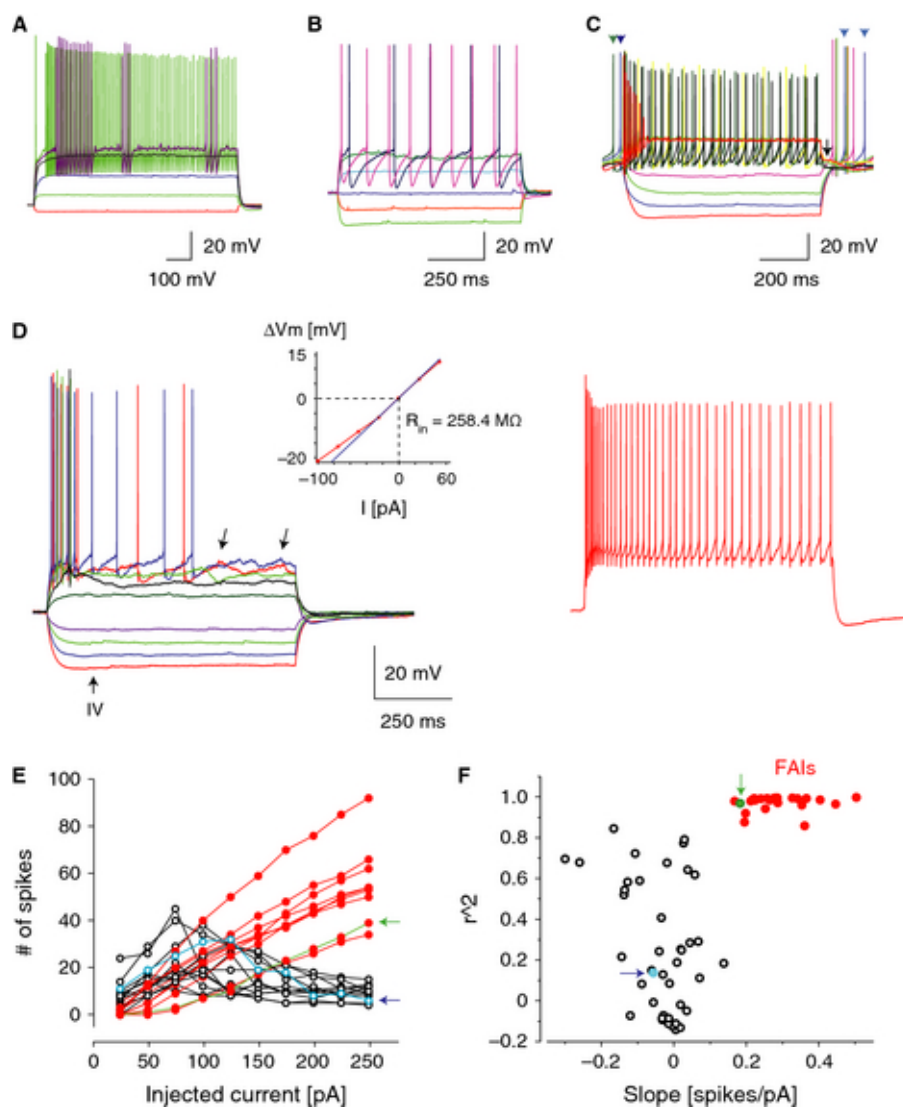


Figure 2. Electrophysiological identification of FAIs. (A) Membrane potential responses of a typical FSI to injected current pulses. Note the distinctive ‘stuttering’ firing pattern and sub-threshold membrane potential oscillations. Same cell as in Fig. 3E. (B) Membrane potential responses of a typical NPY-NGF to injected current pulses. Note the large-amplitude, slow AHPs. The neuron was further identified as an NPY-NGF based on characteristic synaptic output shown in Fig. 4E. (C) Membrane potential responses of the most typical novel interneuron not classified as an FAI to injected current pulses. Same as the unclassified non-FAI cell indicated by arrows pointing to open symbols in E and F. Note the features that distinguish this neuron from FAIs, including depolarization block at high amplitudes of injected current, short-duration depolarizing plateau potential (arrow) and spontaneous activity (arrowheads). Also note the resemblance of these characteristics to those exhibited by THINs. (D) Membrane potential responses of a typical FAI to injected current pulses (25-pA steps from  $-100$  pA, including traces in left and right panels). Same FAI as indicated by arrows pointing to closed symbols in E and F. Note the pronounced spike frequency adaptation and irregular membrane potential fluctuations (left panel, arrows). Inset shows the current–voltage relationship of this neuron. The thin line is a linear fit restricted to the current range  $-25$  to  $25$  pA used to calculate slope conductance and  $R_{in}$ . Right panel shows the response of the cell to a high-amplitude current pulse ( $275$  pA). The  $V_{m-rest}$  was  $-62$  mV in this cell. (E and F) Cluster analysis of novel interneurons (see Materials and methods). (E) The number of action potentials fired in response to current injection is plotted as a function of the injected current amplitude for unclassified novel neurons (open symbols) and FAIs (closed symbols). Note the pronounced reduction in action potential number above a certain current amplitude in the non-classified neurons

but not in FAIs. Only a subset of cells are shown for each group to avoid overcrowding.

(F) Linear functions were fitted to each cell's current–frequency relationship and the coefficients of determination ( $r^2$ ) were plotted as a function of the slopes of the fitted lines. Neurons pre-classified as FAIs correspond to the cluster of closed symbols. Note the clear separation of this group from the remaining novel HTR3a-Cre neurons. Arrows indicate the corresponding cells in the graphs in E and F.

**Table 1.** Electrophysiological properties of Htr3a-Cre interneurons.

Parameter	FSI (57)	NGF (5)	FAI (25)	Unclassified (43/22*)
Input resistance (M $\Omega$ )	84.1 $\pm$ 6.7	232.3 $\pm$ 34.8	362.0 $\pm$ 21.0	601.1 $\pm$ 48.3
Resting membrane potential (mV)	-82.0 $\pm$ 0.7	-73.1 $\pm$ 5.8	-66.2 $\pm$ 1.2	-66.1 $\pm$ 1.1
Membrane time constant (ms)	6.72 $\pm$ 0.51	14.67 $\pm$ 3.76	22.43 $\pm$ 1.97	34.61 $\pm$ 2.42
Percent spontaneously active	0	0	0	46.5
Percent exhibiting ADP or plateau potential	0	0	0	34.9

All values are means  $\pm$  SEM.

\*Only a subset of the unclassified cells (22 cells which were not spontaneously active) was used for calculating resting membrane potential and input resistance at rest.

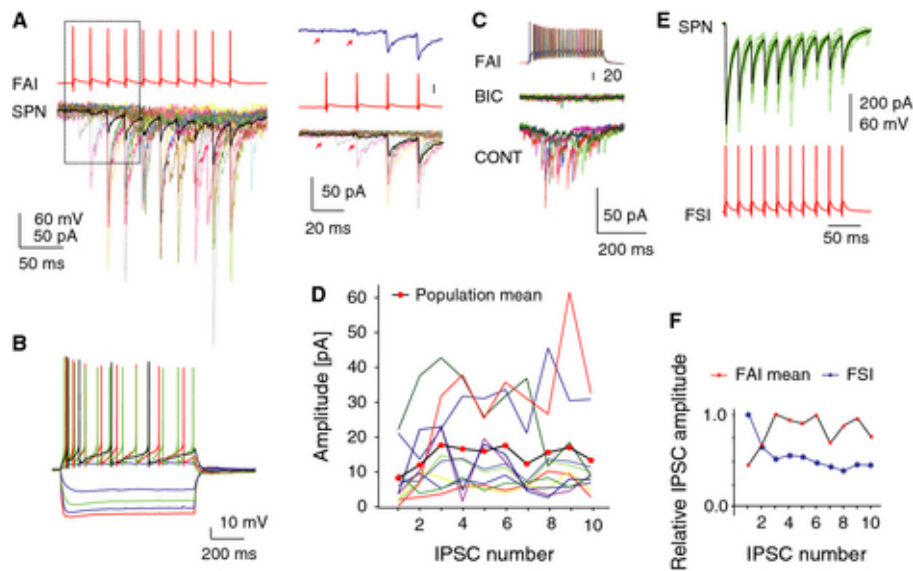


Figure 3. Characterization of synaptic transmission between FAIs and SPNs. (A) IPSC trains in an SPN elicited by trains of presynaptic action potentials in an FAI; same cell as in B. The thick trace is the average, and thin traces are individual responses. Right panel shows the first four IPSCs at higher time resolution. Top trace is the average response. Note the failure of transmission at the first spike (arrows) and the pronounced facilitation of the response. (B) Membrane potential responses of the FAI recorded in A to injected current pulses. (C) The IPSCs elicited from an FAI are blocked by bicuculline ( $10 \mu\text{M}$ ). (D) IPSC trains recorded in 11 FAI–SPN pairs. Thin lines are the average responses for each pair; the thick line is the population mean. Note the facilitation of the response through the first three IPSCs. (E) Paired recording from an FSI and an SPN. Same FSI as in Fig. 2A. Note the typical large-amplitude IPSCs, exhibiting a low failure rate and short-term depression (top panel). (F) Comparison of the normalized amplitudes of the population means of the IPSCs elicited from FAIs and the IPSCs recorded from the FSI–SPN pair shown in E. Note the different short-term dynamics of the two connections.

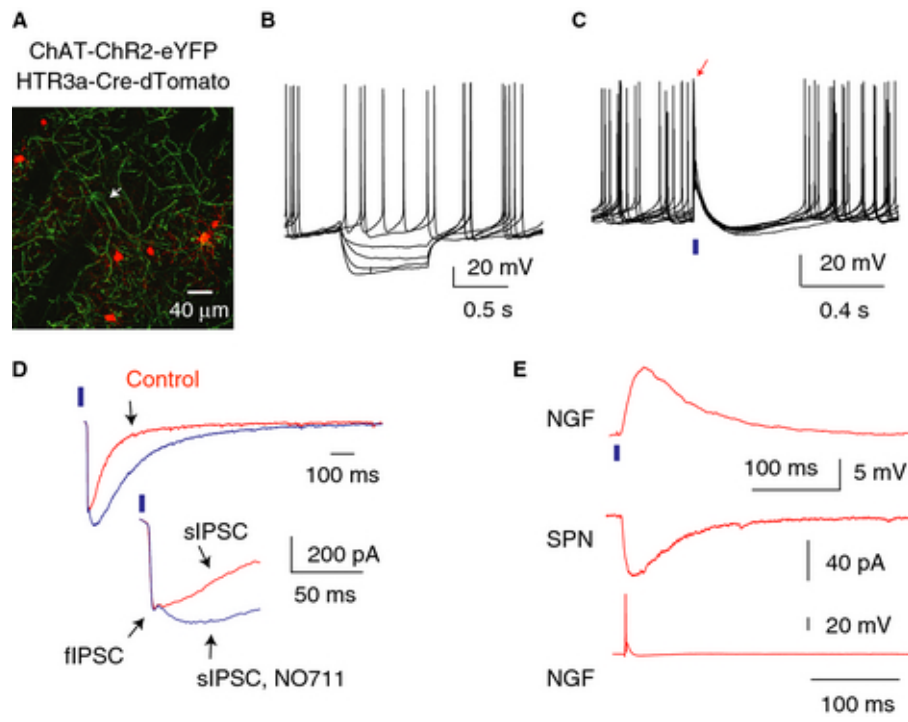


Figure 4. Characterization of optogenetic responses in slices prepared from double transgenic ChAT-ChR2-EYFP; HTR3a-Cre mice. (A) Double transgenic visualization of cholinergic profiles with ChR2-eYFP and HTR3a-Cre interneurons with targeted expression of tdTomato (red) in double transgenic mice. The arrow points to a ChAT interneuron. Note the absence of colocalization of the two markers. (B) Voltage responses of a ChR2-EYFP-expressing ChAT interneuron to injected current pulses demonstrating typical electrophysiological properties of these cells, including spontaneous activity. (C) Brief light pulses (2 ms, blue bar) elicit single action potentials (arrow) and reset pacemaking in a spontaneously active ChAT interneuron. (D) Optogenetic activation of cholinergic interneurons and axons with 2-ms pulses of blue light (blue bars) elicits large-amplitude postsynaptic responses in an SPN, top and bottom traces. Note that application of the GABA transport blocker NO711 (10  $\mu$ M) significantly increases the decay time constant of the late phase of the response (sIPSC). Also note that a relatively small, early fast component (fIPSC) was not affected by this drug. Inset shows the fIPSC–sIPSC transition at higher time resolution (bottom traces). (E) Top trace. Optogenetic stimulation (2-ms pulses of blue light, blue bar) elicited a large-amplitude EPSP in the HTR3a-Cre NPY-NGF interneuron. Same cell as in Fig. 2B. Paired recording from this neuron (bottom trace) and a nearby SPN (middle trace) demonstrates that the interneuron elicited a slow IPSC in the SPN (middle trace). Note that the intrinsic (Fig. 2B) and synaptic properties of the neuron are typical for NPY-NGF interneurons.

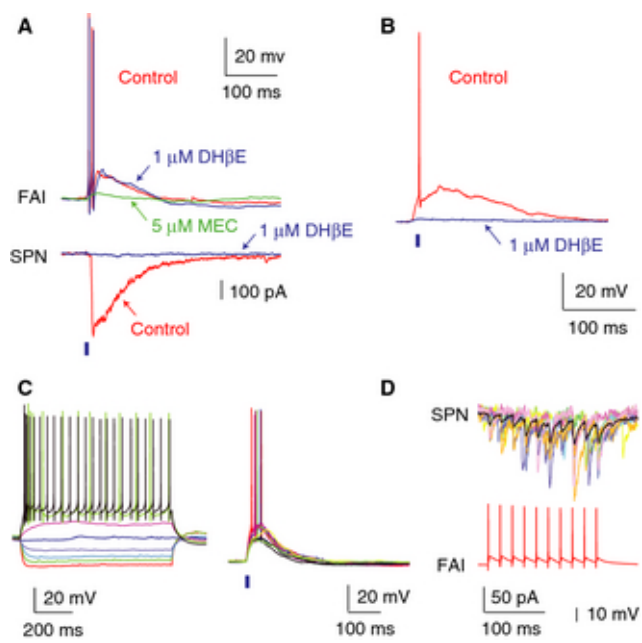


Figure 5. Nicotinic cholinergic synaptic responses of FAIs. (A) Simultaneous recording from an FAI and an SPN. Optogenetic activation of cholinergic inputs (2-ms pulse of blue light, blue bar) elicited a large-amplitude IPSC in the SPN (bottom) and an EPSP giving rise to action potentials in the FAI (top). Application of DH $\beta$ E (1  $\mu$ M) had no significant effect on the EPSP or action potential firing in the FAI (top traces, arrow), but completely blocked the IPSC in the SPN (bottom traces, arrow). Subsequent application of MEC (5  $\mu$ M) inhibited the EPSP in the FAI by  $\sim$ 80% (top traces, arrow). (B) Optogenetic activation of cholinergic inputs (2-ms pulse of blue light, blue bar) elicited an EPSP and the firing of an action potential in another FAI. The EPSP in this neuron was blocked by DH $\beta$ E (1  $\mu$ M, arrow). (C) Left panel: voltage responses to injected current pulses in a tdTomato-expressing HTR3a-Cre interneuron identified as an FAI. Right panel: optogenetic activation of cholinergic inputs (2-ms pulse of blue light, blue bar) elicited an EPSP and during some stimuli the firing of several action potentials in the same FAI. (D) Paired recording from the same FAI as in C and a nearby SPN demonstrated facilitating synaptic transmission to the SPN (top traces, thick line is the average IPSC) in response to a presynaptic spike train (bottom trace).

CHAPTER 3:  
Neostriatal GABAergic Interneurons Mediate Cholinergic  
Inhibition of Spiny Projection Neurons

Thomas W. Faust, Maxime Assous, James M. Tepper and Tibor Koós

Center for Molecular and Behavioral Neuroscience, Rutgers University, Newark, New  
Jersey 17102

Published in:

Faust TW, Assous M, Tepper JM, Koós T (2016) Neostriatal GABAergic Interneurons  
Mediate Cholinergic Inhibition of Spiny Projection Neurons. *J Neurosci* 36:9505–11.

## Abstract

Synchronous optogenetic activation of striatal cholinergic interneurons *ex vivo* produces a disynaptic inhibition of spiny projection neurons composed of biophysically distinct GABA<sub>Afast</sub> and GABA<sub>Aslow</sub> components. This has been shown to be due, at least in part, to activation of nicotinic receptors on GABAergic NPY-neurogliaform interneurons that monosynaptically inhibit striatal spiny projection neurons. Recently, it has been proposed that a significant proportion of this inhibition is actually mediated by activation of presynaptic nicotinic receptors on nigrostriatal terminals that evoke GABA release from the terminals of the dopaminergic nigrostriatal pathway. To disambiguate these two mechanisms, we crossed mice in which channelrhodopsin is endogenously expressed in cholinergic neurons with Htr3a-Cre mice, in which Cre is selectively targeted to several populations of striatal GABAergic interneurons, including the striatal NPY-neurogliaform interneuron. Htr3a-Cre mice were then virally transduced to express halorhodopsin to allow activation of channelrhodopsin and halorhodopsin, individually or simultaneously. Thus we were able to optogenetically disconnect the interneuron-spiny projection neuron (SPN) cell circuit on a trial-by-trial basis. As expected, optogenetic activation of cholinergic interneurons produced inhibitory currents in SPNs. During simultaneous inhibition of GABAergic interneurons with halorhodopsin, we observed a large, sometimes near complete reduction in both fast and slow components of the cholinergic-evoked inhibition, and a delay in IPSC latency. This demonstrates that the majority of cholinergic-evoked striatal GABAergic inhibition is derived from GABAergic interneurons. These results also reinforce the notion that a semiautonomous circuit of striatal GABAergic interneurons is responsible for transmitting behaviorally relevant cholinergic signals to

spiny projection neurons.

## Significance Statement

The circuitry between neurons of the striatum has been recently described to be far more complex than originally imagined. One example of this phenomenon is that striatal cholinergic interneurons have been shown to provide intrinsic nicotinic excitation of local GABAergic interneurons, which then inhibit the projection neurons of the striatum. As deficits of cholinergic interneurons are reported in patients with Tourette syndrome, the normal functions of these interneurons are of great interest. Whether this novel route of nicotinic input constitutes a major output of cholinergic interneurons remains unknown. The study addressed this question using excitatory and inhibitory optogenetic technology, so that cholinergic interneurons could be selectively activated and GABAergic interneurons selectively inhibited to determine the causal relationship in this circuit.

## Introduction

Cholinergic interneurons (CINs) represent one of the largest groups of striatal interneurons and the only non-GABAergic population. They exert a strong muscarinic control over striatal function and exhibit conditioned phasic responses to various behaviorally relevant stimuli (Goldberg and Reynolds, 2011; for review, see Goldberg et al., 2012).

In addition, a diverse population of striatal GABAergic interneurons provides inhibition to spiny projection neurons (SPNs) through several known routes (Tepper and

Koós, 2016). In perhaps the most well described case, fast-spiking interneurons (FSIs) receive glutamatergic input from cortex and intralaminar thalamus (Rudkin and Sadikot, 1999; Sidibé and Smith, 1999; Ramanathan et al., 2002), and provide strong feedforward inhibition to SPNs (Kita et al., 1990; Bennett and Bolam, 1994; Kita, 1996; Koós and Tepper, 1999; Koós et al., 2004; Mallet et al., 2005; Gittis et al., 2010; Planert et al., 2010; Szydlowski et al., 2013). Pharmacological inhibition of non-NMDA glutamate receptors in these neurons produces obvious motor deficits (Gittis et al., 2011).

However, more recently, many other types of striatal GABAergic interneurons have been identified that are driven by different sources. Striatal TH-expressing interneurons, NPY-expressing neurogliaform interneurons (NGFs) and fast-adapting interneurons (FAIs) receive nicotinic excitation *ex vivo*, and provide potent GABA<sub>A</sub>slow and/or GABA<sub>A</sub>fast inhibition to SPNs (Ibáñez-Sandoval et al., 2011, 2015; English et al., 2012; Luo et al., 2013; Faust et al., 2015). CINs are also responsible for their own feedback inhibition through an as yet unidentified source (Sullivan et al., 2008). When synchronously activated, CINs produce a large and long-lasting IPSC in SPNs in brain slices that contain distinct GABA<sub>A</sub>slow and GABA<sub>A</sub>fast components. This inhibition is also observed *in vivo* as a reduction of SPN firing following CIN activation (English et al., 2012). Based on the synaptic connections and inhibition kinetics determined from the *ex vivo* optogenetic and paired recording experiments, it appears that this cholinergic inhibition is mediated through striatal interneurons. This observation suggests that striatal interneurons under cholinergic control may influence striatal information processing in a cortical-independent manner.

In addition to the nicotinic innervation of striatal interneurons, CINs also provide a source of nicotinic input to nigrostriatal and mesoaccumbens dopamine terminals that

evokes dopamine release in both dorsal and ventral striatum (Cachope et al., 2012; Threlfell et al., 2012). With the recent demonstration that nigrostriatal terminals can co-release GABA and produce inhibition in SPNs with slow decay kinetics in ex vivo optogenetic experiments (Tritsch et al., 2012, 2014), it has been reported that the majority of the nicotinic-induced inhibition of SPNs is caused by GABA release from these terminals rather than by local interneurons, and that following either nigrostriatal pathway lesion or depletion of dopaminergic vesicles, a significant proportion of nicotinic-induced inhibition is reduced in the optogenetic experiments (Nelson et al., 2014). These data suggest that nigrostriatal terminals are the predominant source of this inhibition, and/or that the disynaptic pathway from CINs to SPNs via GABAergic interneurons is dopamine-sensitive. Therefore, we sought to determine the interneuronal contribution to the cholinergic-induced inhibition by using optogenetics to disconnect interneurons from this disynaptic circuit. If inhibition of ACh-activated striatal GABAergic interneurons failed to affect the CIN-induced SPN inhibition, then the novel, non-canonical mode of GABAergic inhibition of SPNs (Nelson et al., 2014) would be verified. On the other hand, if the CIN-induced inhibition of SPNs were due to activation of the NGF and/or other GABAergic interneurons, then the SPN inhibition ought to be reduced or blocked.

## Materials and Methods

### Subjects

All procedures used in this study were performed in agreement with the National Institutes of Health Guide for the Care and Use of Laboratory Animals and with the approval of the

Rutgers University Institutional Animal Care and Use Committee. Double-transgenic Htr3a-Cre ChAT-ChR2 mice [Tg(Htr3a-Cre)NO152Gsat/Mmucd, UC Davis; Tg(Chat-COP4\*H134R/EYFP,Slc18a3)6Gfng/J, Jackson Laboratories] were generated and maintained as hemizygotes (Zhao et al., 2011; Gerfen et al., 2013). Mice were housed in groups of up to four per cage and maintained on a 12 h light cycle (07:00 A.M.– 07:00 P.M.) with ad libitum access to food and water. A total of seven mice were used, including both males and females.

### **Intracerebral virus injection**

Mice were anesthetized with isofluorane (1–3%) and placed in a stereotaxic frame. Following a subcutaneous injection of bupivacaine, the scalp was retracted. A craniotomy was drilled above the site of injection, and 0.6  $\mu$ L AAV5 Efla DIO HR3.0-eYFP (HR3.0) was injected into dorsal neostriatum at three sites described by the following coordinates (from bregma): +0.74 mm AP, +1.6 mm ML, –1.75/–2.25/–3.6 mm DV, for a total volume of 1.8  $\mu$ L. Injections were performed using glass pipettes pulled and cut to an inner diameter of 40–50  $\mu$ m and an outer diameter of 60–70  $\mu$ m. Virus was injected at a rate of 9.2 nL/5 s with Nanoject II Auto-Nanoliter Injector (Drummond Scientific Company). Following viral injection, mice were treated with ketoprofen and buprenorphine for analgesia, and allowed to recover and express the viral transgene for 4–6 weeks before experimentation.

### **Slice preparation and visualized in vitro whole-cell recording**

Mice aged 3–7 months were anesthetized with ketamine (100 mg/kg) and transcardially perfused with an ice-cold/partially frozen N-methyl D-glucamine (NMDG)-based solution

comprised of the following (in mM): 103 NMDG, 2.5 KCl, 1.2 NaH<sub>2</sub>PO<sub>4</sub>, 30 NaHCO<sub>3</sub>, 20 HEPES, 25 glucose, 101 HCl, 10 MgSO<sub>4</sub>, 2 thiourea, 3 sodium pyruvate, 12 N-acetyl cysteine, and 0.5 CaCl<sub>2</sub> (saturated with 95% O<sub>2</sub>/5% CO<sub>2</sub>, measured to be 300–310 mOsm and 7.2–7.4 pH). The brain was removed, blocked and 350 μm slices cut on a Vibratome 3000. Slices were then incubated in oxygenated NMDG-based solution at 35°C for 5 min, after which they were maintained in oxygenated normal external solution at 25°C until placed in the recording chamber constantly perfused with oxygenated external solution at 30°C. External solution was composed of the following (in mM): 124 NaCl, 2.5 KCl, 26 NaHCO<sub>3</sub>, 1.2 NaH<sub>2</sub>PO<sub>4</sub>, 1 MgCl<sub>2</sub>, 2 CaCl<sub>2</sub>, 10 glucose, and 3 sodium pyruvate. Whole-cell voltage-clamp recordings of SPNs were obtained at –70 mV using a CsCl-based internal solution containing the following (in mM): 125 CsCl, 2 MgCl<sub>2</sub>, 10 HEPES, 4 Na<sub>2</sub>ATP, 0.4 GTP plus 2 μl/ml AlexaFluor 594 for SPN verification. Current-clamp recordings were obtained with normal internal solution containing the following (in mM): 130 K-methanesulfonate, 10 KCl, 2 MgCl<sub>2</sub>, 10 HEPES, 4 Na<sub>2</sub>ATP, 0.4 GTP plus 0.1– 0.3% biocytin, pH 7.3–7.4. Pipettes typically exhibited a DC impedance of 3–4 M measured in the recording chamber.

### **In vitro optical stimulation**

Optogenetic stimulation of channelrhodopsin-2 (ChR2)-expressing neurons in vitro consisted of 1–2 ms duration blue light pulses (465 nm, 1.25 mW/mm<sup>2</sup> illumination intensity) delivered from an LED coupled to a 200 m multimode optical fiber (PlexBright, Plexon) placed at 30° above the slice aiming at the recorded neurons. Optogenetic stimulation of HR3.0 consisted of 1 s duration yellow light pulses by wide-field illumination using a high-power (750 mW) LED (590 nm, 5 mW/mm<sup>2</sup> illumination

intensity). Optogenetic pulses were delivered at 30 s intervals. Because of the pronounced depression in this synaptic pathway (Nelson et al., 2014), we omitted the first ChR-evoked trace from subsequent statistical analysis.

## Results

Whole-cell recordings were obtained from SPNs in slices from the ChAT-Chr2 Htr3a-Cre double-transgenic mice described above. A schematic of the experimental protocol is shown in Figure 1A. Cholinergic neurons were stimulated with a 2 ms pulse from a blue LED causing postsynaptic GABAergic interneurons to fire, as shown for one representative neuron in Figure 1B. On alternate trials, a 1 s long wide-angle yellow LED was simultaneously activated as shown in Figure 1B. The yellow light hyperpolarized the GABAergic interneuron and blocked the spiking in response to activation of ChR2, leaving only a subthreshold depolarization (yellow traces). This example verifies the efficacy of the optogenetic activation of cholinergic interneurons consistently evoking spiking in the GABAergic interneurons, and the complete blockade of the ChAT-ChR2-induced spiking by simultaneous activation of halorhodopsin in the interneuron.

Next we repeated the optical stimulation protocol while recording SPNs in voltage-clamp. Optogenetic activation (1–2 ms blue light pulse) of CINs evoked a large IPSC in SPNs. Simultaneous illumination with yellow light, activating halorhodopsin selectively in the Htr3a-Cre GABAergic interneurons produced a dramatic reduction in the amplitude of the EPSC (Fig. 2), thus demonstrating that a significant proportion of the IPSC originates from local interneurons. In several SPNs there was a distinct delay in IPSC onset and peak

following halorhodopsin activation (Fig. 3). This indicates a delay in the latency of the intervening interneurons to fire action potentials following activation of CINs. In one SPN we observed failures on a number of trials both with and without halorhodopsin activation (Fig. 3B, bottom). This also strongly suggests that the sources for this inhibition are neurons rather than axon terminals.

Because the NPY-NGF interneuron generates only GABA<sub>A</sub>slow inhibition (Ibáñez-Sandoval et al., 2011; English et al., 2012), we assumed that the fast and slow components of the IPSC that were reduced in this preparation arose from distinct neuronal sources providing either GABA<sub>A</sub>fast or GABA<sub>A</sub>slow inhibition. We sought to differentiate these two components as much as possible to determine whether their reduction by halorhodopsin was similar in amount and occurred independently. Although the peaks of the GABA<sub>A</sub> fast and slow components constitute a variable mixed response of GABA<sub>A</sub>fast and GABA<sub>A</sub>slow currents, they represent their respective maximal contributions to the response and occur with a substantial delay between them (Figs. 2, 4A). Therefore, we measured the current reduction at both of these time points to approximate the GABA<sub>A</sub>fast and GABA<sub>A</sub>slow components. For example, if the IPSC contribution arising from NPY-NGF interneurons was completely abolished, we would expect this to reduce the slow-peak component much more than that of the fast-peak. The peak of the slow component was observed in a small number of cells (n = 9) to occur distinct from the fast component on average  $41.0 \pm 2.6$  ms (mean SEM) after the blue light pulse (Fig. 4A).

The IPSC fast-peak amplitude and latency, and the average amplitude during an interval approximating the slow peak (35–45 ms), were used to determine the proportion of SPNs that experienced significant reductions in inhibition amplitude or latency (Fig.

4A). Comparing control and HR3.0 trials, 66.7% (8/12) of SPNs exhibited a significant reduction of fast-peak amplitude, 25% (3/12) of SPNs exhibited a significant increase in the fast-peak latency, and 64.7% (11/17) of SPNs exhibited a significant reduction in the slow-peak amplitude ( $p < 0.05$ , paired sample t test, or paired sample Wilcoxon signed rank test). As a group, SPNs from the double-transgenic animals exhibited a significant reduction in fast-peak amplitude [Fig. 4B, left;  $n = 12$ ; control  $281.8 \pm 310.4$  pA, median  $\pm$  interquartile range (IQR), HR3.0  $98.0 \pm 164.7$  pA, median  $\pm$  IQR;  $p = 4.88e-3$ ,  $z = -2.63$ ,  $W = 5$ ; paired sample Wilcoxon signed rank test] a significant increase in fast-peak latency (Fig. 4C, left;  $n = 12$ ; control  $15.0 \pm 4.4$  ms, median  $\pm$  IQR; HR3.0  $17.8 \pm 3.7$  ms, median IQR;  $p = 5.37e-3$ ,  $z = -2.59$ ,  $W = 5.5$ ; paired sample Wilcoxon signed rank test) and a significant reduction in slow-peak amplitude (Fig. 4D, left;  $n = 17$ ; control  $184.5 \pm 177.1$  pA, median  $\pm$  IQR; HR3.0  $51.0 \pm 100.9$ , median  $\pm$  IQR;  $p = 1.07e-3$ ,  $z = -3.03$ ,  $W = 12$ ; paired sample Wilcoxon signed rank test).

To control for any potential artifact of the yellow light illumination itself, we performed the same recordings on a limited number of SPNs from ChAT-ChR2 single-transgenic animals (Fig. 2B). In these recordings, no SPNs exhibited any reduction of the fast-or slow-peak amplitude, or an increase in fast-peak latency as a result of yellow light application [using the same criterion as for the double-transgenic (Dbl-Tgn) group of  $p < 0.05$ , paired sample t test or paired sample Wilcoxon signed rank test]. Compared with this group, the double-transgenic group evidenced a significant reduction in fast-peak amplitude (Fig. 4B, right; Dbl-Tgn:  $n = 12$ ;  $48.3 \pm 44.1\%$  median  $\pm$  IQR; ChAT-ChR2:  $n = 8$ ,  $7.7 \pm 28.4\%$ , median  $\pm$  IQR;  $p = 6.2e-3$ ,  $z = 2.74$ ,  $U = 84$ ; Mann–Whitney test), a significant increase in fast-peak latency (Fig. 4C, right; Dbl-Tgn:  $n = 12$ ,  $12.9 \pm 3.9\%$ ,

mean  $\pm$  SEM; ChAT-ChR2:  $n = 8$ ,  $1.7 \pm 2.7\%$ , mean  $\pm$  SEM;  $p = 4.6e-2$ ,  $t = 2.1384$ ; two sample t test) and a significant reduction of slow-peak amplitude (Fig. 4D, right; Dbl-Tgn:  $n = 17$ ,  $37.1 \pm 54.0\%$ , median  $\pm$  IQR; ChAT-ChR2:  $n = 11$ ,  $6.7 \pm 17.9\%$ , median  $\pm$  IQR;  $p = 3.54e-3$ ,  $z = 2.92$ ,  $U = 156$ ; Mann–Whitney test).

We observed a wide range of IPSC amplitudes in SPNs in response to ChAT-ChR2 activation, and a wide range of IPSC reductions in the double-transgenic group. We aimed to test the concern that the variability in IPSC reduction was a function of initial IPSC amplitude. If nigrostriatal terminals were responsible for a consistent amount of inhibition to SPNs, we would expect IPSC amplitude and percentage reduction to be positively correlated, as larger IPSCs that rely more on interneurons and would be reduced more by HR3.0. Conversely, if interneurons were responsible for a consistent amount of inhibition to SPNs, we would expect IPSC amplitude and percentage reduction to be negatively correlated, as larger IPSCs that rely more on nigrostriatal terminals would be reduced less by HR3.0. Because the ChR2-induced IPSC exhibits a strong and long-lasting paired-pulse depression (Nelson et al., 2014), we used the initial IPSC amplitudes from each SPN to describe the maximal response. There was no correlation between initial amplitude and percentage reduction (fast-peak slope =  $-0.025$ ,  $r^2 = -0.035$ ; slow-peak slope =  $-0.029$ ,  $r^2 = -0.020$ ; Pearson's product-moment correlation; Fig. 5 A, B). Therefore, we assume that the variability of IPSC reduction is due to variable interneuron control by HR3.0. It is also possible that the lack of correlation reflects the scenario in which relative contributions of interneurons and nigrostriatal terminals vary independently of each other and IPSC amplitude, but even in this case, the strong average HR3.0-mediated IPSC reduction is proof that the interneuron source accounts for a large part of the inhibition, for both small

and large IPSCs.

Although there was a large range in percentage reduction for both the fast-peak responses and the slow-peak responses, we were unsure what the relationship between them was. Both fast- and slow-peak responses contain varying contributions from GABA<sub>A</sub> fast and slow sources, depending on the SPN. If there were SPNs in which one component was reduced much more than the other (Fig. 3A), this would indicate that GABA<sub>A</sub> fast and slow inhibitory sources are being suppressed independently by HR3.0. Contrary to this notion, we found a significant correlation between fast- and slow-peak reduction (Fig. 4C;  $r^2 = 0.86$ , slope = 0.636,  $p < 0.01$ ; Pearson's product-moment correlation). This suggests that although there are distinct sources of this inhibition, their decoupling from the cholinergic circuit may occur through a common mechanism.

## Discussion

By hyperpolarizing populations of striatal interneurons with HR3.0, we were able to reduce both the fast and slow components of cholinergic-mediated GABAergic inhibition in SPNs in a fast and reversible manner, causally demonstrating an interneuronal source of this inhibition. However, the rate of reduction was highly variable among SPNs, with some exhibiting no reduction and others up to 79.6% reduction for the fast peak and 90.5% reduction for the slow peak. This high ceiling of the reduction indicates that interneurons are the primary source of this cholinergic-induced inhibition under these conditions. As there are fewer interneurons per SPN than nigrostriatal terminals per SPN, we expect a greater variability for the interneuronal contribution based on which interneurons are

successfully decoupled from the circuit by HR3.0.

If the inhibition originates mostly from interneurons targeted in the Htr3a-Cre mouse, why did this paradigm sometimes fail? Incomplete or absent reduction of the IPSC can be ascribed to several technical failures. First, it is clear that not all interneurons responsible for generating ACh-linked IPSCs are targeted in the Htr3a-Cre mouse. For example, TH interneurons are not targeted in this Cre mouse, and provide powerful inhibition of SPNs as well as receive strong excitation via nicotinic receptors (Luo et al., 2013; Ibáñez-Sandoval et al., 2015). Striatal NPY-PLTS interneurons are also not targeted in the Htr3a-Cre mouse (Faust et al., 2015). Among the GABAergic interneurons that are targeted, the magnitude of the IPSC reduction is likely a function of both transfection efficiency, as well as the location of SPNs within the transfection field. Last, failure of HR3.0-induced hyperpolarization to completely prevent action potential initiation and subsequent GABA release would result in an incomplete reduction of the IPSC. If we assume that nigrostriatal terminals produce a consistent inhibition among SPNs, then the maximal reduction we were able to produce in our preparation represents the minimal contribution from GABAergic interneurons.

How can these results and interpretations be reconciled with the notion that release of GABA from nigrostriatal terminals also inhibits SPNs in the same manner? If there were a large, consistent nigrostriatal contribution, we would have expected a lower ceiling of IPSC reduction, rather than the 80–90% we observed. Some divergence in results may derive from the different ChR2 expression levels in the ChAT-ChR2 mouse used in this study versus the viral expression under ChAT-Cre targeting (English et al., 2012; Nelson et al., 2014). In our preparation, CINs consistently fired action potentials upon blue light

stimulation. Yet if Chr2-mediated acetylcholine release is different between these two preparations, this may affect the amount of nigrostriatal GABA release and additionally explain the differences in IPSC amplitudes observed. Perhaps most important to our preparation, nigrostriatal dopamine neurons load GABA by a non-canonical mechanism and display a strong synaptic rundown of GABAergic inhibition (Tritsch et al., 2012, 2014), that is well outside of the range of their autoreceptor-mediated depression of dopamine release (Phillips et al., 2002). Taking these differences into account, it is likely that the recovery time of vesicular GABA may be much longer than that observed for dopamine or for other inhibitory synapses in the striatum (Planert et al., 2010). In our hands, the use of Chr2.0-eYFP and blue light for locating the transfection field may have depleted the nigrostriatal vesicular pool of GABA for the duration of these experiments. Another potential explanation of these differences may be that nigrostriatal deletion or depletion alters the strength of the disynaptic interneuronal circuits in a rapid manner, similar to that observed in SPN–SPN connections (Taverna et al., 2008).

The reductions in the GABA<sub>A</sub> fast-peak amplitude and latency came as a surprise to us, considering we did not believe that any striatal interneurons targeted in Htr3a-Cre transgenic fit the criteria necessary to be a major source of this inhibition. These criteria include a strong inhibition of SPNs and a DH $\beta$ E-sensitive suprathreshold input from CINs. The FAI, which is targeted in the Htr3a-Cre mouse, is excited by cholinergic activation, but as a population is not DH $\beta$ E-sensitive, and exhibits on average a low release probability, low-amplitude IPSC at the SPN cell body (Faust et al., 2015). The other novel interneurons targeted in the Htr3a-Cre resembled TH interneurons, but similarly did not fit the criteria (Faust et al., 2015). If none of these neurons are responsible for the fast component of the

inhibition, why was it reduced?

Our results indicate that a source of the fast inhibition is not only being reduced by HR3.0 activation but that these sources' increased latency to fire action potentials in response to ChAT-ChR2 activation is the result of an outward current in those interneurons not always strong enough to prevent action potentials but only to delay them. The two sources for this outward current could be either a polysynaptic disinhibitory circuit or electrical synapses between interneurons. This unknown synaptic source would also be the candidate for the reduction of the fast component of the IPSC.

This study verifies that striatal GABAergic interneurons are responsible for cholinergic-induced inhibition of SPNs under our *ex vivo* conditions. Although these interneuronal sources are incompletely described and relatively rare (Ibáñez-Sandoval et al., 2011), they provide a majority of the inhibition to SPNs from CINs. If these results did not demonstrate this, it could be argued that this unique excitatory input to rare GABAergic interneurons is an oddity non-integral to normal striatal function. An extension of these results implies that striatal cholinergic circuits have complex machinery and operate in a semiautonomous manner from cortical control. We suggest that the characteristic brief firing rate changes of CINs that are associated with stimuli of innate and learned significance may be transmitted with high fidelity to projection neurons through nicotinic control of the activity of specialized classes of GABAergic interneurons.

## References

- Bennett BD, Bolam JP (1994) Synaptic input and output of parvalbumin-immunoreactive neurons in the neostriatum of the rat. *Neuroscience* 62:707–719.
- Cachope R, Mateo Y, Mathur BN, Irving J, Wang HL, Morales M, Lovinger DM, Cheer JF (2012) Selective activation of cholinergic interneurons enhances accumbal phasic dopamine release: setting the tone for reward processing. *Cell Rep* 2:33–41.
- English DF, Ibáñez-Sandoval O, Stark E, Tecuapetla F, Buzsáki G, Deisseroth K, Tepper JM, Koós T (2012) GABAergic circuits mediate the reinforcement-related signals of striatal cholinergic interneurons. *Nat Neurosci* 15:123–130.
- Faust TW, Assous M, Shah F, Tepper JM, Koós T (2015) Novel fast adapting interneurons mediate cholinergic-induced fast GABAA inhibitory postsynaptic currents in striatal spiny neurons. *Eur J Neurosci* 42:1764–1774.
- Gerfen CR, Paletzki R, Heintz N (2013) GENSAT BAC Cre-recombinase driver lines to study the functional organization of cerebral cortical and basal ganglia circuits. *Neuron* 80:1368–1383.
- Gittis AH, Nelson AB, Thwin MT, Palop JJ, Kreitzer AC (2010) Distinct roles of GABAergic interneurons in the regulation of striatal output pathways. *J Neurosci* 30:2223–2234.
- Gittis AH, Leventhal DK, Fensterheim BA, Pettibone JR, Berke JD, Kreitzer AC (2011) Selective inhibition of striatal fast-spiking interneurons causes dyskinesias. *J Neurosci* 31:15727–15731.
- Goldberg JA, Reynolds JN (2011) Spontaneous firing and evoked pauses in the tonically active cholinergic interneurons of the striatum. *Neuroscience* 198:27–43.
- Goldberg JA, Ding JB, Surmeier DJ (2012) Muscarinic modulation of striatal function and circuitry. *Handb Exp Pharmacol* 208:223–241.
- Ibáñez-Sandoval O, Tecuapetla F, Ünal B, Shah F, Koós T, Tepper JM (2011) A novel functionally distinct subtype of striatal neuropeptide Y interneuron. *J Neurosci* 31:16757–16769.
- Ibáñez-Sandoval O, Xenias HS, Tepper JM, Koós T (2015) Dopaminergic and cholinergic modulation of striatal tyrosine hydroxylase interneurons. *Neuropharmacology* 95:468–476.
- Kita H (1996) Glutamatergic and GABAergic postsynaptic responses of striatal spiny neurons to intrastriatal and cortical stimulation recorded in slice preparations. *Neuroscience* 70:925–940.
- Kita H, Kosaka T, Heizmann CW (1990) Parvalbumin-immunoreactive neurons in the rat neostriatum: a light and electron microscopic study. *Brain Res* 536:1–15.

- Koós T, Tepper JM (1999) Inhibitory control of neostriatal projection neurons by GABAergic interneurons. *Nat Neurosci* 2:467–472.
- Koós T, Tepper JM, Wilson CJ (2004) Comparison of IPSCs evoked by spiny and fast-spiking neurons in the neostriatum. *J Neurosci* 24:7916–7922.
- Luo R, Janssen MJ, Partridge JG, Vicini S (2013) Direct and GABA-mediated indirect effects of nicotinic ACh receptor agonists on striatal neurones. *J Physiol* 591:203–217.
- Mallet N, Le Moine C, Charpier S, Gonon F (2005) Feedforward inhibition of projection neurons by fast-spiking GABA interneurons in the rat striatum in vivo. *J Neurosci* 25:3857–3869.
- Nelson AB, Hammack N, Yang CF, Shah NM, Seal RP, Kreitzer AC (2014) Striatal cholinergic interneurons drive GABA release from dopamine terminals. *Neuron* 82:63–70.
- Phillips PE, Hancock PJ, Stamford JA (2002) Time window of autoreceptor-mediated inhibition of limbic and striatal dopamine release. *Synapse* 44: 15–22.
- Planert H, Szydlowski SN, Hjorth JJ, Grillner S, Silberberg G (2010) Dynamics of synaptic transmission between fast-spiking interneurons and striatal projection neurons of the direct and indirect pathways. *J Neurosci* 30:3499–3507.
- Ramanathan S, Hanley JJ, Deniau JM, Bolam JP (2002) Synaptic convergence of motor and somatosensory cortical afferents onto GABAergic interneurons in the rat striatum. *J Neurosci* 22:8158–8169.
- Rudkin TM, Sadikot AF (1999) Thalamic input to parvalbumin-immunoreactive GABAergic interneurons: organization in normal striatum and effect of neonatal decortication. *Neuroscience* 88:1165–1175.
- Sidibé M, Smith Y (1999) Thalamic inputs to striatal interneurons in monkeys: synaptic organization and co-localization of calcium binding proteins. *Neuroscience* 89:1189–1208.
- Sullivan MA, Chen H, Morikawa H (2008) Recurrent inhibitory network among striatal cholinergic interneurons. *J Neurosci* 28:8682–8690.
- Szydlowski SN, Pollak Dorocic I, Planert H, Carlén M, Meletis K, Silberberg G (2013) Target selectivity of feedforward inhibition by striatal fast-spiking interneurons. *J Neurosci* 33:1678–1683.
- Taverna S, Ilijic E, Surmeier DJ (2008) Recurrent collateral connections of striatal medium spiny neurons are disrupted in models of Parkinson's disease. *J Neurosci* 28:5504–5512.
- Tepper JM, Koós T (2016) Striatal GABAergic interneurons. In: *Handbook of basal*

ganglia structure and function, Ed 2 (Steiner H, Tseng K, eds.), in press.

Threlfell S, Lalic T, Platt NJ, Jennings KA, Deisseroth K, Cragg SJ (2012) Striatal dopamine release is triggered by synchronized activity in cholinergic interneurons. *Neuron* 75:58–64.

Tritsch NX, Ding JB, Sabatini BL (2012) Dopaminergic neurons inhibit striatal output through non-canonical release of GABA. *Nature* 490:262–266.

Tritsch NX, Oh WJ, Gu C, Sabatini BL (2014) Midbrain dopamine neurons sustain inhibitory transmission using plasma membrane uptake of GABA, not synthesis. *Elife* 3:e01936.

Zhao S, Ting JT, Atallah HE, Qiu L, Tan J, Gloss B, Augustine GJ, Deisseroth K, Luo M, Graybiel AM, Feng G (2011) Cell-type specific optogenetic mice for dissecting neural circuitry function. *Nat Methods* 8:745–752.

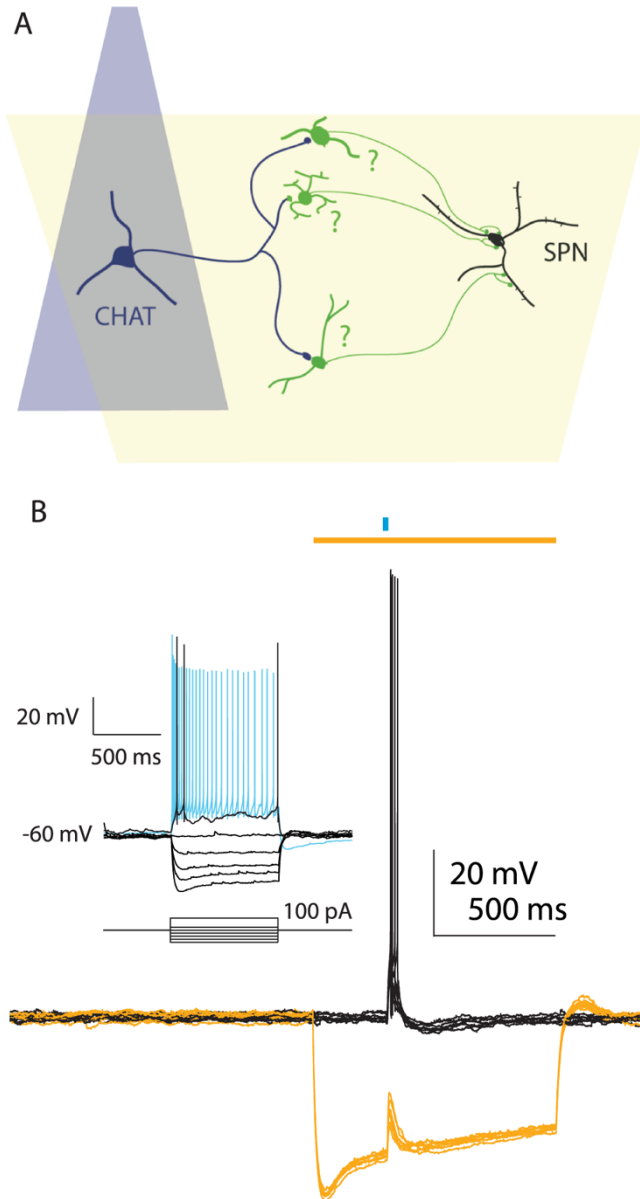


Figure 1. Schematic for examining interneuronal contributions to cholinergic-induced inhibition. A. Diagram of tissue from double transgenic animals in which cholinergic interneurons (CHAT, dark blue) are activated with a focal blue LED and Htr3a-Cre interneurons (green) are inhibited with a wide angle yellow LED (yellow). B. Example of decoupling an interneuron from the nicotinic circuit. Blue bar at top: 2 ms blue LED stimulus, yellow bar at top: 1 s yellow LED stimulus. Activation of CINs produces nicotinic EPSP and action potentials in the fast-adapting interneuron (black traces).

Concurrent inhibition with yellow light hyperpolarizes neuron and prevents EPSP from reaching spike threshold (yellow traces). Inset: current-voltage responses of the HR3.0-expressing fast-adapting interneuron.

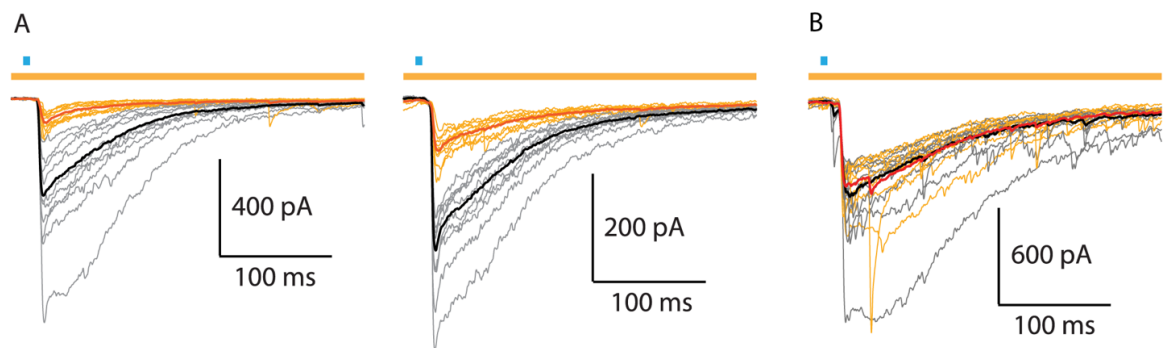


Figure 2. Cholinergic-induced inhibition in SPNs before and after inhibition of Htr3a-Cre interneurons. A. Voltage clamp recordings of SPNs from Db1 Tgn mice following cholinergic activation. Blue bar at top: 1-2 ms blue LED stimulus, yellow bar at top: 1 s yellow LED stimulus. Thin gray traces represent individual control trials following blue LED pulse. Thin yellow traces represent individual HR3.0 trials during simultaneous blue and yellow LED pulses. These two trial types were acquired on an alternating schedule. Black traces represent average of control trials (n=9, excluding first trial). Red traces represent average of HR3.0 trials (n=10). B. Voltage clamp recording of SPN from single transgenic ChAT-ChR2 mouse following cholinergic activation, using the same color scheme used as in A. Note the lack of IPSC reduction during yellow LED pulses.

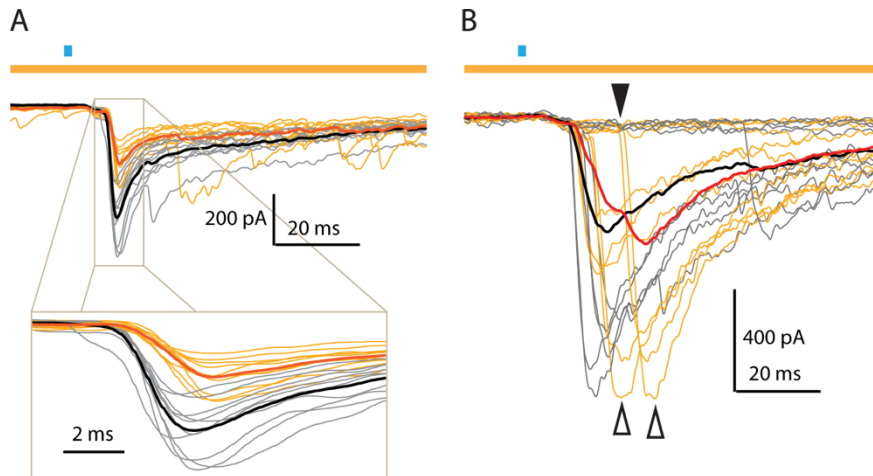


Figure 3. Inhibition of Htr3a-Cre interneurons delays cholinergic-induced IPSC. A. Example SPN from Dbl Tgn mouse, using same color scheme as in Figure 2. Note that the main effect of HR3.0 in this neuron was the reduction of the fast component and the delay in its onset and peak, observable in the inset. B. Example SPN from Dbl Tgn mouse, using same color scheme as in Figure 2. Note the increased delay of IPSC onset (black arrow) and peak (white arrows) primarily on HR3.0 trials. Note also the failures experienced by this SPN on both trial types, indicative of unitary sources (individual neurons) failing to fire action potentials.

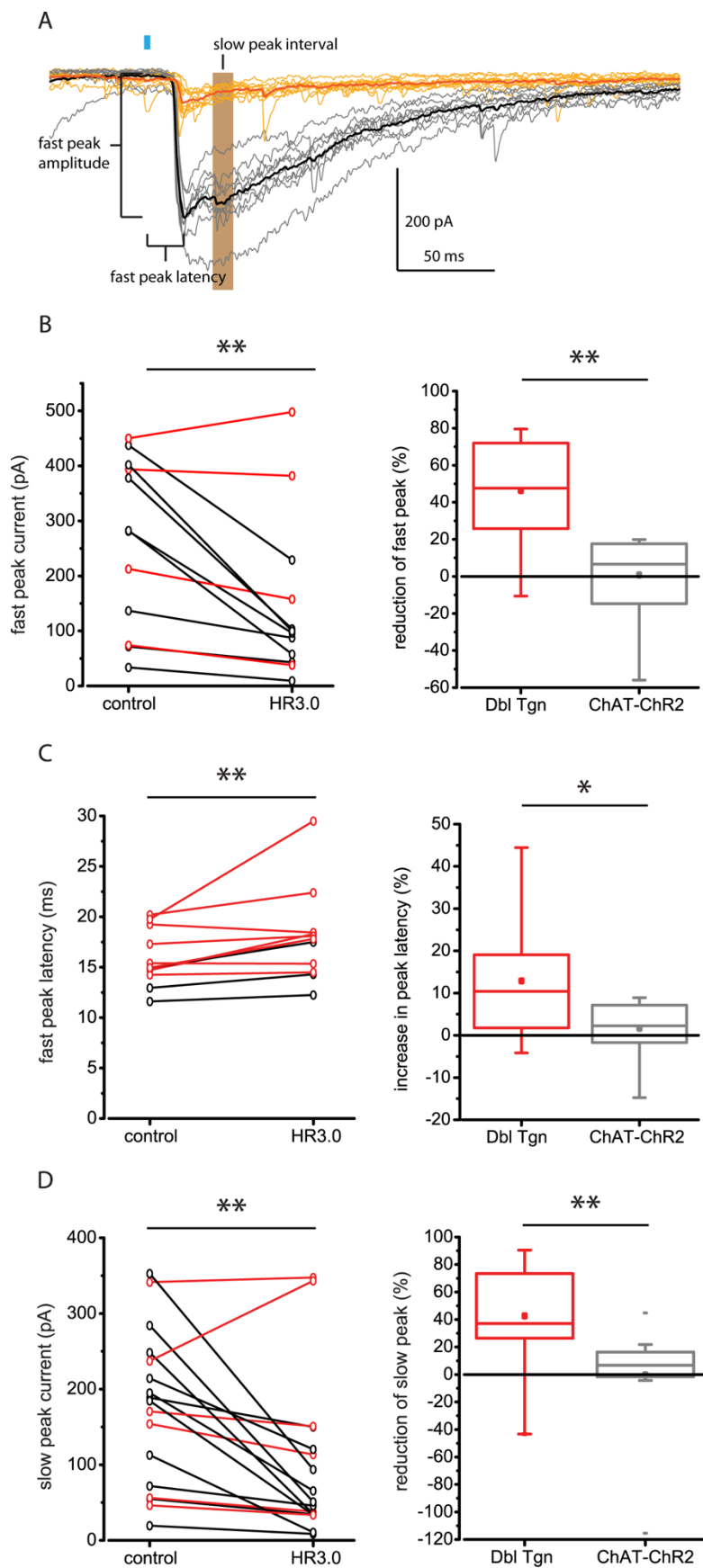


Figure 4. Statistical analysis of HR3.0 effect on IPSC kinetics. A. Example voltage clamp recording of SPN from Dbl Tgn mouse as in Figure 2, following the same color scheme. For this SPN, note the presence of both GABA<sub>A</sub> fast and GABA<sub>A</sub> slow peaks for the control traces (black, gray). The IPSC fast peak amplitude, latency and slow peak interval used to quantify IPSC amplitude and delay are detailed. Blue bar: 2 ms blue LED stimulus. B-D. Left panels: within-group examination of HR3.0 effect on IPSC amplitude and latency for individual Dbl Tgn SPNs. Black traces represent average responses in SPNs where HR3.0 significantly affected the IPSC amplitude or latency ( $p < 0.05$ , paired sample t-test or paired sample Wilcoxon signed rank test of individual control and HR3.0 trials, such as the thin gray and yellow traces in A). Red traces represent average responses in SPNs where HR3.0 failed to do so ( $p > 0.05$ ). \*\*  $p < 0.01$ , paired sample wilcoxon signed rank test, using average responses for each SPN. Right panels: between-group examination of normalized % IPSC reduction or delay in SPNs from Dbl Tgn mice or single transgenic ChAT-ChR2 control mice. Box plot bars represent minimum (bottom attached bar), Q1 (box bottom), Q2 (middle line), Q3 (box top), and maximum values (top attached bar. Mean represented by central dot. Detached bars represent outliers (values lesser or greater than  $Q1, Q3 \pm 1.5$  IQR). Note the large range in slow and fast peak IPSC reduction for the Dbl Tgn group. \*\*  $p < 0.01$ , Mann-Whitney test, \*  $p < 0.05$ , two sample t-test.

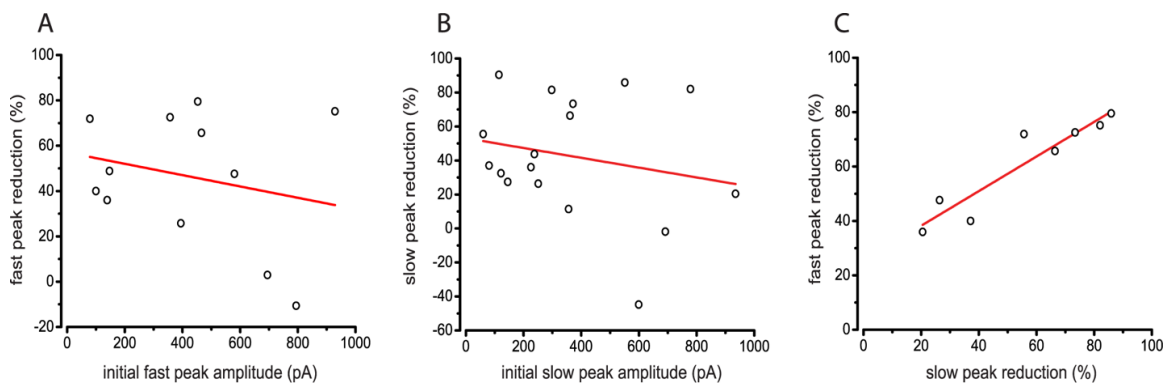


Figure 5. Relationship between IPSC reduction and amplitude. A. Correlation between the IPSC first acquired trace (largest gray traces, Figure 2a) and percent reduction for the fast peak. B. Correlation between the IPSC first acquired trace (largest gray traces, Figure 2a) and percent reduction for the slow peak. Although there are negative trends in both A and B, no significant correlations were observed. C. Correlation between fast peak and slow peak percent reduction for all SPNs exhibiting significant reductions in at least one of these two components. Note the strong linear correlation between these two responses.

CHAPTER 4:

Neostriatal patch and matrix neurons differentially encode reward  
prediction

Thomas W. Faust, Charles R. Gerfen and Tibor Koós

Center for Molecular and Behavioral Neuroscience, Rutgers University, Newark, New  
Jersey 17102

## Abstract

The neostriatal patch occupies a unique position in the striatum in that its projection neurons alone monosynaptically innervate dopaminergic neurons of the SNc. Given its distinct anatomical differences from the matrix and reciprocal connections with SNc dopaminergic neurons, the patch may play a key role in controlling the phasic dopaminergic representation of behavioral events. Therefore, we sought to characterize the synaptic inputs from the patch to SNc dopaminergic neurons and determine the coding of prediction-based behavioral sequences by patch SPNs. We observed that in the SepW1\_NP67 BAC transgenic line, SPNs in the patch were selectively targeted compared to the matrix, but that some striatal interneurons were targeted as well. Stimulation of patch axons in the substantia nigra produced a mixed GABA<sub>A</sub> and GABA<sub>B</sub> inhibition in dopaminergic neurons but only GABA<sub>A</sub> inhibition in GABAergic neurons. During a prediction-based instrumental task in which SNc dopaminergic neurons were observed to encode reward prediction error, a subset of both patch and matrix SPNs produced large responses immediately prior to and after reward delivery or reward omission, with no differences between these two trial types. Patch SPNs responded more selectively to the UCS of specific trial types (fixed or variable), while matrix SPNs had more similar responses for both trial types. We believe that these responses from patch SPNs may constitute a prediction signal with which dopaminergic neurons suppress reward-associated responses and successfully encode RPE.

## Significance Statement

The neostriatal patch and matrix compartments have been known to have different afferent and efferent targets for decades, yet their respective roles in executing the limbic and motor functions of the striatum have remained obscure. As the patch inhibits midbrain dopamine neurons, it may control dopaminergic encoding of rewarding stimuli. Using transgenic mice and optogenetic identification of patch neurons, we were able to distinguish how patch and matrix neurons encode behavioral stimuli in comparison to dopaminergic neurons. The coding of patch neurons to predicted reward events suggests that they have a role in generating the prediction-based coding of dopaminergic coding.

## Introduction

Survival and reproductive success of animals depends on the ability to seek, predict and successfully exploit resources in an environment. Dopaminergic neurons of the ventral midbrain have long been thought of as a critical node for limbic networks, controlling behaviors of motivation, incentive salience, reward-seeking, and reward learning (Wise, 2004; Berridge, 2007; Palmiter, 2008; Bromberg-Martin et al., 2010; Salamone and Correa, 2012). These neurons encode reward prediction errors (RPE) to behaviorally-relevant appetitive stimuli (Schultz, 1998), responding to better than expected outcomes by firing bursts and worse than expected outcomes by brief pauses in firing. Disruption of the normal phasic dopaminergic coding pattern has profound consequences for reinforcement learning (Zweifel et al., 2009; Tsai et al., 2009; Kim et al., 2012; Steinberg et al., 2013; Sharpe et al., 2017; Chang et al., 2016), indicating that some of the behavioral functions of dopaminergic neurons are mediated through these phasic signals.

The RPE coding pattern of dopaminergic neurons and the circuit mechanisms which both control it and in turn are influenced by it can be examined in the context of the temporal difference learning model (TD model) (Sutton and Barto, 1981; Schultz et al., 1997). Based on these assumptions, the RPE coding of midbrain dopaminergic neurons requires afferent sources of both prediction and outcome information. Neuronal sources representing reward prediction are expected to receive dopamine input, undergo experience-dependent synaptic remodeling that is dopamine-sensitive, and transmit a prediction signal to dopaminergic neurons around the time of outcome. Under a most simple hypothetical scenario, as animals receive predictable rewards, the reward-associated phasic dopamine signal would induce synaptic plasticity in the downstream structure representing prediction, which would then, over the course of many predictable trials, provide increasing inhibition to dopaminergic neurons around the time of reward until the reward-associated dopamine signal has been reduced, as is observed experimentally (Ljungberg et al., 1992; Mirenowicz and Schultz, 1994; Hollerman et al., 1998).

If this model accurately describes how RPE coding is generated in dopaminergic neurons, the striatum may represent the best source of input representing reward prediction, due to its massive dopaminergic innervation, dopamine-dependent synaptic plasticity (Reynolds et al., 2001; Shen et al., 2008; Yagishita et al., 2014), and monosynaptic or multisynaptic inhibition of dopaminergic neurons. Within the striatum, the spiny projection neurons (SPNs) of the striatal patches are perhaps the best candidates to transmit this prediction signal, due to their reciprocal monosynaptic connections with substantia nigra pars compacta (SNc) dopaminergic neurons and the lateral habenula (LHb)-projecting

entopeduncular nucleus (EP) (Gerfen, 1984; Gerfen, 1985; Rajakumar et al., 1993; Fujiyama et al., 2011; Wallace et al., 2017). As these recipient and downstream structures all produce RPE signals (Bromberg-Martin and Hikosaka, 2011; Stephenson-Jones et al., 2016), they may share a common source of prediction input in the patch.

Striatal SPNs have been repeatedly characterized to be active around the time of reward (Jog et al., 1999; Schmitzer-Torbert and Redish, 2004; Gage et al., 2010). Yet based on this limited information, we have not known whether these responses were due to reward delivery, expectation, or perhaps a coincident behavioral event such as the termination of a motivated action. Similarly, we have not known the identity of recorded SPNs active at these epochs, whether striatonigral or striatopallidal, patch or matrix. Selective targeting of the patch has recently become experimentally feasible with the development of new transgenic mouse lines (Gerfen et al., 2013; Crittenden et al., 2016). Here we attempt to identify the synaptic inputs from the neostriatal patches to SNc dopaminergic neurons, and determine how patch SPNs encode behavioral events in the context of normal RPE coding by dopaminergic neurons. For patch neurons to successfully encode a prediction signal, we expect that they should similarly encode reward prediction despite differing outcomes, in behaviors where SNc dopaminergic neurons encode deviations from predicted outcomes.

## Materials and Methods

### **Animals**

All procedures used in this study were performed in accordance with the National Institute of Health's Guide for the Care and Use of Laboratory Animals and also in accordance with

the Rutgers University institutional animal care and use committee. NP67 mice (Tg(SepW1-Cre)NP67Gsat/Mmucd, University of Davis) (Gerfen et al., 2013) and double transgenic NP67 x Rosa26/stop/EGFP mice were maintained and used as hemizygotic, and housed in groups of up to four per cage with ad libitum access to food and water. During training and recording mice were kept on a reverse light cycle (dark period from 10:00 A.M.–10:00 P.M.), and trained and recorded during the dark cycle. A total of 24 NP67 mice, one NP67 x Rosa26/stop/EGFP mouse, and 3 wild type mice were used, including males and females.

### **Intracerebral virus injection**

All virus injections were conducted with BSL-2 precautions within a biosafety cabinet. Mice were anesthetized with isoflurane (1.5–3%, delivered with O<sub>2</sub>, 1 L/min) and placed into a stereotaxic frame. A subcutaneous injection of bupivacaine was administered prior to scalp incision and retraction. 1.0 µl AAV5-EF1a-DIO-hChR2(H134R)-EYFP or AAV5-FLEX-CAG-tdtomato (UNC Vector Core) was injected into dorsal neostriatum at the following coordinates (from bregma): +0.5 mm AP, +2.25 mm ML, –3.35 mm DV, which transfected almost all of dorsolateral striatum while greatly limiting or excluding transfection of cortex. Injections were performed using glass pipettes pulled and cut to an inner diameter of 30–40 µm and an outer diameter of 50–60 µm. Virus was injected at a rate of 4.6 nL/5 s with Nanoject II Auto-Nanoliter Injector (Drummond Scientific Company). Following viral injection, mice were treated with 10 mg/kg enrofloxacin (Baytril) to prevent infection. For analgesia, mice were treated with 5mg/kg ketoprofen daily and 0.1mg/kg buprenorphine every 12 hours, for three days during which they were closely monitored. Following surgery, mice were allowed to recover and viral transgene

was allowed to express for a period of at least 3 weeks before microelectrode drive implantation and 4 weeks before slice preparation.

### **Slice preparation and in vitro whole-cell recording**

Mice were aged 4-8 months prior to slice preparation. Mice were deeply anesthetized with 150/25 mg/kg ketamine/xylazine, i.p. Slices were prepared as detailed in (Faust et al., 2014), with the exception that all slices were cut using a Leica VT1200S, recovered in normal external solution containing 2.4 mM  $\text{Ca}^{2+}$ , and recorded in normal external solution containing 1.2 mM  $\text{Ca}^{2+}$ . Pipettes typically exhibited a DC impedance of 2-3 M $\Omega$  prior to formation of cell membrane seal. All cells were recorded with normal internal solution. Unless otherwise stated cells recorded in voltage clamp were held at -45 mV.

### **Immunohistochemistry**

Mice were deeply anesthetized with 150/25 mg/kg ketamine/xylazine, i.p. Brain fixation was accomplished by transcardial perfusion of 20 mL of ice-cold artificial cerebrospinal fluid (adjusted to pH 7.2–7.4), followed by 90–100 mL of 4% (w/v) paraformaldehyde, 15% (v/v) picric acid in phosphate buffer. Brains were extracted and post-fixed overnight in the same fixative solution at 4 °C. Fixed tissue was cut into 50–60  $\mu\text{m}$  thick sections using a Vibratome 1500 (The Vibratome Company). Sections were incubated in 10% (v/v) methanol, 3% (v/v) hydrogen peroxide in phosphate-buffered saline (PBS), followed by 1% (w/v) sodium borohydride in PBS. Sections were blocked in 10% (v/v) normal donkey or goat serum, 3% (w/v) bovine serum albumin, and 0.5% (v/v) Triton X-100 in PBS overnight at 4 °C. Sections were incubated in the following secondary antibodies overnight at 4 °C: mouse anti-calbindin, 1:1500 (Sigma, catalog #C8666), rabbit anti-neuropeptide-Y (NPY), 1:1000 (Abcam, catalog #Ab30914), rabbit anti-parvalbumin (PV), 1:1500

(Immunostar, catalog #24428), rabbit anti-tyrosine hydroxylase (TH), 1:1500 (Millipore, catalog #ab152). For calbindin staining, sections were incubated in 1:400 goat anti-mouse Alexa Fluor® 594 (Life Technologies, catalog #R-37121) overnight at 4 °C. For NPY and PV staining, sections were incubated in 1:500 donkey anti-rabbit Alexa Fluor® 488 (Life Technologies, catalog #A-21206) overnight at 4 °C. For TH staining, sections were incubated in 1:500 donkey anti-rabbit Alexa Fluor® 594 (Life Technologies, catalog #A-11032) overnight at 4 °C. Sections were mounted with Vectashield (Vector Laboratories), and imaged using an Olympus Fluoview 1000 laser scanning confocal System (Olympus).

### **Behavior**

Mice were maintained on water restriction for a maximum of 6 days/week during shaping, training and recording, during which they consumed liquid only during performance of the behavior, unless they failed to consume 1 mL of sucrose during a session, after which they were allowed 1 hour of ad libitum water. Mice were shaped, trained and recorded in a custom built 16 x 75 cm corridor with a central nosepoke and two reward ports at either end of the corridor (see Fig 3). Control of the behavioral apparatus was accomplished by FPGA (Digilent) with custom programs for the various stages of shaping and training. Mice were shaped to initiate trials by nosepoking into the central nosepoke, which produced either a high tone (6.7 kHz) or a low tone (2.2 kHz, pulsed at 50 Hz). Following trial initiation mice would collect single small rewards (20 µL, 10% sucrose) at a single reward port paired with the given tone. After several sessions mice learned to successfully execute this behavioral sequence in rapid succession. Training then began by presenting either tone pseudorandomly on half of the trials following nosepoke and allowing the mice to choose to enter either port. Correct port entry was rewarded and incorrect port entry was not.

During these first sessions the nosepoke wait duration time was gradually increased to 400 ms. Over multiple sessions mice increased their correct choices following successful trial initiation. Once performance on both trial types exceeded 80% for at least three consecutive sessions, one trial type was switched from a fixed schedule reward of 20  $\mu$ L to a 50% variable schedule reward of 40  $\mu$ L. At this final stage of training the fixed trials were presented on 33 percent of trial initiations and the variable trials on 67 percent, pseudorandomly. This generated an equal distribution of three trial types, fixed reward delivery, variable reward delivery, and variable reward omission. The sides of tone and trial type were counterbalanced amongst the mice.

### **Multi-tetrode and fiberoptic drive fabrication and implantation**

Moveable multitetrode drives based on a custom design were fabricated from acrylic and brass construction using a MicroMill DSLS 3000 (MicroProto Systems). Eight tetrodes were attached to the drive in a circular pattern around a stationary fiberoptic using polyimide coated capillary tubing (Polymicro Technologies), for an array diameter of 500  $\mu$ m. 20  $\mu$ m tungsten tetrode wire was used for tetrode recordings in the substantia nigra, while 12.7  $\mu$ m wire was used for tetrode recordings in the dorsal striatum (California fine wire). Tetrodes were electroplated in 2:1 1% (v/v) polyethylene glycol 8000:gold plating solution (Neuralynx) (Ferguson et al., 2009), to a final impedance of 30-40 k $\Omega$ . The central fiberoptic (Thorlabs) was etched in hydrofluoric acid to a tapered fiber tip, polished, and mounted into the center of the tetrode array at the same initial depth as the tetrode tips. Mice were anesthetized with isoflurane (1.5–3%, delivered with O<sub>2</sub>, 1 L/min) and placed into a stereotaxic frame. A subcutaneous injection of bupivacaine was administered prior to scalp incision and retraction. The skull surface was cleaned using 10% (v/v) hydrogen

peroxide and a combination of metabond (Parkell) and dental cement (A-M Systems) were used to mount the multitetrode drive to the skull. Drive weight including dental cement was 1.5-2.0 g. The ground screw was threaded into a craniotomy on the frontal bone in contact with the surface of the brain, while the reference screw was threaded into a craniotomy on the occipital bone in contact with the surface of the cerebellum. Tetrodes were lowered into a craniotomy of the same coordinates as the virus injection, to an initial depth of 1.5 mm. The dura mater was removed for this craniotomy, and following drive implantation the exposed craniotomy was filled with silicone gel as artificial dura (Dow Corning, 3-4680 Silicone gel kit). Conductive tape was used to create a mechanical and electrical barrier against disturbances, and was connected to the ground screw on the frontal bone and the ground on the printed circuit board to which the headstage connected. Following multielectrode drive implantation, mice were treated with 10 mg/kg enrofloxacin (Baytril) to prevent infection. For analgesia, mice were treated with 5mg/kg ketoprofen daily and 0.1mg/kg buprenorphine every 12 hours, for three days during which they were closely monitored. Mice were allowed to recover for a week prior to resuming behavior and beginning to record neural signals.

### **In vivo recording**

Neural activity was recorded using a unitary gain headstage amplifier (Plexon) connected to a programmable amplifier (RC Electronics Inc.) for a combined 1,000-10,000x amplification in open band (1Hz-20 kHz). Signals were recorded at 31.25 kHz referenced to the ground screw implanted above cerebellum using custom software in Igor (WaveMetrics). Behavioral events (nosepokes, reward port entry) were detected by IR beam detection (Med Associates) and transmitted from the FPGA to the acquisition

computer. Optogenetic detection of neurons was accomplished with a series of 50 laser pulses (20 ms) delivered every three seconds several minutes prior to the start of behavior. Tetrodes were advanced at 40  $\mu\text{m}$  steps, from an initial depth of 1500  $\mu\text{m}$  to a final depth of up to 3000  $\mu\text{m}$ . Tetrodes would be advanced at a maximum of 80  $\mu\text{m}/\text{day}$  during the search for cells of interest.

### **Analysis and statistics**

Acquired tetrode recordings were re-referenced to median values to remove common mode noise using custom written code in C++. Noise introduced in some mice from the piezoelectric buzzers was reduced with a masking algorithm using custom written code in Python. Spikes were detected and clustered using Klustakwik (Kenneth Harris). Using custom written software in Igor (WaveMetrics), clusters of spikes were then combined and compared to nearby clusters to select well isolated units which displayed clear moats in principal component space, and no cross-correlation with neighbors. These units usually had spike amplitudes of at least 200  $\mu\text{V}$ . Putative SNc dopaminergic units were identified by their long, multiphasic spike waveforms, tonic firing rates between 2 and 9 Hz, and decreases in tonic firing rate after 0.5mg/kg quinpirole i.p. SPNs were identified by their long spike waveforms, low firing rates, and bursty autocorrelogram. Putative patch SPNs were optogenetically identified using 20 ms laser pulses delivered prior to the start of behavior. Responsive units fired well above their baseline firing rates to a maximal rate of 200 Hz, although multiple light-responsive neurons at a tetrode had the effect of contaminating spike waveforms and artificially reducing light-evoked firing in many units. Putative matrix units were identified as SPN units unresponsive to laser pulses that were recorded in the transfection field, here defined as the tetrode path between the first and last

optogenetically identified units. In 4/6 NP67 mice, a minority of the putative FSI units that exhibited fast spike waveforms and high tonic firing rates were responsive to laser pulses. These were also used to determine the limits of the transfection field when applicable. Peri-event time histograms were generated in Igor for further analysis. UCS-responsive patch and matrix units were identified by unbiased clustering of the firing rates containing the peak UCS response (k-means). The interval containing the peak UCS response was selected as the PETH between the peaks of the first derivative of the average UCS response. This yielded several groups, the largest of which was firing at or close to 0 Hz during this interval and was discarded from further analysis. Statistics and figures were produced in Matlab (MathWorks).

## Results

At first, we attempted to verify that neostriatal patches were selectively targeted in the NP67 mouse. Viral transfection of dorsal striatum in NP67 mice (AAV5 EF1a DIO ChR2-EYFP) revealed a pattern of targeted neurons clustered in patches (Fig 1a). Counterstaining a NP67 x Rosa26-EGFP mouse for matrix-enriched calbindin determined that these targeted cell groups correspond to the calbindin-poor patches (Fig 1b). In double transgenic mice some extrastriatal areas were targeted, including cortex, but amongst striatal neighbors the globus pallidus (GP) was not targeted (data not shown). In vitro whole cell recording of striatal neurons expressing either ChR2-EYFP or tdTomato revealed targeted neurons of several types. SPNs in the patch, exopatch SPNs in the matrix (Smith et al., 2016), a small number of both fast-spiking interneurons (FSI,  $n = 2$ ) and neuropeptide Y (NPY)-expressing neurogliaform interneurons (NPY-NGF,  $n = 2$ ) were targeted in NP67

mice (Fig 1c). A small fraction of targeted striatal neurons expressed parvalbumin and NPY, respective markers of FSIs and NPY-NGFs (Fig 1d), however in both cases the majority of counterstained interneurons were not targeted, indicating at least for FSIs that not all interneurons of this type are targeted in NP67 mice (Fig 1d, bottom row).

Patch axon fields in the substantia nigra displayed a distinct innervation pattern targeting the ventral dendrites and ventral cell body layer of SNc dopaminergic neurons (Fig 2a). For all subsequent experiments, dorsolateral striatum was targeted as dorsomedial viral transfection innervated only the very ventromedial portion of the SNc and its ventral dendrites (data not shown), perhaps due to a topographic organization of patch projections along the mediolateral axis.

Whole cell recordings of SNc dopaminergic and SNr GABAergic neurons revealed differences in their inhibition by the patch (Fig 2b-h). High frequency stimulation of patch axons generated compound IPSCs composed of GABA<sub>A</sub> and GABA<sub>B</sub> currents in SNc neurons (Fig 2d), while in SNr neurons this stimulus generated only GABA<sub>A</sub> currents (Fig 2e). In several SNr neurons (2/5 attempted) this IPSC was not fully reduced by GABA<sub>A</sub> antagonist bicuculline (10  $\mu$ M). The residual bicuculline-insensitive component was blocked by picrotoxin (100  $\mu$ M). The distributions of GABA<sub>A</sub> IPSC amplitude between SNc and SNr neurons were observably different in two ways. SNr neurons had larger GABA<sub>A</sub> IPSC amplitude than SNc neurons (SNc n = 33, 23.7  $\pm$  42.7 pA median  $\pm$  IQR; SNr n = 13, 239.6  $\pm$  60.1 pA mean  $\pm$  SEM, p = 7.6e-4, z = 3.3666, rank sum = 444, Wilcoxon rank sum test), and while the SNr GABA<sub>A</sub> IPSC was highly variable between neurons, it was normally distributed while the SNc GABA<sub>A</sub> IPSC was not (Figure 2f). GABA<sub>A</sub> IPSCs in SNc neurons had significantly lower reversal potentials than those of

SNr neurons (Fig 2f) (SNc  $n = 8$ ,  $-85.1 \pm 2.3$  mV mean  $\pm$  SEM; SNr  $n = 9$ ,  $-76.5 \pm 1.7$  mV,  $p = 7.4e-3$ ,  $t = 3.0917$ , two sample t-test), indicating a space clamp error and a larger electrotonic distance from the soma to the source of the IPSC in those neurons. GABA<sub>A</sub> and GABA<sub>B</sub> currents in SNc neurons displayed a positively correlated relationship to each other ( $n = 33$ ,  $r = 0.6381$ ,  $p = 6.5e-05$ , Pearson's product moment correlation) (Fig 2h), suggesting that they arise from the same synapses. GABA<sub>B</sub> amplitudes were substantially smaller than GABA<sub>A</sub> amplitudes ( $n = 33$ , GABA<sub>A</sub>,  $23.7 \pm 42.7$  pA median  $\pm$  IQR; GABA<sub>B</sub>,  $20.5 \pm 29.9$  pA median  $\pm$  IQR,  $p = 1.7e-3$ ,  $z = 3.1358$ , rank = 456, Wilcoxon sign rank test). In some SNc neurons inhibition from high frequency stimulation of the patch was strong enough to interrupt the pace-making firing pattern of the neurons (Fig 2i).

Next, we sought to investigate when during motivated behaviors the patch might provide SNc neurons, as well as their other downstream targets, with inhibition that could control their firing patterns. We therefore designed an instrumental task in which patch and matrix SPN coding could be investigated within the context of RPE coding by dopaminergic neurons. In this task, mice initiate trials at a central nosepoke which elicited one of two instructive tones. Entry into the correct reward port for one of the tones resulted in a fixed schedule delivery of a small reward (20 $\mu$ L sucrose) on every trial. For the other tone, correct responses at the reward port resulted in larger rewards (40 $\mu$ L sucrose) delivered at a variable schedule on only half of correct trials (Fig 3a). Excluding errors, this task generated the following three trial types: small fixed reward delivery which corresponds to no RPE, large variable reward delivery which corresponds to positive RPE, and large variable reward omission which corresponds to negative RPE, while the average expected value for either trial is equal. Mice performed slightly better on the variable side

during recording sessions ( $n = 9$ , fixed = 85.2  $\pm$  3.1 percent correct mean  $\pm$  SEM; variable 94.2  $\pm$  1.1 percent correct mean  $\pm$  SEM,  $p = 0.012$ ,  $t = 3.2535$ , paired-sample t-test) (Fig 3b).

Chronic tetrode recordings in the SNc of putative dopaminergic neurons revealed a RPE coding pattern (Fig 4), although there appeared to be some residual phasic response to the fixed reward in some units. The majority of units displayed phasic responses to both variable reward delivery and omission, however, indicating that on average these neurons represented RPE in the context of this behavior. Within the same behavior, we recorded optogenetically-identified patch and matrix SPNs from NP67 mice. Both populations exhibited heterogeneous responses during behavioral sequences, with many units active prior to nosepoke, and smaller subpopulations with brief phasic responses in series from the nosepoke to the UCS (Fig 5a,c). Average perievent time histograms (PETH) revealed that for both groups, the largest average responses occurred immediately prior to and after the UCS, with similar responses to the variable reward delivery and omission, in both patch and matrix groups (Fig 5b,d).

Because there were differences between trial types observed in the average responses from the CS and UCS, and because striatal motor and sensory responses are known to display preferences for contralateral representations, we compared both patch and matrix unit responses to ipsilateral or contralateral rewards. Sorting responses by reward side revealed some elevated contralateral firing between the CS and UCS for both patch and matrix groups (Fig 6), but no observable differences for the peak amplitude observed around reward delivery.

Next, we focused on these UCS responses as they were the largest phasic responses in both groups and occurred immediately prior to the UCS-associated RPE coding of SNc dopaminergic neurons. As the majority of SPN units are silent during this and most other behavioral epochs, clustering of all units based on firing rates during this period yielded a small number of units in both patch and matrix responsible for the vast majority of the UCS response ( $n = 24$  of 318, for 7.5% of matrix units and 11 of 88, for 12.5% patch units) (Fig 7a). Distributions of UCS-responsive units were not significantly different between the two groups ( $\chi^2$  test,  $p = 0.1429$ ,  $\chi^2 = 2.1464$ ).

Based on the apparent differences both within and between groups for these phasic responses, we wanted to test whether these observations reflected different distributions of responses in these populations. For the variable trials in particular, this would indicate whether the responses are capable of accurately representing reward expectation or prediction. Within groups, there were no significant differences between any trial types for both matrix units ( $n = 24$ , fixed reward 22.2 +/- 40.5, variable reward 18.9 +/- 53.5, variable omission 20.8 +/- 50.8 Hz peak firing rate, median +/- IQR,  $p = 0.93$ ,  $\chi^2 = 0.1474$ , Friedman test) and for patch units ( $n = 11$ , fixed reward 6.3 +/- 9.5, variable reward 8.1 Hz +/- 11.3, variable omission 11.1 Hz +/- 12.7 Hz peak firing rate, median +/- IQR,  $p = 0.31$ ,  $\chi^2 = 2.36$ , Friedman test) (Fig 7b). In comparison with patch units, matrix units had significantly larger responses for the fixed reward ( $p = 0.016$ ,  $z = 2.3993$ , rank = 500, Wilcoxon rank sum test), but not for either variable UCS (variable reward,  $p = 0.16$ ,  $z = 1.4037$ , rank = 472; variable omission,  $p = 0.21$ ,  $z = 1.2441$ , rank sum = 467.5, Wilcoxon rank sum test).

As neither ipsilateral or contralateral differences, nor statistical testing between and within groups could explain the observed differences, we next examined variation between

unit responses to different UCS types. Correlation of unit responses to variable trial types or reward trial types yielded the following results. For both matrix and patch units, there was a strong correlation of responses to variable reward delivery and omission (matrix  $n = 24$ ,  $r = 0.9852$ ,  $p = 2.3e-18$ ; patch  $n = 11$ ,  $r = 0.99$ ,  $p = 7.8e-9$ , Pearson's product moment correlation) (Fig 7b). The responses of matrix and patch units between fixed and variable rewards however, were quite different. Matrix units displayed a strong correlation of responses to both reward types, while patch units did not (matrix  $n = 24$ ,  $r = 0.7419$ ,  $p = 3.3e-05$ ; patch  $n = 11$ ,  $r = 0.0127$ ,  $p = 0.97$ , Pearson's product moment correlation). This indicates that although both patch and matrix units respond quite similarly during reward delivery or omission, patch units have much greater selectivity between reward types, displaying much larger responses to one or the other.

## Discussion

Using a combination of in vitro synaptic physiology and in vivo recording in behaving mice, we determined that patch neurons targeted in the SepW1\_NP67 BAC transgenic mouse provide distinct types of inhibition to dopaminergic and GABAergic neurons of the substantia nigra, and that patch and matrix neurons respond similarly to the delivery or omission of expected rewards within close temporal proximity to the RPE responses of SNc dopaminergic neurons. We believe that this response, primarily in patch SPNs, is capable of providing a prediction signal required for the successful encoding of RPE by SNc dopaminergic neurons, as predicted by the TD model.

Considering that the SNc remains one of the exclusive targets of patch SPNs, the limited or seemingly absent inhibition in many SNc dopaminergic neurons remains

paradoxical (Fig 2f). This does not exclude an under-sampling error due to in vitro limitations. Apparent differences in inputs may follow specific patterns of innervation, with patch axons primarily targeting the SNc ventral tier and ventral dendrites (Fig 2a) (Crittenden et al., 2016). Innervation patterns may underlie some of the observed heterogeneity in IPSC amplitude, as in our hands dorsal and ventral tier neurons were not labeled or otherwise verified. For SNc neurons receiving input, the small IPSC amplitude and lower than expected GABA<sub>A</sub> reversal potential indicate that patch SPNs target dendritic regions of SNc dopaminergic neurons electrotonically distal from the soma.

Although the patch has long been observed to innervate the SNr, we did not expect to observe such large and consistent inhibition in SNr neurons, in contrast to that observed in SNc neurons. While the kinetics and underlying receptors responsible for the inhibition are different between the dopaminergic and GABAergic neurons of the substantia nigra, the size and frequency of this inhibition cannot be ignored. The coding consequences of this input are expected to be different than for SNc dopaminergic neurons, however, as these synapses were observed to exhibit no GABA<sub>B</sub> current and strong synaptic depression. Thus the current frequency relationship between SNc and SNr neurons to patch firing rate may result in SNr neurons being more sensitive to single spikes and SNc neurons more sensitive to bursts in patch SPNs, resulting in different responses and postsynaptic consequences for the same code generated. This may be even more pronounced in vivo, where the GABA<sub>A</sub> reversal potential of SNc neurons is expected to be much higher than in whole cell recording with normal internal solution (Gulácsi et al., 2003).

Both patch and matrix populations displayed large phasic responses around the time of the UCS that were almost identical between variable reward delivery and omission trials.

The lack of difference between the firing responses to these two UCS types indicates that these SPNs encode an internal representation of the task that generalizes amongst these two conditions. Although alternative candidates exist, the fact that the activity of these SPNs does not differ between trial types at later time points where the animal's behavior does (i.e.: reward consumption vs. running to return to the center port), suggests that these signals do not represent the animal's momentary behavior but that they encode some more abstract aspect of the behavior that is invariant to the particular outcome encountered on a given trial. One particularly interesting possibility is that SPN firing around delivery represents the reward prediction information. There were patch and matrix units phasically active exclusively following reward delivery, but these were relatively rare and as a population did not generate the largest UCS-associated responses observed (Fig 5). Therefore, we believe that the reward-related responses reported in other studies are likely to be of the type we observed, although we cannot discount regional and task-specific differences.

We were somewhat surprised by the relative lack of coding differences between patch and matrix SPNs, given that the patch and matrix compartments are innervated by different cortical layers (Gerfen, 1989; Kincaid and Wilson, 1996), and in some cases cortical regions (Kincaid and Wilson, 1996; Flaherty and Graybiel, 1994; Ragsdale and Graybiel, 1990; Eblen and Graybiel, 1995). The lack of fine temporal, kinematic and sensory control during the task may account for some of this apparent lack of difference, as well as the limited sampling of diversely and sparsely coding populations of neurons. However, since SPNs of both structures were active around the time of the UCS, and exhibited indistinguishable responses to variable reward delivery and omission, we are not

able to exclude the possibility that the striatum is transmitting a prediction signal to downstream targets that is responsible for RPE signals in SNc dopaminergic neurons and LHb-projecting EP neurons. In contrast to the matrix, patch SPNs had distinctly different responses for the UCS at either reward port, for fixed or variable trial types. These differences may explain the apparent amplitude differences between patch and matrix SPNs, and allow for the patch to uniquely represent the expected value of specific states, in this case fixed or variable trials.

It is difficult to exhaustively determine what information is represented by individual SPNs or populations of SPNs, as they receive diverse types of cortical inputs and respond heterogeneously during behavioral sequences. However, we can analyze them in the context of their postsynaptic consequences. For matrix responses to the UCS, and indeed patch responses as well, there are many potential postsynaptic effects through nigrocollicular, nigrothalamic and nigropeduncular pathways, however for dopamine neurons there are also several options. If the UCS-responding matrix population is composed mostly of direct pathway neurons, the simplest explanation of the response effect is that SNc dopaminergic neurons would be disinhibited. If the UCS-responding matrix population is composed both of direct and indirect pathway neurons, then the simplest explanation is that there would be little to no effect on SNc neuron firing due to coincident inhibition and disinhibition of SNr neurons (Celada et al., 1999). In either scenario, other consequences may be possible depending on patch input specificity and the diversity of SNr neurons and their intrinsic connections. The strongest effects of matrix SPN bursting during the UCS may not be on dopaminergic neurons but on other output targets of the basal ganglia, and the consequence of these matrix responses remains an empirical question.

Lastly, although there were slight differences in the percentage of UCS-responsive units in patch and matrix compartments, the majority of patch neurons (87.5%) was not active around the time of the UCS. Based on the *in vitro* synaptic physiology, we expect the somatic current evoked from this subpopulation to be a fraction of that observed following 50 Hz stimulation of all transfected axons. Whatever postsynaptic consequences patch SPN bursting may have for dopaminergic neurons, we do not expect it to control the pace-making firing pattern of SNc dopaminergic neurons or to be monosynaptically responsible for their decreases in firing following the omission of predicted rewards.

If patch inhibition of SNc dopaminergic neurons is not capable of preventing their tonic firing, how might it influence the RPE coding of these neurons? Their dendritic targeting and prolonged GABA<sub>B</sub>-mediated inhibition have the potential to interfere with several known dendritic processes. Postsynaptic calcium influx on SNc dopaminergic neuron dendrites primarily occurs through NMDA receptors located on spines (Hage et al., 2016). Another route of dendritic calcium influx occurs by action potential backpropagation, which nonlinearly increases dendritic calcium and postsynaptic excitatory gain (Hage and Khaliq, 2015). As both NMDA receptors and intracellular calcium appear to be required for burst firing in dopaminergic neurons (Kitai et al., 1999; Zweifel et al., 2009), patch inhibition of these dendritic regions may cause back-propagating action potentials to fail, shunt excitatory inputs, or prevent the occurrence of regenerative potentials responsible for burst firing (Evans et al., 2017). Patch input may also interfere with synaptic plasticity. If reward-related burst firing of SNc dopaminergic neurons is generated in dendritic regions targeted by patch SPNs, then patch activation

could gradually reduce these bursts without affecting tonic firing patterns, and allow for SNc dopaminergic neurons to accurately encode RPE.

## References

Berridge KC (2007) The debate over dopamine's role in reward: the case for incentive salience. *Psychopharmacology* 191:391–431.

Bromberg-Martin ES, Hikosaka O (2011) Lateral habenula neurons signal errors in the prediction of reward information. *Nat Neurosci* 14: 1209–1216.

Bromberg-Martin ES, Matsumoto M, Hikosaka O (2010) Dopamine in motivational control: rewarding, aversive, and alerting. *Neuron* 68:815–834.

Celada P, Paladini CA, Tepper JM (1999) GABAergic control of rat substantia nigra dopaminergic neurons: role of globus pallidus and substantia nigra pars reticulata. *Neuroscience* 89:813–825.

Chang CY, Esber GR, Marrero-Garcia Y, Yau HJ, Bonci A, Schoenbaum G (2016) Brief optogenetic inhibition of dopamine neurons mimics endogenous negative reward prediction errors. *Nat Neurosci* 19:111–116.

Crittenden JR, Tillberg PW, Riad MH, Shima Y, Gerfen CR, Curry J, Housman DE, Nelson SB, Boyden ES, Graybiel AM (2016) Striosome–dendron bouquets highlight a unique striatonigral circuit targeting dopamine-containing neurons. *PNAS* 113:11318–11323.

Eblen F, Graybiel AM (1995). Highly restricted origin of prefrontal cortical inputs to striosomes in the macaque monkey. *J Neurosci* 15:5999–6013.

Evans RC, Zhu M, Khaliq ZM (2017) Dopamine Inhibition Differentially Controls Excitability of Substantia Nigra Dopamine Neuron Subpopulations through T-Type Calcium Channels. *J Neurosci* 37:3704–3720.

Faust TW, Assous M, Tepper JM, Koós T (2016) Neostriatal GABAergic Interneurons Mediate Cholinergic Inhibition of Spiny Projection Neurons. *J Neurosci* 36:9505–11.

Ferguson JE, Boldt C, Redish AD (2009) Creating low-impedance tetrodes by electroplating with additives. *Sensors and Actuators A: Physical* 156:388–93.

Flaherty AW, Graybiel AM (1994) Input-output organization of the sensorimotor striatum in the squirrel monkey. *J Neurosci* 14:599–610.

- Fujiyama F, Sohn J, Nakano T, Furuta T, Nakamura KC, Takeshi Kaneko T (2011) Exclusive and common targets of neostriatofugal projections of rat striosome neurons: a single neuron-tracing study using a viral vector. *Eur J Neurosci* 33:668–677.
- Gage GJ, Stoetzner CR, Wiltschko AB, Berke JD (2010) Selective activation of striatal fast-spiking interneurons during choice execution. *Neuron* 67:466–479.
- Gerfen CR (1984) The neostriatal mosaic: compartmentalization of corticostriatal input and striatonigral output systems. *Nature* 311:461–464.
- Gerfen CR (1985) The neostriatal mosaic. I. Compartmental organization of projections from the striatum to the substantia nigra in the rat. *J Comp Neurol* 236:454–476
- Gerfen CR. The neostriatal mosaic: striatal patch-matrix organization is related to cortical lamination (1989) *Science* 246:385–388.
- Gerfen CR, Paletzki R, Heintz N (2013) GENSAT BAC cre-recombinase driver lines to study the functional organization of cerebral cortical and basal ganglia circuits. *Neuron* 80:1368–83.
- Gulácsi A, Lee CR, Sük A, Viitanen T, Kaila K, Tepper JM, Freund TF (2003) Cell type-specific differences in chloride-regulatory mechanisms and GABAA receptor-mediated inhibition in rat substantia nigra. *J Neurosci* 23:8237–8246.
- Hage TA, Khaliq ZM (2015) Tonic firing rate controls dendritic Ca<sup>2+</sup> signaling and synaptic gain in substantia nigra dopamine neurons. *J Neurosci* 35:5823–5836.
- Hage TA, Sun Y, Khaliq ZM (2016) Electrical and Ca<sup>2+</sup> signaling in dendritic spines of substantia nigra dopaminergic neurons. *eLife* 5:e13905.
- Hollerman JR, Schultz W (1998) Dopamine neurons report an error in the temporal prediction of reward during learning. *Nat Neurosci* 1: 304–309.
- Jog MS, Kubota Y, Connolly CI, Hillegaart V, Graybiel AM (1999) Building neural representations of habits. *Science* 286:1745–1749.
- Kim KM, Baratta MV, Yang A, Lee D, Boyden ES, Fiorillo CD (2012) Optogenetic mimicry of the transient activation of dopamine neurons by natural reward is sufficient for operant reinforcement. *PloS one* 7:e33612.
- Kincaid AE, Wilson CJ (1996) Corticostriatal innervation of the patch and matrix in the rat neostriatum. *J Comp Neurol* 374:578–592.
- Kitai ST, Shepard PD, Callaway JC, Scroggs R (1999) Afferent modulation of dopamine neuron firing patterns. *Curr Opin Neurobiol* 9:690–697.

- Ljungberg T, Apicella P, Schultz W (1992) Responses of monkey dopamine neurons during learning of behavioral reactions. *J Neurophys* 67:145–163.
- Mirenowicz J, Schultz W (1994) Importance of unpredictability for reward responses in primate dopamine neurons. *J Neurophys* 72:1024–1027.
- Palmiter RD (2008) Dopamine signaling in the dorsal striatum is essential for motivated behaviors. *Ann NY Acad Sci* 1129:35–46.
- Ragsdale CW Jr, Graybiel AM (1990) A simple ordering of neocortical areas established by the compartmental organization of their striatal projections. *PNAS* 87:6196–6199.
- Rajakumar N, Elisevich K, Flumerfelt BA (1993) Compartmental origin of the striato-entopeduncular projection in the rat. *J Comp Neurol* 331:286–296.
- Reynolds JNJ, Hyland BI, Wickens JR (2001) A cellular mechanism of reward-related learning. *Nature* 413:67–70.
- Salamone JD, Correa M (2012) The mysterious motivational functions of mesolimbic dopamine. *Neuron* 76:470–485.
- Schmitzer-Torbert N, Redish AD (2004) Neuronal activity in the rodent dorsal striatum in sequential navigation: separation of spatial and reward responses on the multiple T task. *J Neurophys* 91:2259–2272.
- Schultz W (1998) Predictive reward signal of dopamine neurons. *J Neurophys* 80:1–27.
- Schultz W, Dayan P, Montague PR (1997) A neural substrate of prediction and reward. *Science* 275:1593–1599.
- Sharpe MJ, Chang CY, Liu MA, Batchelor HM, Mueller LE, Jones JL, Niv Y, Schoenbaum G (2017) Dopamine transients are sufficient and necessary for acquisition of model-based associations. *Nat Neurosci*.
- Shen W, Flajolet M, Greengard P, Surmeier DJ (2008) Dichotomous dopaminergic control of striatal synaptic plasticity. *Science* 321:848–851.
- Smith JB, Klug JR, Ross DL, Howard CD, Hollon NG, Ko VI, Hoffman H, Callaway EM, Gerfen CR, Jin X (2016) Genetic-based dissection unveils the inputs and outputs of striatal patch and matrix compartments. *Neuron* 91:1069–1084.
- Steinberg EE, Keiflin R, Boivin JR, Witten IB, Deisseroth K, Janak PH (2013) A causal link between prediction errors, dopamine neurons and learning. *Nat Neurosci* 16:966–973.
- Stephenson-Jones M, Yu K, Ahrens S, Tucciarone JM, van Huijstee AN, Mejia LA, Penzo MA, Tai LH, Wilbrecht L, Li B (2016) A basal ganglia circuit for evaluating

action outcomes. *Nature* 539:289–293.

Sutton RS, Barto AG (1981) Toward a Modern Theory of Adaptive Networks: Expectation and Prediction. *Psychol Rev* 88:135–170.

Tsai HC, Zhang F, Adamantidis A, Stuber GD, Bonci A, De Lecea L, Deisseroth K (2009) Phasic firing in dopaminergic neurons is sufficient for behavioral conditioning. *Science* 324:1080–1084.

Wallace ML, Saunders A, Huang KW, Philson AC, Goldman M, Macosko EZ, McCarroll SA, Sabatini BL (2017) Genetically distinct parallel pathways in the entopeduncular nucleus for limbic and sensorimotor output of the basal ganglia. *Neuron* 94:138–152.

Wise RA (2004) Dopamine, learning and motivation. *Nature rev neurosci* 5:483–494.

Yagishita S, Hayashi-Takagi A, Ellis-Davies GC, Urakubo H, Ishii S, Kasai H (2014) A critical time window for dopamine actions on the structural plasticity of dendritic spines. *Science* 345:1616–1620.

Zweifel LS, Parker JG, Lobb CJ, Rainwater A, Wall VZ, Fadok JP, Darvas M, Kim MJ, Mizumori SJ, Paladini CA, Phillips PE (2009) Disruption of NMDAR-dependent burst firing by dopamine neurons provides selective assessment of phasic dopamine-dependent behavior. *PNAS* 106:7281–7288.

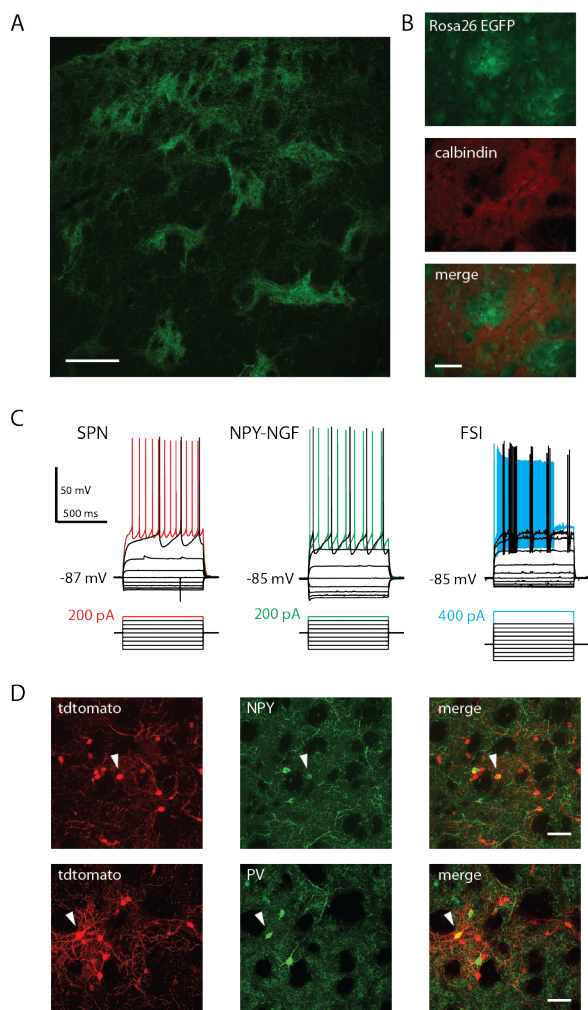


Figure 1. Targeting of striatal neurons in the SepW1\_NP67 transgenic mouse. A. Fluorescent micrograph of dorsal striatum expressing Cre-dependent ChR2-EYFP in patches following viral transfection. Scale bar = 200  $\mu\text{m}$ . B. Calbindin counterstaining of matrix in NP67 x Rosa26/stop/EGFP double transgenic mouse. Note the lack of colocalization. Scale bar = 50  $\mu\text{m}$ . C. Current clamp recordings of targeted striatal neurons in NP67 mice. Depolarizing current pulses reveal characteristic voltage responses for all three neurons. Left: SPN experiences  $I_A$ -mediated ramp potential prior to regular spiking pattern. Middle: NPY-NGF displays characteristic deep and slow afterhyperpolarization and regular firing pattern. Right: FSI exhibits subthreshold membrane potential oscillations,

fast spike waveform and stuttering firing pattern. D. Immunolabeling of tdTomato-expressing striatal neurons for interneuronal markers NPY and PV. White arrows indicate colocalized neurons. Scale bar = 50  $\mu\text{m}$ .

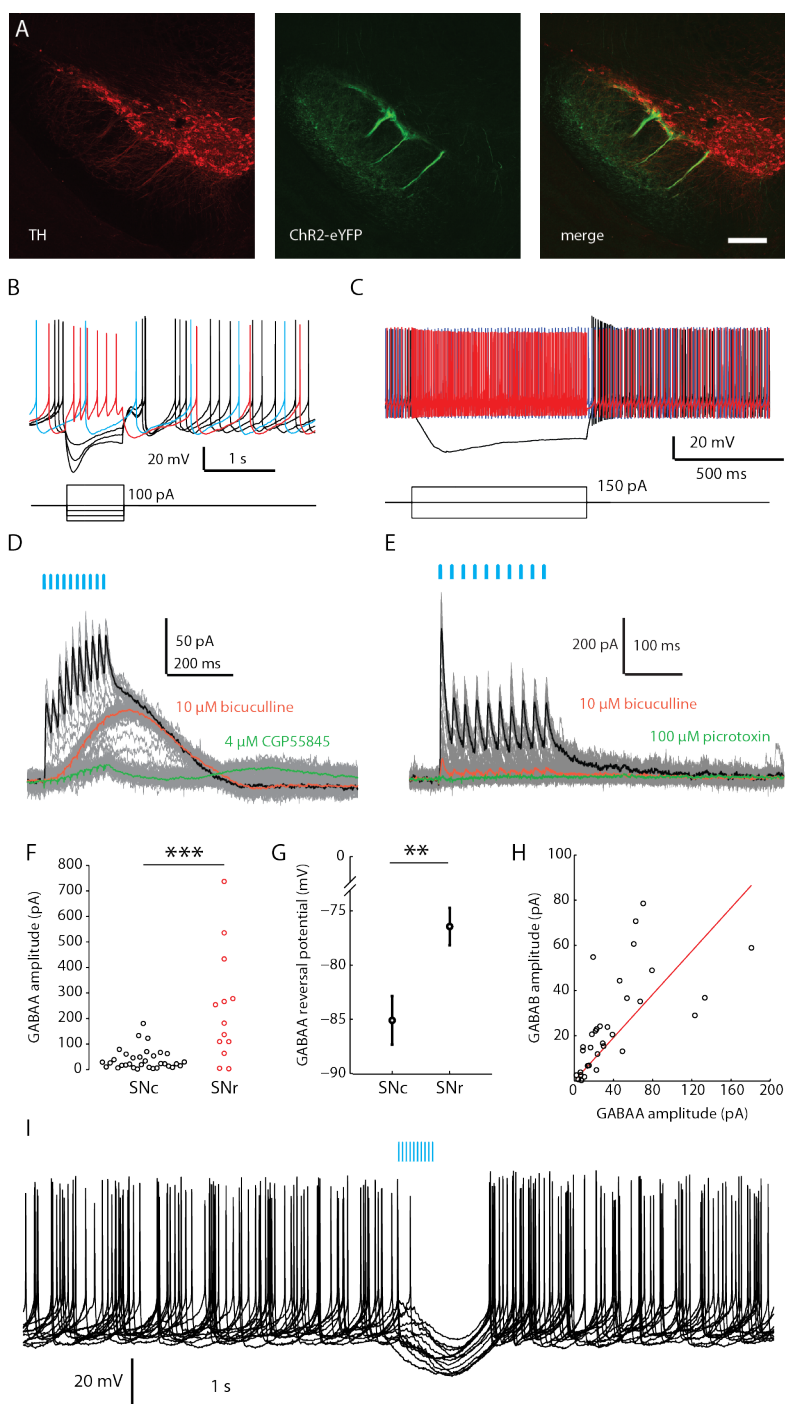


Figure 2. Inhibition of substantia nigra dopaminergic and GABAergic neurons by the patch.

A. Patch axon field innervation of the substantia nigra, with TH immunolabeling of dopaminergic neurons. Note the strong innervation of the SNc ventral dendrites. Scale bar = 200  $\mu\text{m}$ . B. Current clamp recording of SNc dopaminergic neuron. C. Current clamp recording of SNr GABAergic neuron. D-E. Voltage clamp recording of SNc and SNr neurons in B-C, following optogenetic stimulation of patch axons at 50 Hz for 10 pulses (blue bars), with the average IPSC in black, individual traces in gray. The average IPSC following bicuculline (10  $\mu\text{M}$ ) is in red, and the average IPSC following either CFP55845 (4  $\mu\text{M}$ ) or picrotoxin (100  $\mu\text{M}$ ) is in green. F. Peak GABA<sub>A</sub> IPSC responses in all recorded SNc and SNr neurons. G. GABA<sub>A</sub> IPSC reversal potentials for SNc and SNr neurons. H. Correlation between GABA<sub>A</sub> and GABA<sub>B</sub> IPSC peak amplitude, with red line illustrating linear regression constrained to have intercept of zero. I. Current clamp recording of SNc dopaminergic neuron receiving large inhibition from the patch, with multiple traces overlaid. Patch axon stimulus is the same as in D-E (blue bars). \*\*  $p < 0.01$ , \*\*\*  $p < 0.001$ .

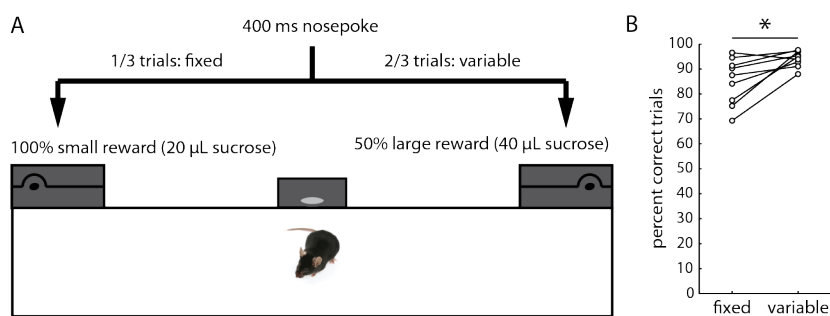


Figure 3. Schematic for instrumental task. A. Diagram of behavioral apparatus with flowchart for behavioral sequence. B. Behavioral performance of all recorded mice for fixed and variable trial types. \*  $p < 0.05$ .

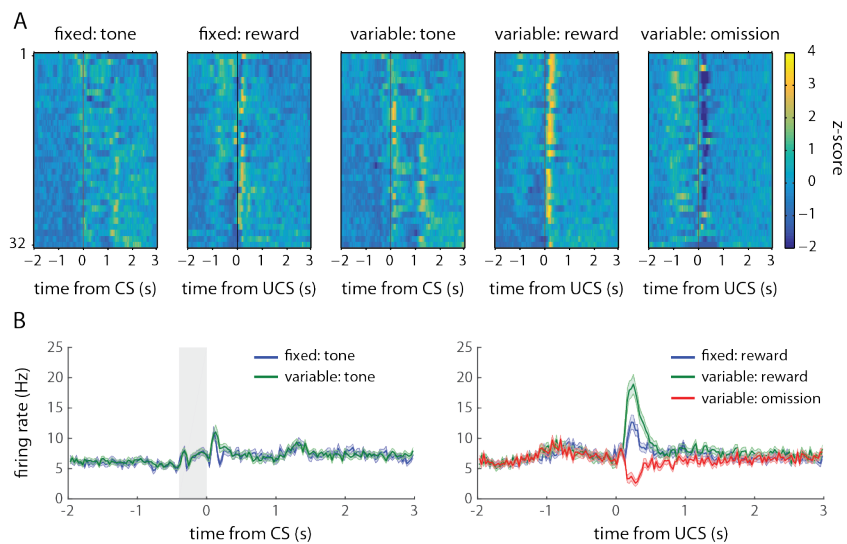


Figure 4. SNc dopaminergic neurons encode RPE in the instrumental task. A. Heat maps of smoothed z-score PETHs from all dopaminergic units, sorted by center of mass, for all CS and UCS events. B. PETHs of average responses to CS and UCS for fixed and variable trial types, expressed as mean  $\pm$  SEM.

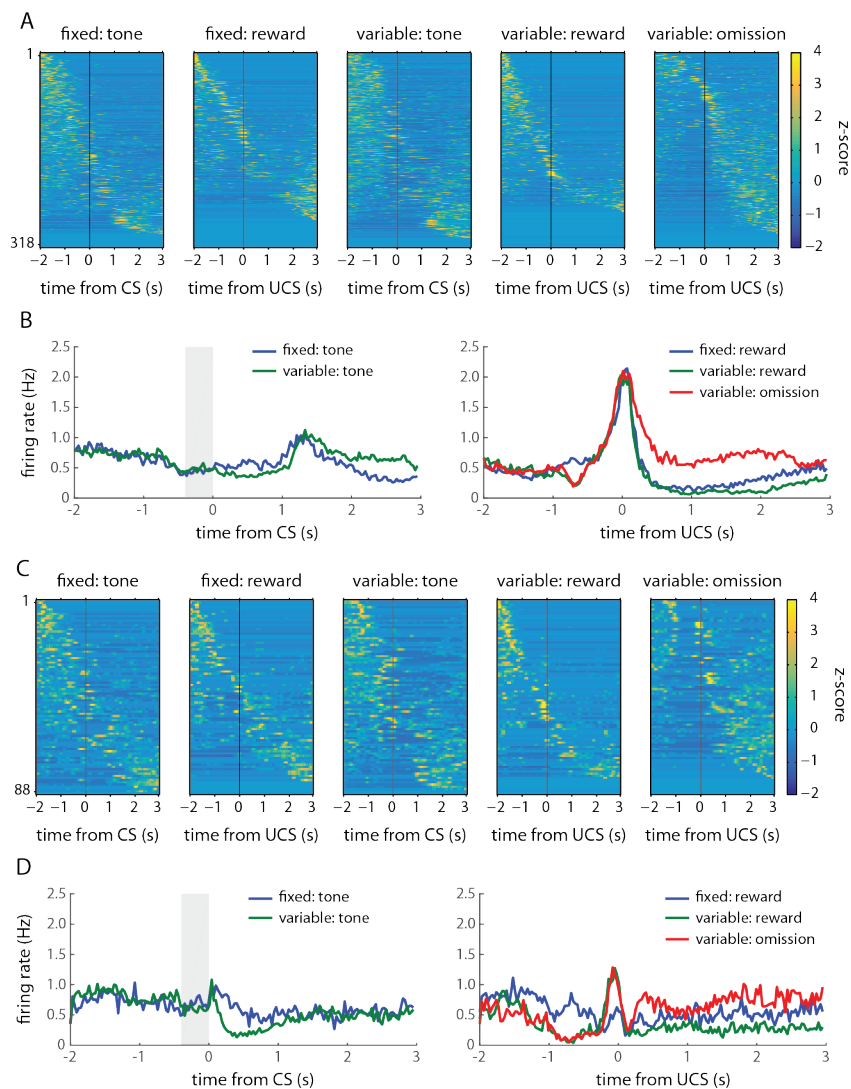


Figure 5. Matrix and patch SPN responses during the instrumental task. A. Heat maps of smoothed z-score PETHs from all matrix units, sorted by center of mass, for all CS and UCS events. B. PETHs of average matrix unit responses to CS and UCS for fixed and variable trial types. C-D. Same as for A-B but for all patch units.

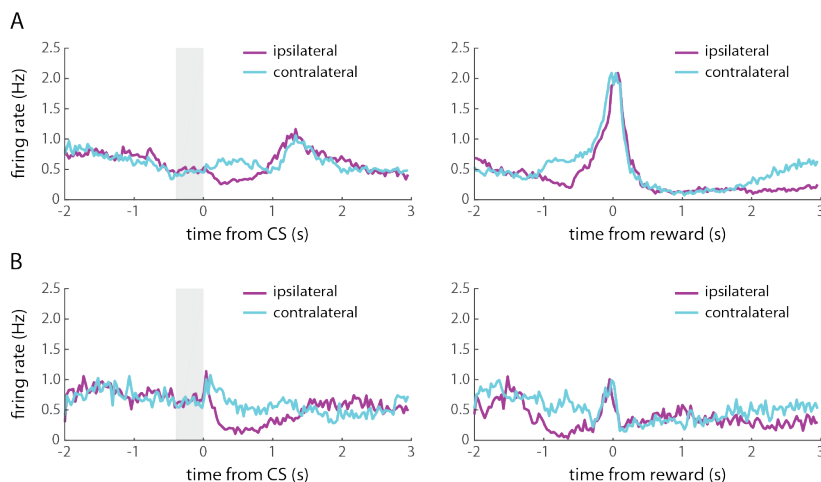


Figure 6. Contralateral responses in matrix and patch SPNs are increased between the CS and UCS. A-B. PETHs of average matrix (A) and patch (B) unit responses to CS and UCS (rewards) for ipsilateral and contralateral reward ports. Note the increased contralateral responses between CS and UCS, but lack of contralateral differences for the peak UCS response amplitude.

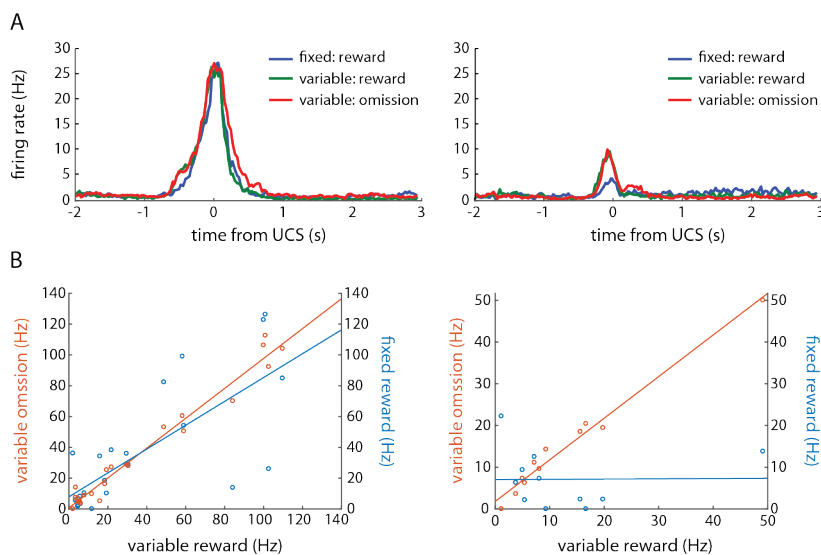


Figure 7. Differential coding of patch and matrix neurons to reward expectation. A. PETH of average responses for UCS-responsive matrix units (left) and patch units (right) to the UCS. B. Correlation of unit peak firing rate responses (Hz) to different UCS trial types.

Left: UCS-responsive matrix units, right: UCS-responsive patch units. Orange: correlation of responses to variable reward delivery and variable reward omission, blue: correlation of responses to variable reward delivery and fixed reward delivery (blue).

CHAPTER 5:  
General Discussion

In the first of this series of studies, I characterized the striatal targeting and some synaptic physiology in the Htr3a-Cre BAC transgenic mouse line. In this mouse, four observable types of striatal interneurons were targeted, two of which were previously unidentified and three of which receive nicotinic excitation. The focal cell type of this study, termed the fast-adapting cell, exhibits novel synaptic connections in the striatal microcircuit. It is possible that this type of interneuron receives nicotinic excitation from CINs, but as connected pairs were not recorded, it remains possible that fast-adapting interneurons receive their nicotinic excitation from the pedunculopontine tegmental nucleus (Dautan et al., 2014). The discovery of this neuron, as well as the THIN-resembling spontaneously active neurons, increases the number of striatal GABAergic interneuron types. Their receipt of nicotinic input lends additional evidence to the theory that the striatal microcircuit is semiautonomous from cortical control.

Because three of the targeted interneurons in this transgenic mouse line received nicotinic input, and because one of them was the NPY-NGF, I surmised that double transgenic Htr3a-Cre x ChAT-ChR2 mice would be an appropriate preparation to causally test the hypothesis that GABAergic interneurons mediate the cholinergic inhibition of SPNs. In a simple and informative series of experiments, I determined that the vast majority of GABAergic inhibition was derived from local interneurons, rather than nigrostriatal terminals. This results provides meaningful insight into this phenomenon of cholinergic-mediated inhibition, as it is observed both in vitro and in vivo (English et al., 2012). Compared to this, cholinergic-mediated dopamine release is substantially attenuated in vivo (Cachope et al., 2012). These two observations cast doubt on the efficacy by which

cholinergic interneurons inhibit SPNs through nigrostriatal terminals, but it remains an experimental question.

In the last and principal study in this thesis, I examined striatal targeting in the SepW1\_NP67 BAC transgenic mouse (Gerfen et al., 2013), characterized synaptic inputs from neostriatal patches to the substantia nigra dopaminergic and GABAergic neurons, and observed divergence in the coding patterns of patch and matrix neurons during a prediction-based instrumental task. These results advance the field in several different ways. First, identification of heterogeneous striatal targeting in the NP67 mouse will inform future experimentation with this line, and reveal errors in the published literature. Characterization of *in vitro* synaptic physiology will contribute to our understanding of patch inhibition of downstream targets and SNc dopaminergic neurons' dendritic information processing. And lastly characterization of patch and matrix SPN coding properties will aid future investigations of their representation of behavioral events and contribution to downstream targets' information processing.

In contrast to the observations of others (Smith et al., 2016), we observed targeting of unknown proportions of at least two interneuron types in the striatum of the NP67 mouse. This was observed *in vitro*, *in vivo* and with immunocytochemistry. While off-target effects are not uncommon in BAC transgenic animals, the basis for this targeting remains unknown, but potentially troublesome for experiments requiring specific targeting of patch SPNs. This would also imply that the viral tracing in the aforementioned study, which stated that there are negligible differences of innervation between patch and matrix compartments, may have been contaminated by interneurons.

This thesis is not the first attempt to characterize the postsynaptic inhibition of dopaminergic neurons by the striatum. The first optogenetic investigations of this synaptic input revealed no inhibition (Chuhma et al., 2011; Xia et al., 2011), from either dorsal striatum to the SNc or ventral striatum to the VTA, respectively. At least for the SNc, this failure could be due to selective innervation of ventral tier neurons by patch axons, or mediolateral topography of innervation which would be masked by matrix axons. More recently, ventral striatal inhibition of VTA dopaminergic neurons has been successfully characterized (Edwards et al., 2017), and these inputs produce almost exclusively a GABA<sub>B</sub> current in these neurons.

The mechanisms by which dopaminergic neurons encode RPE has previously been attempted to be explained using the recordings of a diverse population of neurons identified as monosynaptically providing input to dopaminergic neurons (Tian et al., 2016). The synaptic weights for all recorded presynaptic neurons were fit using a linear model to best approximate the observed dopaminergic firing pattern. In this model, increasing numbers of presynaptic neurons recorded from diverse brain regions provided an increasingly better fit, and monosynaptically connected neurons provided a better fit than unconnected neurons. However, amongst the diverse responses of presynaptic neurons were a minority which either partially or fully recapitulated the RPE signal. As the authors did not disclose the assigned synaptic weights, it could be reasonably assumed that neurons with similar responses to dopaminergic neurons were assigned larger synaptic weights, while those with much different responses were assigned smaller synaptic weights, which would ultimately produce the best fit. Additionally, synaptic weights were assigned by neuron rather than by presynaptic structure, which allows for no testable hypotheses of whether individual

structures exert greater or lesser control over dopaminergic firing. While the model used in this study might explain how dopaminergic neurons integrate presynaptic inputs, it may be that not all synaptic inputs are integrated linearly, or that all synaptic inputs primarily control the pace-making activity of dopaminergic neurons. The study also failed to explain how RPE would be generated in presynaptic neurons.

Ultimately, causal experiments will determine how dopaminergic neurons integrate postsynaptic inputs to generate RPE, and whether or not patch SPNs provide SNc dopaminergic neurons with a prediction signal necessary for this. These experiments can take many forms, but the most informative and elegant ones would be fully reversible, utilizing inhibitory optogenetics or perhaps pharmacogenetics. This was the approach that I wanted to take to causally determine whether patch inhibition successfully reduces SNc dopaminergic burst firing to predicted rewards, as I had done previously (Faust et al., 2015). However, several structural impediments quickly presented themselves. First, nonselective targeting of striatal neurons remains problematic, so any manipulations would have to exclude them. The use of inhibitory opsins in the patch terminal fields of the substantia nigra could circumvent this issue, but recent evidence of the failures of terminal inhibition by these opsins may make in this strategy intractable for the near future (Mahn et al., 2016). Remaining options include mu-opioid receptor-dependent lesioning (Jenrette et al., 2017), or the generation of a SPN-specific, cre-dependent virus. Based on the results of this thesis I predict that removal of patch inhibition from SNc dopaminergic neurons will interfere with their successful encoding of RPE.

## CHAPTER 6:

### References

- Ainslie GW (1974) Impulse control in pigeons. *J Exp Anal Behav* 21:485–489.
- Andén NE, Carlsson A, Dahlström A, Fuxe K, Hillarp NÅ, Larsson K (1964) Demonstration and mapping out of nigro-neostriatal dopamine neurons. *Life Sci* 3:523–530.
- Balcita-Pedicino JJ, Omelchenko N, Bell R, Sesack SR (2011) The inhibitory influence of the lateral habenula on midbrain dopamine cells: ultrastructural evidence for indirect mediation via the rostromedial mesopontine tegmental nucleus. *J Comp Neurol* 519:1143–1164.
- Bayer HM, Glimcher PW (2005) Midbrain dopamine neurons encode a quantitative reward prediction error signal. *Neuron* 47:129–141.
- Bennett BD, Bolam JP. Characterization of calretinin-immunoreactive structures in the striatum of the rat. *Brain Res* 609:137–148.
- Berridge KC (2007) The debate over dopamine's role in reward: the case for incentive salience. *Psychopharmacology* 191:391–431.
- Bertler Å, Rosengren E (1959) Occurrence and distribution of dopamine in brain and other tissues. *Cell Mol Life Sci* 151:10–11.
- Bliss TVP, Collinridge GL (1993) A synaptic model of memory: long-term potentiation in the hippocampus. *Nature* 361:31–39.
- Bolam JP, Clarke DJ, Smith AD, Somogyi P (1983) A type of aspiny neuron in the rat neostriatum accumulates [<sup>3</sup>H]  $\gamma$ -aminobutyric acid: Combination of golgi-staining, autoradiography, and electron microscopy. *J Comp Neurol* 213:121–134.
- Bolam JP, Powell JF, Wu JY, Smith AD (1985) Glutamate decarboxylase-immunoreactive structures in the rat neostriatum: A correlated light and electron microscopic study including a combination of Golgi impregnation with immunocytochemistry. *J Comp Neurol* 237:1–20.
- Boyes J, Bolam JP (2003) The subcellular localization of GABA(B) receptor subunits in the rat substantia nigra. *Eur J Neurosci* 18:3279–3293.
- Brazhnik E, Shah F, Tepper JM (2008) GABAergic afferents activate both GABAA and GABAB receptors in mouse substantia nigra dopaminergic neurons in vivo. *J Neurosci* 28:10386–10398.
- Bromberg-Martin ES, Hikosaka O (2011) Lateral habenula neurons signal errors in the prediction of reward information. *Nat Neurosci* 14: 1209–1216.
- Bromberg-Martin ES, Matsumoto M, Hikosaka O (2010) Dopamine in motivational

control: rewarding, aversive, and alerting. *Neuron* 68:815–834.

Brown PL, Palacorolla H, Brady D, Riegger K, Elmer GI, Shepard PD (2017) Habenula-induced inhibition of midbrain dopamine neurons is diminished by lesions of the rostromedial tegmental nucleus. *J Neurosci* 37:217–225.

Cachope R, Mateo Y, Mathur BN, Irving J, Wang HL, Morales M, Lovinger DM, Cheer JF (2012) Selective activation of cholinergic interneurons enhances accumbal phasic dopamine release: setting the tone for reward processing. *Cell Rep* 2:33–41.

Cagniard B, Balsam PD, Brunner D, Zhuang X (2006) Mice with chronically elevated dopamine exhibit enhanced motivation, but not learning, for a food reward. *Neuropsychopharmacology* 31:1362–1370.

Calu DJ, Roesch MR, Haney RZ, Holland PC, Schoenbaum G (2010) Neural Correlates of Variations in Event Processing during Learning in Central Nucleus of Amygdala. *Neuron* 68:991–1001.

Cannon CM, Palmiter RD (2003) Reward without dopamine. *J Neurosci* 23:10827–10831.

Carlsson A, Lindqvist M, Magnusson TO (1957) 3,4-Dihydroxyphenylalanine and 5-hydroxytryptophan as reserpine antagonists. *Nature* 180:1200.

Carlsson A, Lindqvist M, Magnusson T, Waldeck B (1958) On the presence of 3-hydroxytyramine in brain. *Science* 127:471.

Celada P, Paladini CA, Tepper JM (1999) GABAergic control of rat substantia nigra dopaminergic neurons: role of globus pallidus and substantia nigra pars reticulata. *Neuroscience* 89:813–825.

Cepeda C, Buchwald NA, Levine MS (1993) Neuromodulatory actions of dopamine in the neostriatum are dependent upon the excitatory amino acid receptor subtypes activated. *PNAS* 90:9576–9580.

Ciocchi S, Herry C, Grenier F, Wolff SBE, Letzkus JJ, Vlachos I, Ehrlich I, Sprengel R, Deisseroth K, Stadler MB, Müller C, Andreas Lüthi A (2010) Encoding of conditioned fear in central amygdala inhibitory circuits. *Nature* 468:277–282.

Chesselet MF, Graybiel AM (1986) Striatal neurons expressing somatostatin-like immunoreactivity: evidence for a peptidergic interneuronal system in the cat. *Neuroscience* 17:547–571.

Chang CY, Esber GR, Marrero-Garcia Y, Yau HJ, Bonci A, Schoenbaum G (2016) Brief optogenetic inhibition of dopamine neurons mimics endogenous negative reward prediction errors. *Nat Neurosci* 19:111–116.

- Chiodo LA, Antelman SM, Caggiula AR, Lineberry CG (1980) Sensory stimuli alter discharge rate of dopamine (DA) neurons: evidence for two functional types of DA cells in the substantia nigra. *Brain Research* 189:544–549.
- Chuhma N, Tanaka KF, Hen R, Rayport S (2011) Functional connectome of the striatal medium spiny neuron. *J Neurosci* 31:1183–1192.
- Cowan RL, Wilson CJ, Emson PC, Heizmann CW (1990) Parvalbumin-containing gabaergic interneurons in the rat neostriatum. *J Comp Neurol* 302:197–205.
- Cragg SJ (2003) Variable dopamine release probability and short-term plasticity between functional domains of the primate striatum. *J Neurosci* 23:4378–4385.
- Crittenden JR, Tillberg PW, Riad MH, Shima Y, Gerfen CR, Curry J, Housman DE, Nelson SB, Boyden ES, Graybiel AM (2016) Striosome–dendron bouquets highlight a unique striatonigral circuit targeting dopamine-containing neurons. *PNAS* 113:11318–11323.
- Dahlström A, Fuxe K (1964) Evidence for the existence of monoamine-containing neurons in the central nervous system. I. Demonstration of monoamines in the cell bodies of brain stem neurons. *Acta Physiol Scand Suppl* 232: 1–55.
- Dautan D, Huerta-Ocampo I, Witten IB, Deisseroth K, Bolam JP, Gerdjikov T, Mena-Segovia J (2014) A major external source of cholinergic innervation of the striatum and nucleus accumbens originates in the brainstem. *J Neurosci* 34:4509–4518.
- Day JJ, Jones JL, Wightman RM, Carelli RM (2010) Phasic nucleus accumbens dopamine release encodes effort-and delay-related costs. *Biol Psychiatry* 68:306–309.
- Day JJ, Roitman MF, Wightman RM, Carelli RM (2007) Associative learning mediates dynamic shifts in dopamine signaling in the nucleus accumbens. *Nat Neurosci* 10:1020–1028.
- Dodson PD, Dreyer JK, Jennings KA, Syed EC, Wade-Martins R, Cragg SJ, Bolam JP, Magill PJ (2016) Representation of spontaneous movement by dopaminergic neurons is cell-type selective and disrupted in parkinsonism. *PNAS* 113:E2180–2188.
- Duvarci S, Popa D, Paré D (2011) Central Amygdala activity during fear conditioning. *J Neurosci* 31:289–294.
- Eblen F, Graybiel AM (1995). Highly restricted origin of prefrontal cortical inputs to striosomes in the macaque monkey. *J Neurosci* 15:5999–6013.

Edwards NJ, Tejeda HA, Pignatelli M, Zhang S, McDevitt RA, Wu J, Bass CE, Bettler B, Morales M, Bonci A (2017) Circuit specificity in the inhibitory architecture of the VTA regulates cocaine-induced behavior. *Nat Neurosci*.

Ehringer H, Hornykiewicz O (1960) Verteilung von noradrenalin and dopamin im gehirn des menschen und ihr verhalten bei erkrankungen des extrapyramidalen systems. *Klin Wschr* 38: 1126–1239

English DF, Ibáñez-Sandoval O, Stark E, Tecuapetla F, Buzsáki G, Deisseroth K, Tepper JM, Koós T (2012) GABAergic circuits mediate the reinforcement-related signals of striatal cholinergic interneurons. *Nat Neurosci* 15:123–230.

Eshel N, Tian J, Bukwich M, Uchida N (2016) Dopamine neurons share common response function for reward prediction error. *Nat Neurosci* 19:479–486.

Faust TW, Assous M, Shah F, Tepper JM, Koós T (2015) Novel fast adapting interneurons mediate cholinergic-induced fast GABAA inhibitory postsynaptic currents in striatal spiny neurons. *Eur J Neurosci* 42:1764–1774.

Faust TW, Assous M, Tepper JM, Koós T (2016) Neostriatal GABAergic interneurons mediate cholinergic inhibition of spiny projection neurons. *J Neurosci* 36:9505–9511.

Fiorillo CD (2013) Two dimensions of value: dopamine neurons represent reward but not aversiveness. *Science* 341:546–549.

Fiorillo CD, Tobler PN, Schultz W (2005) Evidence that the delay-period activity of dopamine neurons corresponds to reward uncertainty rather than backpropagating TD errors. *Behav Brain Funct* 1:7.

Fiorillo CD, Yun SR, Song MR (2013) Diversity and homogeneity in responses of midbrain dopamine neurons. *J Neurosci* 33:4693–4709.

Flaherty AW, Graybiel AM (1994) Input-output organization of the sensorimotor striatum in the squirrel monkey. *J Neurosci* 14:599-610.

Floresco SB, West AR, Ash B, Moore H, Grace AA (2003) Afferent modulation of dopamine neuron firing differentially regulates tonic and phasic dopamine transmission. *Nat Neurosci* 6:968–973.

Fudge JL, Haber SN (2000) The central nucleus of the amygdala projection to dopamine subpopulations in primates. *Neuroscience* 97:479–494.

Fujiyama F, Sohn J, Nakano T, Furuta T, Nakamura KC, Takeshi Kaneko T (2011) Exclusive and common targets of neostriatofugal projections of rat striosome neurons: a single neuron-tracing study using a viral vector. *Eur J Neurosci* 33:668–677.

- Freedman LJ, Cassell MD (1994) Distribution of dopaminergic fibers in the central division of the extended amygdala of the rat. *Brain Res* 633:243–252.
- Friedman A, Homma D, Gibb LG, Amemori KI, Rubin SJ, Hood AS, Riad MH, Graybiel AM (2015) A corticostriatal path targeting striosomes controls decision-making under conflict. *Cell* 161:1320–1333.
- Gage GJ, Stoetzner CR, Wiltschko AB, Berke JD (2010) Selective activation of striatal fast-spiking interneurons during choice execution. *Neuron* 67:466–479.
- Galarraga E, Herná-López S, Reyes A, Barral J, Bargas J (1997) Dopamine facilitates striatal EPSPs through an L-type Ca<sup>2+</sup> conductance. *Neuroreport* 8:2183–2186.
- Gan JO, Walton ME, Phillips PE (2010) Dissociable cost and benefit encoding of future rewards by mesolimbic dopamine. *Nat Neurosci* 13:25–27.
- Gerfen CR (1984) The neostriatal mosaic: compartmentalization of corticostriatal input and striatonigral output systems. *Nature* 311:461–464.
- Gerfen CR (1985) The neostriatal mosaic. I. Compartmental organization of projections from the striatum to the substantia nigra in the rat. *J Comp Neurol* 236:454–476
- Gerfen CR. The neostriatal mosaic: striatal patch-matrix organization is related to cortical lamination (1989) *Science* 246:385–388.
- Gerfen CR, Baimbridge KG, Miller JJ (1985) The neostriatal mosaic: compartmental distribution of calcium-binding protein and parvalbumin in the basal ganglia of the rat and monkey. *PNAS* 82:8780–8784.
- Gerfen CR, Baimbridge KG, Thibault J (1987) The neostriatal mosaic: III Biochemical and developmental dissociation of patch-matrix mesostriatal systems. *J Neurosci* 7:3935–3944.
- Gerfen CR, Engber TM, Mahan LC, Susel Z, Chase TN, Monsma FJ, Jr, Sibley DR (1990) D1 and D2 dopamine receptor-regulated gene expression of striatonigral and striatopallidal neurons. *Science* 250:1429–1432.
- Gerfen CR, Herkenham M, Thibault J (1987) The neostriatal mosaic: II. Patch-and matrix-directed mesostriatal dopaminergic and non-dopaminergic systems. *J Neurosci* 7:3915–3934.
- Gerfen CR, Paletzki R, Heintz N (2013) GENSAT BAC cre-recombinase driver lines to study the functional organization of cerebral cortical and basal ganglia circuits. *Neuron* 80:1368–1383.
- Gerfen CR, Young WS (1988) Distribution of striatonigral and striatopallidal peptidergic

neurons in both patch and matrix compartments: an in situ hybridization histochemistry and fluorescent retrograde tracing study. *Brain Res* 460:161–167.

Giros B, Jaber M, Jones SR, Wightman RM, Caron MG (1996) Hyperlocomotion and indifference to cocaine and amphetamine in mice lacking the dopamine transporter. *Nature* 379:606–612.

Gittis AH, Nelson AB, Thwin MT, Palop JJ, Kreitzer AC (2010) Distinct roles of GABAergic interneurons in the regulation of striatal output pathways. *J Neurosci* 30:2223–2234.

Gong S, Zheng C, Doughty ML, Losos K, Didkovsky N, Schambra UB, Nowak NJ, Joyner A, Leblanc G, Hatten ME, Heintz N (2003) A gene expression atlas of the central nervous system based on bacterial artificial chromosomes. *Nature* 425:917–925.

Gonon FG (1988) Nonlinear relationship between impulse flow and dopamine released by rat midbrain dopaminergic neurons as studied by in vivo electrochemistry. *Neuroscience* 24:19–28.

Gonzales C, Chesselet MF (1990) Amygdalonigral pathway: an anterograde study in the rat with *Phaseolus vulgaris* leucoagglutinin (PHA-L). *J Comp Neurol* 297:182–200

Grace AA, Bunney BS (1983) Intracellular and extracellular electrophysiology of nigral dopaminergic neurons—1. Identification and characterization. *Neuroscience* 10:301–315.

Grace AA, Bunney BS (1983) Intracellular and extracellular electrophysiology of nigral dopaminergic neurons—3. Evidence for electrotonic coupling. *Neuroscience* 10:333–348.

Grace AA, Bunney BS (1984) The control of firing pattern in nigral dopamine neurons: single spike firing. *J Neurosci* 4:2866–2876.

Grace AA, Bunney BS (1984) The control of firing pattern in nigral dopamine neurons: burst firing. *J Neurosci* 4:2877–2890.

Graybiel AM, Ragsdale CW Jr (1978) Histochemically distinct compartments in the striatum of human, monkeys, and cat demonstrated by acetylthiocholinesterase staining. *PNAS* 75:5723–5726.

Ragsdale CW Jr, Graybiel AM (1990) A simple ordering of neocortical areas established by the compartmental organization of their striatal projections. *PNAS* 87:6196–6199.

Greif GJ, Lin YJ, Liu JC, Freedman JE (1995) Dopamine-modulated potassium channels on rat striatal neurons: specific activation and cellular expression. *J Neurosci* 15:4533–4544.

Hallett PJ, Spoelgen R, Hyman BT, Standaert DG, Dunah AW (2006) Dopamine D1

activation potentiates striatal NMDA receptors by tyrosine phosphorylation-dependent subunit trafficking. *J Neurosci* 26:4690–4700.

Hamid AA, Pettibone JR, Mabrouk OS, Hetrick VL, Schmidt R, Vander Weele CM, Kennedy RT, Aragona BJ, Berke JD (2016) Mesolimbic dopamine signals the value of work. *Nat Neurosci* 19:117–126.

Hart AS, Rutledge RB, Glimcher PW, Phillips PE (2014) Phasic dopamine release in the rat nucleus accumbens symmetrically encodes a reward prediction error term. *J Neurosci* 34:698–704.

Hasue RH, Shammah-Lagnado SJ (2002) Origin of the dopaminergic innervation of the central extended amygdala and accumbens shell: A combined retrograde tracing and immunohistochemical study in the rat. *J Comp Neurol* 454:15–33.

Herkenham M, Nauta WJ (1977) Afferent connections of the habenular nuclei in the rat. A horseradish peroxidase study, with a note on the fiber-of-passage problem. *J Comp Neurol* 173:123–146.

Herkenham M, Pert CB (1981) Mosaic distribution of opiate receptors, parafascicular projections and acetylcholinesterase in rat striatum. *Nature* 291:415–418.

Hernández-Echeagaray E, Starling AJ, Cepeda C, Levine MS (2004) Modulation of AMPA currents by D2 dopamine receptors in striatal medium-sized spiny neurons: are dendrites necessary?. *Eur J Neurosci* 19:2455–2463.

Hernández-López S, Tkatch T, Perez-Garci E, Galarraga E, Bargas J, Hamm H, Surmeier DJ (2000) D2 dopamine receptors in striatal medium spiny neurons reduce L-Type Ca<sup>2+</sup> currents and excitability via a novel PLCβ1–IP3–calcineurin-signaling cascade. *J Neurosci* 20:8987–8995.

Hollerman JR, Schultz W (1998) Dopamine neurons report an error in the temporal prediction of reward during learning. *Nat Neurosci* 1: 304–309.

Hong S, Zhou TC, Smith M, Saleem KS, Hikosaka O (2011) Negative reward signals from the lateral habenula to dopamine neurons are mediated by rostromedial tegmental nucleus in primates. *J Neurosci* 31: 11457–11471.

Howe MW, Dombeck DA (2016) Rapid signalling in distinct dopaminergic axons during locomotion and reward. *Nature* 535:505–510.

Howe MW, Tierney PL, Sandberg SG, Phillips PE, Graybiel AM (2013) Prolonged dopamine signaling in striatum signals proximity and value of distant rewards. *Nature* 500:575–579.

Ibáñez-Sandoval O, Tecuapetla F, Unal B, Shah F, Koós T, Tepper JM (2010) Electrophysiological and morphological characteristics and synaptic connectivity of tyrosine hydroxylase-expressing neurons in adult mouse striatum. *J Neurosci* 30:6999–7016.

Ibáñez-Sandoval O, Tecuapetla F, Unal B, Shah F, Koós T, Tepper JM (2011) A novel functionally distinct subtype of striatal neuropeptide Y interneuron. *J Neurosci* 31:16757–16769.

Ibáñez-Sandoval O, Xenias HS, Tepper JM, Koós T (2015) Dopaminergic and cholinergic modulation of striatal tyrosine hydroxylase interneurons. *Neuropharmacology* 95:468–476.

Jenrette T, Logue J, Horner KA (2017) Striatal patch compartment lesions reduce habitual behaviors. *FASEB J* 31:1059-1056.

Jhou TC, Fields HL, Baxter MG, Saper CB, Holland PC (2009) The rostromedial tegmental nucleus (RMTg), a GABAergic afferent to midbrain dopamine neurons, encodes aversive stimuli and inhibits motor responses. *Neuron* 61:786–800.

Jhou TC, Geisler S, Marinelli M, Degarmo BE, Zahm DS (2009) The mesopontine rostromedial tegmental nucleus: A structure targeted by the lateral habenula that projects to the ventral tegmental area of Tsai and substantia nigra compacta. *J Comp Neurol* 513:566–596.

Jog MS, Kubota Y, Connolly CI, Hillegaart V, Graybiel AM (1999) Building neural representations of habits. *Science* 286:1745–1749.

Kaufling J, Veinante P, Pawlowski SA, Freund-Mercier MJ, Barrot M (2009) Afferents to the GABAergic tail of the ventral tegmental area in the rat. *J Comp Neurol* 513:597–621.

Kawaguchi Y (1993) Physiological, morphological, and histochemical characterization of three classes of interneurons in rat neostriatum. *J Neurosci* 13:4908–4823.

Kim KM, Baratta MV, Yang A, Lee D, Boyden ES, Fiorillo CD (2012) Optogenetic mimicry of the transient activation of dopamine neurons by natural reward is sufficient for operant reinforcement. *PloS one* 7:e33612.

Kincaid AE, Wilson CJ (1996) Corticostriatal innervation of the patch and matrix in the rat neostriatum. *J Comp Neurol* 374:578–592.

Kita H, Kosaka T, Heizmann CW (1990) Parvalbumin-immunoreactive neurons in the rat neostriatum: a light and electron microscopic study. *Brain Res* 536:1–5.

Kitai ST, Surmeier DJ (1992) Cholinergic and dopaminergic modulation of potassium conductances in neostriatal neurons. *Adv Neurol* 60:40–52.

Kerr JN, Wickens JR (2001) Dopamine D-1/D-5 receptor activation is required for long-term potentiation in the rat neostriatum in vitro. *J Neurophys* 85:117–124.

Koós T, Tepper JM (1999) Inhibitory control of neostriatal projection neurons by GABAergic interneurons. *Nat Neurosci* 2:467–472.

Lammel S, Hetzel A, Häckel O, Jones I, Liss B, Roeper J (2008) Unique properties of mesoprefrontal neurons within a dual mesocorticolimbic dopamine system. *Neuron* 57:760–773.

Lammel S, Ion DI, Roeper J, Malenka RC (2011) Projection-specific modulation of dopamine neuron synapses by aversive and rewarding stimuli. *Neuron* 70:855–862.

Lee CR, Abercrombie ED, Tepper JM (2004) Pallidal control of substantia nigra dopaminergic neuron firing pattern and its relation to extracellular neostriatal dopamine levels. *Neuroscience* 129:481–489.

Levine MS, Altemus KL, Cepeda C, Cromwell HC, Crawford C, Ariano MA, Drago J, Sibley DR, Westphal H (1996) Modulatory actions of dopamine on NMDA receptor-mediated responses are reduced in D1A-deficient mutant mice. *J Neurosci* 16:5870–5882.

Ljungberg T, Apicella P, Schultz W (1992) Responses of monkey dopamine neurons during learning of behavioral reactions. *J Neurophys* 67:145–163.

Lobb CJ, Wilson CJ, Paladini CA (2010) A dynamic role for GABA receptors on the firing pattern of midbrain dopaminergic neurons. *J Neurophys* 104:403–413.

Lobb CJ, Wilson CJ, Paladini CA (2011) High-frequency, short-latency disinhibition bursting of midbrain dopaminergic neurons. *J Neurophys* 105:2501–2511.

Luo R, Janssen MJ, Partridge JG, Vicini S (2013) Direct and GABA-mediated indirect effects of nicotinic ACh receptor agonists on striatal neurones. *J Physiol* 591:203–217.

Maeda H, Mogenson GJ (1982) Effects of peripheral stimulation on the activity of neurons in the ventral tegmental area, substantia nigra and midbrain reticular formation of rats. *Brain Res Bull* 8:7–14.

Mahn M, Prigge M, Ron S, Levy R, Yizhar O (2016) Biophysical constraints of optogenetic inhibition at presynaptic terminals. *Nat Neurosci* 19:554–556.

Matsui A, Williams JT (2011) Opioid-sensitive GABA inputs from rostromedial tegmental nucleus synapse onto midbrain dopamine neurons. *J Neurosci* 31:17729–17735.

Matsumoto N, Hanakawa T, Maki S, Graybiel AM, Kimura M (1999). Nigrostriatal dopamine system in learning to perform sequential motor tasks in a predictive manner. *J*

Neurophys 82:978–898.

Matsumoto M, Hikosaka O (2009) Two types of dopamine neuron distinctly convey positive and negative motivational signals. *Nature* 459:837–841.

Miller JD, Sanghera MK, German DC (1981) Mesencephalic dopaminergic unit activity in the behaviorally conditioned rat. *Life Sci* 29:1255–1263.

Mirenowicz J, Schultz W (1994) Importance of unpredictability for reward responses in primate dopamine neurons. *J Neurophys* 72:1024–1027.

Mirenowicz J, Schultz W (1996) Preferential activation of midbrain dopamine neurons by appetitive rather than aversive stimuli. *Nature* 379:449–451.

Muñoz-Manchado AB, Foldi C, Szydlowski S, Sjulson L, Farries M, Wilson C, Silberberg G, Hjerling-Leffler J (2014) Novel striatal GABAergic interneuron populations labeled in the 5HT3aEGFP mouse. *Cereb Cortex* 26:96–105.

Nelson AB, Hammack N, Yang CF, Shah NM, Seal RP, Kreitzer AC (2014) Striatal cholinergic interneurons drive GABA release from dopamine terminals. *Neuron* 82:63–70

Olson PA, Tkatch T, Hernandez-Lopez S, Ulrich S, Ilijic E, Mugnaini E, Zhang H, Bezprozvanny I, Surmeier DJ (2005) G-protein-coupled receptor modulation of striatal CaV1.3 L-type Ca<sup>2+</sup> channels is dependent on a Shank-binding domain. *J Neurosci* 25:1050–1062.

Omelchenko N, Bell R, Sesack SR (2009) Lateral habenula projections to dopamine and GABA neurons in the rat ventral tegmental area. *Eur J Neurosci* 30:1239–1250.

Paladini CA, Celada P, Tepper JM (1999) Striatal, pallidal, and pars reticulata evoked inhibition of nigrostriatal dopaminergic neurons is mediated by GABAA receptors in vivo. *Neuroscience* 89:799–812.

Paladini CA, Iribe Y, Tepper JM (1999) GABAA receptor stimulation blocks NMDA-induced bursting of dopaminergic neurons in vitro by decreasing input resistance. *Brain Res* 832:145–151.

Paladini CA, Tepper JM (1999) GABAA and GABAB antagonists differentially affect the firing pattern of substantia nigra dopaminergic neurons in vivo. *Synapse* 32:165–176.

Palmiter RD (2008) Dopamine signaling in the dorsal striatum is essential for motivated behaviors. *Ann NY Acad Sci* 1129:35–46.

Pan WX, Schmidt R, Wickens JR, Hyland BI (2005) Dopamine cells respond to predicted events during classical conditioning: evidence for eligibility traces in the reward-learning network. *J Neurosci* 25:6235–6242.

- Parker NF, Cameron CM, Taliaferro JP, Lee J, Choi JY, Davidson TJ, Daw ND, Witten IB (2016) Reward and choice encoding in terminals of midbrain dopamine neurons depends on striatal target. *Nat Neurosci* 19:845–854.
- Pawlak V, Kerr JN (2008) Dopamine receptor activation is required for corticostriatal spike-timing-dependent plasticity. *J Neurosci* 28:2435–2446.
- Pert CB, Kuhar MJ, Snyder SH (1976) Opiate receptor: autoradiographic localization in rat brain. *PNAS* 73:3729–3733.
- Prensa L, Parent A (2001) The nigrostriatal pathway in the rat: a single-axon study of the relationship between dorsal and ventral tier nigral neurons and the striosome/matrix striatal compartments. *J Neurosci* 21:7247–7260.
- Price JL, Amaral DG (1981) An autoradiographic study of the projections of the central nucleus of the monkey amygdala. *J Neurosci* 1:1242–1259.
- Puopolo M, Raviola E, Bean BP (2007) Roles of subthreshold calcium current and sodium current in spontaneous firing of mouse midbrain dopamine neurons. *J Neurosci* 27:645–656.
- Rajakumar N, Elisevich K, Flumerfelt BA (1993) Compartmental origin of the striato-entopeduncular projection in the rat. *J Comp Neurol* 331:286–296.
- Raman AV, Pitts MW, Seyedali A, Hashimoto AC, Bellinger FP, Berry MJ (2013) Selenoprotein W expression and regulation in mouse brain and neurons. *Brain Behav* 3:562–574.
- Ramanathan S, Hanley JJ, Deniau JM, Bolam JP (2002) Synaptic convergence of motor and somatosensory cortical afferents onto GABAergic interneurons in the rat striatum. *J Neurosci* 22:8158–8169.
- Rescorla RA, Wagner AR (1972) A theory of Pavlovian conditioning: variations in the effectiveness of reinforcement and non-reinforcement. In AH. Black & W.F. Prokasy (eds.), *Classical conditioning II: current research and theory* (pp. 64–99) New York: Appleton-Century-Crofts.
- Reynolds JNJ, Hyland BI, Wickens JR (2001) A cellular mechanism of reward-related learning. *Nature* 413:67–70.
- Robinson S, Sandstrom SM, Denenberg VH, Palmiter RD (2005) Distinguishing whether dopamine regulates liking, wanting, and/or learning about rewards. *Behav neurosci* 119:5–15.
- Rudkin TM, Sadikot AF (1999) Thalamic input to parvalbumin-immunoreactive GABAergic interneurons: organization in normal striatum and effect of neonatal

decortication. *Neuroscience* 88:1165–1175.

Saddoris MP, Cacciapaglia F, Wightman RM, Carelli RM (2015) Differential dopamine release dynamics in the nucleus accumbens core and shell reveal complementary signals for error prediction and incentive motivation. *J Neurosci* 35:11572–11582.

Saddoris MP, Sugam JA, Stuber GD, Witten IB, Deisseroth K, Carelli RM (2015) Mesolimbic dopamine dynamically tracks, and is causally linked to, discrete aspects of value-based decision making. *Biol psychiatry* 77:903–911.

Salamone JD, Correa M (2012) The mysterious motivational functions of mesolimbic dopamine. *Neuron* 76:470–485.

Satoh T, Nakai S, Sato T, Kimura M (2003) Correlated coding of motivation and outcome of decision by dopamine neurons. *J Neurosci* 23:9913–9923.

Schmitzer-Torbert N, Redish AD (2004) Neuronal activity in the rodent dorsal striatum in sequential navigation: separation of spatial and reward responses on the multiple T task. *J Neurophys* 91:2259–2272.

Schultz W (1986) Responses of midbrain dopamine neurons to behavioral trigger stimuli in the monkey. *J Neurophys* 56:1439–1461.

Schultz W, Apicella P, Ljungberg T (1993) Responses of monkey dopamine neurons to reward and conditioned stimuli during successive steps of learning a delayed response task. *J Neurosci* 13:900–913.

Schultz W, Dayan P, Montague PR (1997) A neural substrate of prediction and reward. *Science* 275:1593–1599.

Schultz W, Romo R (1987) Responses of nigrostriatal dopamine neurons to high-intensity somatosensory stimulation in the anesthetized monkey. *J Neurophys* 57:201–217.

Schultz W, Romo R (1990) Dopamine neurons of the monkey midbrain: contingencies of responses to active touch during self-initiated arm movements. *J Neurophys* 63:592–606.

Schultz W, Ruffieux A, Aebischer P (1983) The activity of pars compacta neurons of the monkey substantia nigra in relation to motor activation. *Exp Brain Res* 51:377–387.

Shan Q, Ge M, Christie MJ, Balleine BW (2014) The acquisition of goal-directed actions generates opposing plasticity in direct and indirect pathways in dorsomedial striatum. *J Neurosci* 34:9196–9201.

Sharpe MJ, Chang CY, Liu MA, Batchelor HM, Mueller LE, Jones JL, Niv Y,

- Schoenbaum G (2017) Dopamine transients are sufficient and necessary for acquisition of model-based associations. *Nat Neurosci*.
- Shen W, Flajolet M, Greengard P, Surmeier DJ (2008) Dichotomous dopaminergic control of striatal synaptic plasticity. *Science* 321:848–851.
- Sidibé M, Smith Y (1999) Thalamic inputs to striatal interneurons in monkeys: synaptic organization and co-localization of calcium binding proteins. *Neuroscience* 89:1189–1208.
- Smith JB, Klug JR, Ross DL, Howard CD, Hollon NG, Ko VI, Hoffman H, Callaway EM, Gerfen CR, Jin X (2016) Genetic-based dissection unveils the inputs and outputs of striatal patch and matrix compartments. *Neuron* 91:1069–1084.
- Stamford JA, Kruk ZL, Palij P, Millar J (1998) Diffusion and uptake of dopamine in rat caudate and nucleus accumbens compared using fast cyclic voltammetry. *Brain Res* 448:381–385.
- Steinberg EE, Keiflin R, Boivin JR, Witten IB, Deisseroth K, Janak PH (2013) A causal link between prediction errors, dopamine neurons and learning. *Nat Neurosci* 16:966–973.
- Steinfels GF, Heym J, Strecker RE, Jacobs BL (1983) Behavioral correlates of dopaminergic unit activity in freely moving cats. *Brain Res* 258:217–228.
- Stephenson-Jones M, Kardamakis AA, Robertson B, Grillner S (2013) Independent circuits in the basal ganglia for the evaluation and selection of actions. *PNAS* 110:E3670–3679.
- Stephenson-Jones M, Yu K, Ahrens S, Tucciarone JM, van Huijstee AN, Mejia LA, Penzo MA, Tai LH, Wilbrecht L, Li B (2016) A basal ganglia circuit for evaluating action outcomes. *Nature* 539:289–293.
- Straub C, Saulnier JL, Begue A, Feng DD, Huang KW, Sabatini BL (2016) Principles of synaptic organization of GABAergic interneurons in the striatum. *Neuron* 92:84–92.
- Sullivan MA, Chen H, Morikawa H (2008) Recurrent inhibitory network among striatal cholinergic interneurons. *J Neurosci* 28:8682–8690.
- Surmeier DJ, Bargas J, Hemmings HC, Nairn AC, Greengard P (1995) Modulation of calcium currents by a D1 dopaminergic protein kinase/phosphatase cascade in rat neostriatal neurons. *Neuron* 14:385–397.
- Sutton RS, Barto AG (1981) Toward a Modern Theory of Adaptive Networks: Expectation and Prediction. *Psychol Rev* 88:135–170.

Sutton RS, Barto AG (1990) Time-derivative models of Pavlovian reinforcement. In M. Gabriel & J. Moore (Eds.), *Learning and computational neuroscience: Foundations of adaptive networks* (p. 497–537). MIT Press.

Szczypka MS, Kwok K, Brot MD, Marck BT, Matsumoto AM, Donahue BA, Palmiter RD (2001) Dopamine production in the caudate putamen restores feeding in dopamine-deficient mice. *Neuron* 30:819–828.

Tecuapetla F, Patel JC, Xenias H, English D, Tadros I, Shah F, Berlin J, Deisseroth K, Rice ME, Tepper JM, Koós T (2010) Glutamatergic signaling by mesolimbic dopamine neurons in the nucleus accumbens. *J Neurosci* 30:7105–7110.

Tepper JM, Martin LP, Anderson DR (1995) GABAA Receptor-Mediated Inhibition of Rat Substantia Nigra Dopaminergic Neurons by Pars Reticulata Projection Neurons. *J Neurosci* 15:3092–3103.

Threlfell S, Lalic T, Platt NJ, Jennings KA, Deisseroth K, Cragg SJ (2012) Striatal dopamine release is triggered by synchronized activity in cholinergic interneurons. *Neuron* 75:58–64.

Tian J, Uchida N (2015) Habenula lesions reveal that multiple mechanisms underlie dopamine prediction errors. *Neuron* 87:1304–1316.

Tian J, Huang R, Cohen JY, Osakada F, Kobak D, Machens CK, Callaway EM, Uchida N, Watabe-Uchida M (2016) Distributed and mixed information in monosynaptic inputs to dopamine neurons. *Neuron* 91:1374–1389.

Tobler PN, Fiorillo CD, Schultz W (2005) Adaptive coding of reward value by dopamine neurons. *Science* 307:1642–1645.

Tritsch NX, Ding JB, Sabatini BL (2012) Dopaminergic neurons inhibit striatal output via non-canonical release of GABA. *Nature* 490:262–266.

Tsai CT, Nakamura S, Iwama K (1980) Inhibition of neuronal activity of the substantia nigra by noxious stimuli and its modification by the caudate nucleus. *Brain Res* 195:299–311.

Tsai HC, Zhang F, Adamantidis A, Stuber GD, Bonci A, De Lecea L, Deisseroth K (2009) Phasic firing in dopaminergic neurons is sufficient for behavioral conditioning. *Science* 324:1080–1084.

Ungerstedt U (1971) Adipsia and aphagia after 6-hydroxydopamine induced degeneration of the nigro-striatal dopamine system. *Acta Physiol Scand* 82:95–122.

- Vincent SR, Johansson O (1983) Striatal neurons containing both somatostatin-and avian pancreatic polypeptide (APP)-like immunoreactivities and NADPH-diaphorase activity: A light and electron microscopic study. *J Comp Neurol* 217:264–270.
- Vuillet J, Kerkerian L, Kachidian P, Bosler O, Nieoullon A (1989) Ultrastructural correlates of functional relationships between nigral dopaminergic or cortical afferent fibers and neuropeptide Y-containing neurons in the rat striatum. *Neurosci Lett* 100:99–104.
- Wallace ML, Saunders A, Huang KW, Philson AC, Goldman M, Macosko EZ, McCarroll SA, Sabatini BL (2017) Genetically distinct parallel pathways in the entopeduncular nucleus for limbic and sensorimotor output of the basal ganglia. *Neuron* 94:138–152.
- Watabe-Uchida M, Zhu L, Ogawa SK, Vamanrao A, Uchida N (2012) Whole-brain mapping of direct inputs to midbrain dopamine neurons. *Neuron* 74:858–873.
- Wickens JR, Begg AJ, Arbuthnott GW (1996) Dopamine reverses the depression of rat corticostriatal synapses which normally follows high-frequency stimulation of cortex in vitro. *Neuroscience* 70:1–5.
- Wieland S, Schindler S, Huber C, Köhr G, Oswald MJ, Kelsch W (2015) Phasic dopamine modifies sensory-driven output of striatal neurons through synaptic plasticity. *J Neurosci* 35:9946–9956.
- Wise RA (2004) Dopamine, learning and motivation. *Nature rev neurosci* 5:483–494.
- Yagishita S, Hayashi-Takagi A, Ellis-Davies GC, Urakubo H, Ishii S, Kasai H (2014) A critical time window for dopamine actions on the structural plasticity of dendritic spines. *Science* 345:1616–1620.
- Yetnikoff L, Lavezzi HN, Reichard RA, Zahm DS (2014) An update on the connections of the ventral mesencephalic dopaminergic complex. *Neuroscience* 282:23–48.
- Xia Y, Driscoll JR, Wilbrecht L, Margolis EB, Fields HL, Hjelmstad GO (2011) Nucleus accumbens medium spiny neurons target non-dopaminergic neurons in the ventral tegmental area. *J Neurosci* 31:7811–7816.
- Zhou QY, Palmiter RD (1995) Dopamine-deficient mice are severely hypoactive, adipsic, and aphagic. *Cell* 83:1197–1209.
- Zweifel LS, Parker JG, Lobb CJ, Rainwater A, Wall VZ, Fadok JP, Darvas M, Kim MJ, Mizumori SJ, Paladini CA, Phillips PE (2009) Disruption of NMDAR-dependent burst firing by dopamine neurons provides selective assessment of phasic dopamine-dependent behavior. *PNAS* 106:7281–7288.